Continental Pans in Southern Africa and their Potential as Paleoclimatic and Paleoecological Geoarchives

Der Fakultät für Mathematik und Naturwissenschaften der Carl von Ossietzky Universität Oldenburg zur Erlangung des Grades und Titels eines

Doktors der Naturwissenschaften

–Dr. rer. nat. –

angenommene Dissertation

von Herrn Lukas Belz

geboren am 15.11.1983 in Wiesbaden

Erstgutachter: Prof. Dr. Heinz Wilkes

Zweitgutachter: PD Dr. Holger Freund

Tag der Disputation: 04.03.2022

Abstract

The impact of human-induced climate change on ecosystems in southern Africa is already visible and measurable. To assess potential hazards of the climate change it is very important to know the regional dynamics of natural climate variability. Reconstruction of paleo-climate conditions is crucial to understand the mechanisms how the local ecosystem is affected by global change. An established method for investigating past terrestrial environmental conditions is the analyses of leaf wax-derived biomarkers primarily long chain n-alkanes and their compound-specific carbon and hydrogen isotopic compositions. From this data conclusions can be drawn on past vegetation and hydrological changes. In central southern Africa environmental archives are rare, due to arid conditions, making paleoclimate studies both challenging and important. A possible archive for leaf wax biomarkers is sediment from pans (playas), local occurring depressions which can get flooded during wet season. This thesis examines the potential of Kalahari pans for reconstructions of environmental conditions using biomarkers.

The first part of the thesis is a study of Omongwa Pan, a Kalahari salt pan located in eastern Namibia. The analyses comprise bulk parameters, n-alkanes n-alkanols, fatty acids, and carbon as well as hydrogen isotopes of n-alkanes. The record reaches back to 27 ka BP and displays the development from the Last Glacial Maximum (23-19 ka BP) to present. The results in general indicate relatively dry conditions. During Heinrich Stadial I (ca. 18-14.8 ka) vegetation changed, as the proportion of C_4 grasses increases. This shift is probably caused by a short phase of intensified summer rainfall, which is linked to a temporary southward shift of the Intertropical Convergence Zone. Conditions were dry during the early Holocene. Results and comparisons with representative terrestrial records from the region indicate, that the catchment of the was part of the summer rainfall zone over the whole time-span of the record.

The second part of the thesis focuses on Koës Pan in south-eastern Namibia. Preceding studies pointed to a northward extension of winter rainfall up to this area during the last glacial. The aim of this study is to reconstruct the process of

Abstract

the shift from winter rainfall to summer rainfall and its environmental implications. The dataset includes bulk parameters, high resolution n-alkanes and their compound-specific carbon and hydrogen isotopic compositions since 19.9 ka BP. The results show abrupt changes pointing to lasting dryer and or warmer conditions around 17.5 ka BP. The shift is probably a result of a switch of the growing season and adapting vegetation in response to the shift from winter to summer rainfall. The change in seasonal rainfall also implies a swapped moisture source from Atlantic to Indian Ocean with impact on n-alkane hydrogen isotopes. Therefore, the application of δD_{31} for a reconstruction of precipitation amount is restricted. The study also displays a highly unusual relative alkane distribution of n-C_{29}, n-C_{31} and n-C_{33} indicating high-resolved change in vegetation and environmental conditions. This highlights the sensitivity of this biomarker. On the other hand, the record reveals that this level of detail can only partly be displayed by well-established molecular proxies such as the average chain length of n-alkanes

This final study compares the Koës Pan record to a new high-resolution n-alkane and carbon isotope record from Omongwa Pan since 16.9 ka BP. The results indicate a comparable, relatively wet phase during the last glacial-interglacial transition at both pans. After 16 ka BP dryer climate affect vegetation at both sites but with different consequences. While at Omongwa Pan vegetation probably changed to an open savanna with poor grass coverage, vegetation at Koës Pan was more similar to the C_4 grasses and dwarf shrub dominated Nama Karoo biome. In the study the Norm$^{13}C_{33}$ index is introduced as a potential proxy for evaporative conditions.

This thesis introduces pans as a capable environmental archive for the application of leaf wax biomarkers in the western Kalahari. It is possible to draw conclusions on climate variations via the applied methods. The resolution of the records even allows the reconstruction of abrupt climate shifts. The small catchment of pans furthermore enables to identify links and boundaries of intracontinental climate change, making pans an interesting option to close paleo-climatic gaps in central southern Africa.

II

Zusammenfassung

Die Auswirkungen des anthropogenen Klimawandels auf Ökosysteme im südlichen Afrika sind bereits erkenn- und messbar. Um die Gefahren des Klimawandels einschätzen zu können ist es von großer Bedeutung, die regionale, natürliche Klimavariabilität zu erkennen. Die Rekonstruierung von Paläoklimabedingungen ist entscheidend, um den Mechanismus wie das lokale Ökosystem durch den globalen Klimawandel beeinträchtigt wird zu verstehen. Eine etablierte Methode, um terrestrische Umweltbedingungen der Vergangenheit untersuchen zu können, ist die Analyse von auf Blattwachsen basierenden Biomarkern, vor allem langkettige n-Alkane und die komponentenspezifische Isotopie ihrer Kohlen- und Wasserstoffatome. Aus diesen Daten können Schlussfolgerungen auf Veränderungen in der Vegetation und Hydrologie gezogen werden. Aufgrund der ariden Bedingungen, sind Umweltarchive im zentralen südlichen Afrika selten, so dass Paläoklimastudien herausfordernd und bedeutend sind. Ein mögliches Archiv für Blattwachs-Biomarker ist das Sediment von Pfannen (Playas), lokal vorkommende Senken, die während der Regenzeit geflutet sein können. Diese Arbeit untersucht das Potential von Kalahari Pfannen für Rekonstruktionen von Umweltbedingungen anhand von Biomarkern.

Der erste Teil dieser Arbeit ist eine Studie der Omongwa Pfanne, eine Kalahari Salzpfanne, die sich im Osten Namibias befindet. Die Analyse umfasst Basisparameter, n-Alkane n-Alkanole, Fettsäuren und Kohlenstoff- und Wasserstoffisotope der n-Alkane. Der Datensatz reicht zurück bis 27 ka BP und stellt die Entwicklung seit dem letzten glazialen Maximum (23-19 ka BP) bis heute dar. Generell zeigen die Ergebnisse relativ trockene Bedingungen auf. Während des Heinrich Stadials I (ca. 18-14,8 ka) veränderte sich die Vegetation, da der Anteil von C_4-Gräsern steigt. Diese Veränderung ist wahrscheinlich durch eine kurze Phase mit intensiviertem Sommerregen verursacht worden. Dieser ist bedingt durch eine temporär südwärts gerichtete Verschiebung der innertropischen Konvergenzzone. Das frühe Holozän ist durch trockene Klimabedingungen geprägt. Die Ergebnisse und Vergleiche mit repräsentativen

terrestrischen Datensätzen aus der Region zeigen an, dass im Einzugsgebiet der Pfanne während des gesamten Zeitraumes Teil der Sommerregenzone war.

Der zweite Teil der Arbeit konzentriert sich auf die Koës Pfanne im südöstlichen Namibia. Vorausgehende Studien deuteten auf eine nordwärts gerichtete Erweiterung des Winterregens während des letzten Glazials in dieses Gebiet. Das Ziel dieser Studie war die Rekonstruktion des Prozesses des Wechsels vom Winterregen zum Sommerregen und die sich daraus ergebenden Folgen für die Umwelt. Der Datensatz enthält Basisparameter sowie n-Alkane und deren Kohlenstoff- und Wasserstoffisotope seit 19,9 ka BP. Die Ergebnisse zeigen abrupte Veränderungen, welche auf länger andauernde trockenere und/oder wärmere Bedingungen deuten. Dieser Wechsel ist wahrscheinlich das Ergebnis einer verschobenen Vegetationsperiode und sich anpassender Vegetation als Reaktion auf den Wechsel von einer Winter- zur einer Sommerregenzeit. Die Wechsel der Regenzeiten beinhaltet auch eine Verschiebung der Herkunft der Feuchtigkeit vom Atlantischen zum Indischen Ozean mit Auswirkungen auf die Zusammensetzung der Wasserstoffisotope in den n-Alkanen. Daher ist die Anwendung des δD_{31} zur Rekonstruktion von Regenmengen nur begrenzt möglich. Die Studie zeigt außerdem eine höchst ungewöhnliche relative Alkan-Verteilung von n-C_{29}, n-C_{31} und n-C_{33} an, die auf hoch aufgelöste kontinuierliche Veränderungen in der Vegetation und bei Umwelteinflüssen hinweisen. Dies verdeutlicht wie sensibel diese Biomarker sind. Auf der anderen Seite deckt der Datensatz auch auf, dass dieser Detailgrad von gut etablierten Proxys, wie etwa der durchschnittliche Kettenlänge, nur teilweise dargestellt werden kann.

Die letzte Studie vergleicht den Datensatz der Koës Pfanne mit einem neuen hochauflösenden n-Alkan- und Kohlenstoffisotopendatensatz aus der Omongwa Pfanne seit 16,9 ka BP. Die Ergebnisse weisen auf eine vergleichbare, relativ feuchte Phase während des letzten Glazialen-Interglazialen Übergangs bei beiden Pfannen hin. Ab 16 ka BP, wird die Vegetation an beiden Orten durch Trockenheit beeinflusst, jedoch mit unterschiedlichen Konsequenzen. Während bei der Omongwa Pfanne im Holozän die Vegetation sich hin zu einer offenen Savanne mit dünner Grasbedeckung entwickelte, entsprach die Vegetation an der Koës Pfanne eher dem durch C_4 Gräser und Zwergsträucher dominierten Nama Karoo

IV

Biom. In der Studie wurde auch der Norm^{13}C$_{33}$-Index als potentieller Proxy für stark evaporative Bedingungen eingeführt.

Diese Arbeit führt Pfannen als geeignete Umweltarchive für die Anwendung von Blattwachs Biomarkern in der westlichen Kalahari ein, Durch die angewandten Methoden können Rückschlüsse auf Klimaveränderungen gezogen werden. Die Auflösung der Datensätze erlaubt sogar die Rekonstruktion von abrupten Klimaveränderungen, was Pfannen zu einer interessanten Option für das Schließen Paläoklimatische Lücken im zentralen Südafrika macht.

Table of Contents

Table of Contents

List of Abbreviations

AA	Arabian Anticyclone
ABF	Angola–Benguela-Front
ACL	Average chain length
AHP	African Humid Period
ASE	Accelerated Solvent Extractor
BP	Before present
C_3 plants	Plants using Calvin cyle
C_4 plants	Plants using Hatch-Slatch cycle
CAB	Congo Air Boundary
cal	Calibrated
CAM	Crassulacean Acid Metabolism
CBC	Calvin-Benson-Cycle
CPI	Carbon Preference Index
DCM	Dichloromethane
EOP	even-over-odd predominance
GC-FID	Gas Chromatograph equipped with Flame Ionization Detector
GC-IRMS	Gas Chromatograph equipped with Isotope Ratio Mass Spectrometer
GC-MS	Gas Chromatograph equipped with Mass Spectrometer
GMT	Generic Mapping Tools
HS1	Heinrich Stadial 1
HSC	Hatch-Slack Cycle
IPCC	Intergovernmental Panel on Climate Change
ITCZ	Intertropical Convergence Zone
ka	Kilo years
L	Major low pressure cell
LGM	Last Glacial Maximum
MeOH	Methanol
MPLC	Medium Pressure Liquid Chromatography
NAA	North Atlantic Anticyclone
NEM	Northerly East African monsoon
NH	Northern Hemisphere
NHC	Northern Hadley Cell
NSO	Fraction containing nitrogen, sulphur, and oxygen
OEP	Odd-over-even predominance
PEP	Phosphoenolpyruvate
PEP-C	Phosphoenolpyruvate carboxylase
PET	Potential evapotranspiration
Rubisco	Ribulose-1,5-bisphosphate carboxylase oxygenase
SAA	South Atlantic Anticyclone
Sed. rate	Sedimentation rate
SEM	Southerly East African monsoon
SH	Southern Hemisphere

List of Abbreviations

SHC	Southern Hadley Cell
SIA	South Indian Anticyclone
SRZ	Summer rainfall zone
TIC	Total inorganic carbon
TOC	Total organic carbon
VPDB	Vienna Pee Dee Belemnite
VSMOW	Vienna Standard Mean Ocean Water
WAM	West African Monsoon
WRZ	Winter rainfall zone
YD	Younger Dryas
YRZ	Year-round rainfall zone
$\delta^{13}C$	Stable carbon isotope composition
$\delta^{18}O$	Stable oxygen isotope composition
δD	Stable hydrogen isotope composition
δD_p	Stable hydrogen isotope composition of precipitation

List of Figures

(abbreviated)

List of Tables

(abbreviated)

1. Introduction

In the wake of anthropogenically induced climate change it is important to understand natural environmental systems and their dynamics. This knowledge allows to estimate the vulnerability of ecosystems and potential hazards for inhabitants and land use. In many regions climate change increases the probability and intensity of extreme weather events like droughts and floods (Held and Soden, 2006). The tendency to extremes makes subtropical semiarid regions with a strongly seasonal occurrence of precipitation especially vulnerable. An example is southern Africa, which location between the Indian and Atlantic Oceans makes climate processes even more complex, in particular in the continental interior. The assessment of weather data since the 1950s determined increases of high-temperature extremes, heavy precipitation events and agricultural and ecological droughts in southern Africa (IPCC, 2021). Climate models predict that this trend will continue when global mean temperature rises by 2°C or more relative to pre-industrial levels (IPCC, 2021). However, the complexity of atmospheric and oceanic processes, especially of abrupt changes and their regional impacts, is still not completely representable in models. Reconstruction of paleo-environmental conditions and of local shifts as a result of global changes are key in understanding mechanisms which will likely play a role in future changes. Periods of major changes in global climate, such as the Last Glacial Maximum (LGM, 23-19 ka BP), the transition phase at the end of the (last) glacial, and the Holocene (11.7 ka BP to present) are crucial to our understanding of the mechanisms that control global climate changes, and thus to our ability to predict future changes. The end of the last glacial featured global climate change through external forcing which led to a rise of temperatures and relocation of atmospheric cells with an impact on southern African precipitation seasonality (Dahl et al., 2005; Broccoli et al., 2006; Chase and Meadows, 2007; Gasse et al., 2008). Most parts of the Holocene showed unstable conditions in central southern Africa with a high spatial variability (Burrough and Thomas, 2013; Chase et al., 2015; Scott and Thackeray, 2015).

Organic matter deposited in sediments can provide valuable information on past environmental conditions at the time and space of its formation. An important way to decipher this information are biomarkers. Biomarkers are organic compounds which can be linked to their biogenetic source (Rullkötter, 2006). Frequently used in numerous studies of terrestrial biomarkers are long chain n-alkanes and n-alkanols (e.g. Meyers, 2003; Rommerskirchen et al., 2003; Schefuß et al., 2003; Kristen et al., 2010). Both are important constituents of the layer of protective leaf waxes of plants resistant to decay over long time scales and can be linked specifically to higher terrestrial plants (Eglinton and Hamilton, 1967; Peters et al., 2005). The distribution of long chain n-alkanes and n-alkanols and their carbon and hydrogen isotopic compositions give insights not only in the vegetation biocenosis, but also the environmental conditions the plants lived in (e.g. Vogts et al., 2009; Kristen et al., 2010; Sachse et al., 2012; Bush and McInerney, 2015).

Reconstruction of climate and environmental conditions using leaf wax proxies is often based on lacustrine and marine archives (e.g. Hinrichs et al., 1998; Schefuß et al., 2011; Rach et al., 2014; Schmidt et al., 2014). The scarce occurrence of lakes in semi-arid to arid regions therefore limits environmental reconstruction to areas where lakes occur. In southern Africa this is mainly in the eastern (Truc et al., 2013; Schmidt et al., 2014), and southern coastal areas (Wündsch et al., 2016). There are few continental lakes which were used for paleoclimatology in central southern Africa, examples include Lake Otjikoto in northern Namibia (Tabares et al., 2020) or Lake Ngami in Botswana (Cordova et al., 2017). Sediment of marine cores integrates terrestrial matter either via dust or riverine input (Rommerskirchen et al., 2006a; Herrmann et al., 2016). Sediments from river systems, especially in dry areas often feature a high variation of catchment size, partly active sidearms and intermediate sedimentation. Records based on terrestrial dust input however are always an integrated signal from a large source area. Consequently, records from marine archives cannot unravel complex processes within the source area. For a reconstruction of intracontinental shifts like changes in rain seasonality, continental archives with limited source areas are crucial. This thesis tests a novel approach in focussing on the reconstruction of environmental conditions in central southern Africa using biomarkers from pan

2

deposits as a promising alternative to lake sediments. Pans are common depressions in the central and western Kalahari which are only flooded infrequently.

1.1 Modern climate in southern Africa

One of the most important factors for the environmental conditions in southern African is the seasonality of precipitation. It is controlled by complex atmospheric and oceanic patterns like the interaction of the southern Hadley Cell (SHC) and the westerlies of the southern Ferrel circulation, which converge across southern Africa (Figure 1-1).

The northern boundary of the Hadley cell is the intertropical convergence zone (ITCZ). This low pressure through migrates southward in austral summer following the high insolation. Another convergence zone connected to the ITCZ is the Congo Air Boundary (CAB). The CAB attracts humid air masses of the South-Atlantic from the west and of the southern Indian Ocean From the east (Nicholson, 2009). The southward shift of the CAB during austral summer causes convection-based summer rainfall (showers) with a high spatial variability over large parts of northwest, central and east of southern Africa (Figure 1-1B; Cockcroft et al., 1987). As the moisture source for central southern Africa is the Indian Ocean, the summer rainfall intensity decreases south-westward with dry conditions during summer at the south western tip of Africa (Figure 1-1C; Nicholson, 2000).

During austral winter the ITCZ is shifted northward and the climate of central southern Africa is controlled by a semi-permanent subtropical anticyclone with stable dry conditions (Tyson et al., 1996). The austral westerlies influenced by the South Atlantic Anticyclone move northward bringing moisture and wind-driven, frontal precipitation to the south western tip of southern Africa, which decreases northward (Figure 1-1A). The area where more than 66 % of precipitation falls between October and March is defined as summer rainfall zone (SRZ), while the area where more than 66 % of precipitation falls between April and September is

defined as winter rainfall zone (WRZ). The area in between where both zones overlap is defined as year-round rainfall zone (YRZ; Chase and Meadows, 2007). The three rainfall zones are mapped in Figure 1-1C.
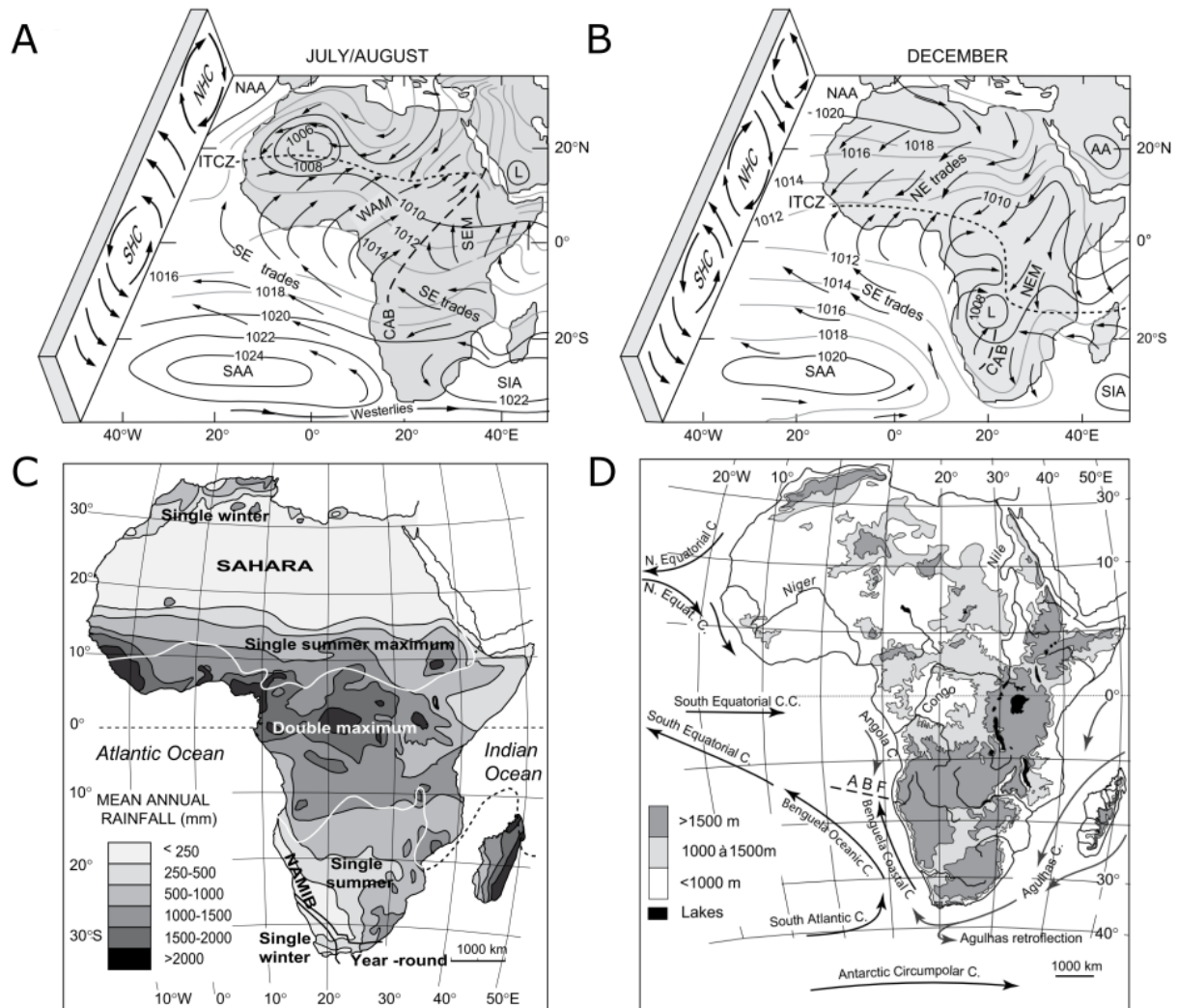
Figure 1-1 Some aspects of the present-day African climate (from Gasse et al., 2008). Low-level wind and pressure patterns during A. austral winter and B. austral summer (modified after Nicholson, 2009); NAA (North Atlantic Anticyclone), SAA (South Atlantic Antic Anticyclone), AA (Arabian Anticyclone), SIA (South Indian Anticyclone), L (major low pressure cells), WAM (West African Monsoon), NEM (northerly East African monsoon), SEM (southerly East African monsoon), dotted line: ITCZ (Intertropical Convergence Zone), dashed line: CAB (Congo Air Boundary). In section: SHC (southern Hadley Cell), NHC (northern Hadley Cell). C. Mean annual rainfall and rainfall seasonality. In the text, the southern single winter area is referred to as winter rainfall zone (WRZ) and the single summer area as summer rainfall zone (SRZ; modified after Griffiths, 1972; Stamp and Morgan, 1972). D. Major African topography and oceanic surface currents; ABF (Angola–Benguela-Front).

4

1.2 Paleoclimate in southern Africa

1.2.1 Last Glacial Maximum

The global climate during the Quaternary (2588 ka BP-today) has been characterized by changes between glacial and interglacial states. These states are caused by cyclic variations of insolation depending on Earth's orbital parameters which affect the distance between Earth and Sun and the angle of insolation, first described by Milanković (1941). The parameters are precession (rotation of Earth's axis, 19 ka cycles), obliquity (angle of axial tilt, 41 ka cycles) and eccentricity (Earth's orbit deviation from a circle; 100 kyr cycles; Hays et al., 1976; Imbrie et al., 1993).

The last glacial stadial culminated in the LGM around 23-19 ka BP (Mix et al., 2001).). In general, the global climate was cooler, windier and dryer. Models predicted that the global mean surface temperature was lowered by about 4.3°C (Bush and Philander, 1999). Cooler conditions were also reconstructed in southern Africa. Studies suggest a northward expansion of the WRZ during the LGM. bringing more precipitation to central southern Africa (van Zinderen Bakker, 1983; Cockcroft et al., 1987; Chase and Meadows, 2007; Stone, 2014). The shift of the WRZ is thought to be the result of a northward migration of the Ferrell Cell and the austral westerlies caused by the glacial accumulation of Antarctic sea ice (Gersonde et al., 2005)

1.2.2 Northern hemisphere cooling events after the LGM

Heinrich Events are repeatedly occurring events which are connected to abrupt cooling shifts (Heinrich Stadials; HS) in the Quaternary. They are characterized by a large occurrence of icebergs and deduced from specific ice-rafted debris layers (Heinrich layers; Heinrich, 1988; Broecker, 1994). The fresh water pulse from the icebergs transported in the North Atlantic lowers the salinity of the surface water;

hence, the water density drops limiting the formation of North Atlantic deep water (NADW). The latter is an important part of the Atlantic meridional overturning circulation (AMOC), which then gets disturbed. This leads to a slowed down heat transfer over the North Atlantic and thus to the cooling of the Northern Hemisphere (Crowley, 1992; Broecker, 1994; Sarnthein et al., 2001). The last HS was HS1 (18-15 ka BP; Labeyrie et al., 2003). Another cooling event on the Northern Hemisphere that took place and disturbed the AMOC in the late Pleistocene was the Younger Dryas (YD; 12.6-11.5 ka BP; Björck et al., 1998). A fresh water pulse from the proglacial Lake Agassiz (Broecker et al., 1989) , or a repeating mechanism of deglaciation (Broecker et al., 2010) are believed the main reasons for the YD. The cooling in the Northern Hemisphere during the HS and YD is thought to have pushed the ITCZ southward, Intensifying summer rainfall in central southern Africa   (Lancaster, 1979; Cockcroft et al., 1987; Dahl et al., 2005).

1.2.3 Holocene

In the Late Pleistocene-early-Holocene, North and West Africa experienced the African humid period (AHP; 14-8.5 ka BP) which was related to an intensified West African monsoon (Shanahan et al., 2015). It did not extend itself to large areas of southern Africa (Burrough and Thomas, 2013). Increased west African monsoon reached Angola and fed the Okavango River which discharged in a system of lakes and pans at that time (Burrough et al., 2007; Cordova et al., 2017). There are hypotheses of a Holocene dualism between North and East on one side and South and West on the other side of southern Africa. However, data compilations on the Holocene show a high environmental and climatic variability in the centre of southern Africa creating a spatially complex and partly inconsistent mosaic of drier and wetter conditions (Thomas and Shaw, 2002; Burrough and Thomas, 2013).

1.3 Vegetation in southern Africa

The variation of environmental conditions within southern Africa leads to high spatial differences in vegetation assemblages. The main controlling element is precipitation but also other factors like temperatures, evaporative conditions and altitude play a role in defining the local botanic biocenosis (Rutherford et al., 2006). In central southern Africa the most important biomes are the Savanna Biome, the Nama Karoo Biome and the Grassland Biome Figure 1-2. The Savanna Biome is characterized by dry winters and wet summer month with high precipitation (Mucina and Rutherford, 2006). The savanna vegetation is mainly a mixture of shrubs, trees and grasses. Vegetation density can switch between a dense and an open grassy state (Bester et al., 2003; Joubert et al., 2008). While grass density mainly depends on precipitation (February et al., 2013; Berry and Kulmatiski, 2017), shrub and tree density is also limited by occurrence of frost or fire, the latter often being caused by high grass density (Joubert et al., 2012, 2013). On the other hand, there are also biotic factors such as intense grazing that are causing processes like shrub encroachment (Joubert et al., 2008). The Nama Karoo biome is characterized by its very dry conditions. Rainfall usually only occurs in late summer with a high spatial variability. Vegetation is dominated by a mixture of savanna grasses and dwarf shrubs and a relatively low species richness compared to adjacent biomes. Soils are too shallow for a high abundance of trees and precipitation is too low for a high grass density (Mucina and Rutherford, 2006). The Grassland Biome today is located in areas with elevated altitudes. The low fraction of shrubs in these grasslands is mainly caused by low temperatures (Bredenkamp et al., 2002).
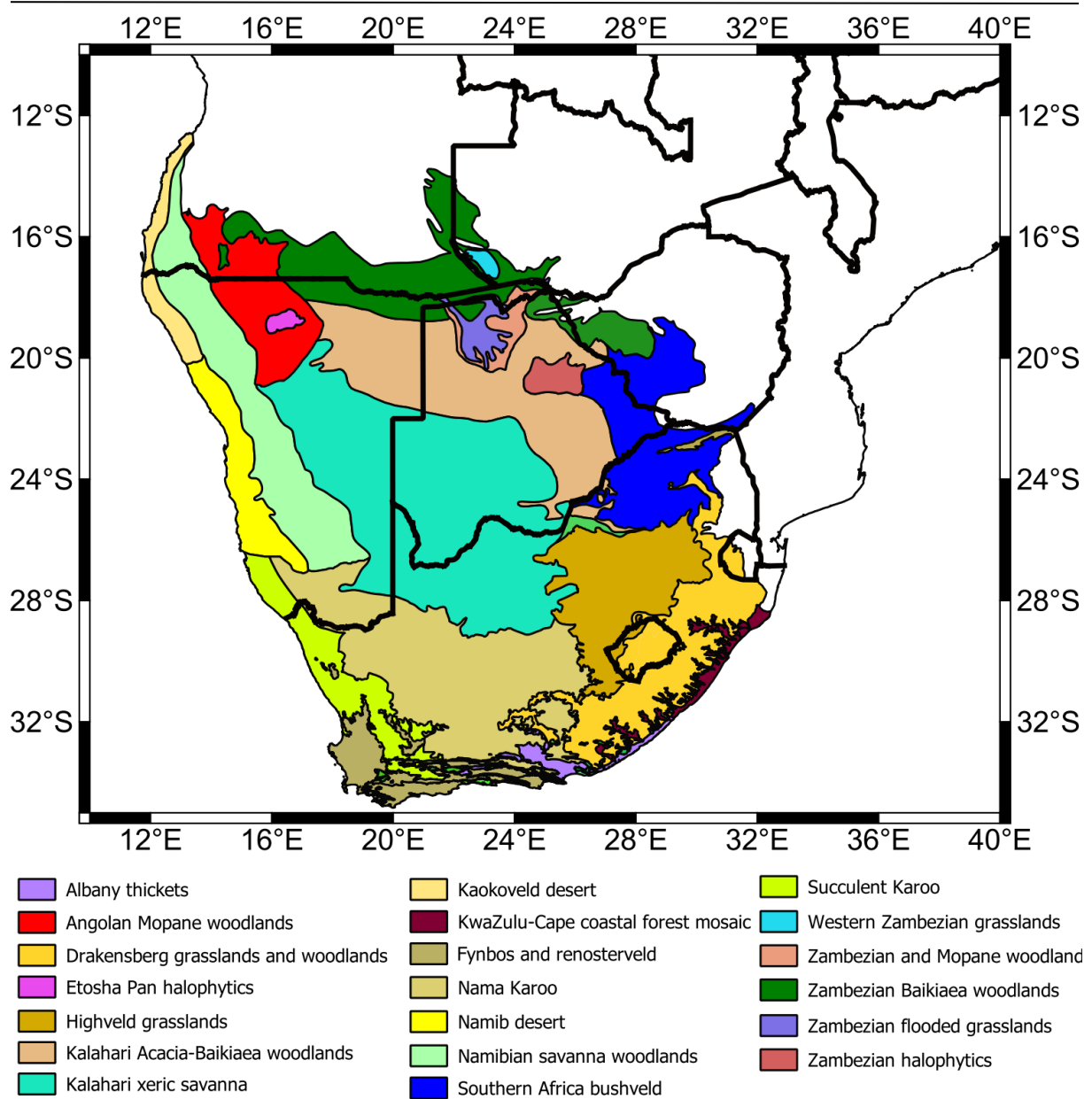
Figure 1-2 Biomes and ecoregions of central and western southern Africa. Datasource: Olson et al. (2001).

1.4 Photosynthetic pathways

Land plants can be distinguished by their Photosynthetic pathways. There are three different types of carbon assimilation during photosynthesis. The Calvin-Benson-Cycle (CBC) the Hatch-Slack Cycle (HSC) and the Crassulacean Acid Metabolism (CAM). The most common pathway in terrestrial plants is the CBC.

At the beginning of the CBC, CO_2 enters the plant via open stomatas into the mesophyll. In the mesophyll cell CO_2 is in equilibrium with aqueous HCO_3^-. Within the CBC, CO_2 is reduced to C_3 molecules (glycerate-3-phosphate) catalysed by enzyme Ribulose-1,5-bisphosphate carboxylase-oxygenase (RuBisCo), which is why plants using this pathway are called C_3 plants (Bassham et al., 1954; Sharkey, 2019). The C_3 molecules are then further metabolized to sugars. In southern Africa, C_3 plants are mainly trees, shrubs and herbs. C_3 grasses are abundant in montane areas of the Grassland Biome in South Africa and Lesotho (Mucina and Rutherford, 2006). However, most grasses in the Savanna and Nama Karoo Biome are C_4 plants. Those plants perform the HSC for the absorption of CO_2 prior to the CBC that is separated spatially. During the HSC, HCO_3^- reacts with phosphoenolpyruvate (PEP) to a C_4 acid (oxaloacetate) and phosphate, catalysed by phosphoenolpyruvate carboxylase (PEP-C). Oxaloacetate is then reduced to malate or aspartate and diffuses to a bundle sheet cell. There, the dicarboxylic acids get decarboxylated forming CO_2 and initiating the CBC. By this, CO_2 is concentrated higher around RuBisCO, compared to the mesophyll cells in C_3 plants, enhancing the efficiency of the CBC. Therefore, CO_2 fixation can be maintained even at lower stomatal conductance, reducing water loss due to evaporation to a minimum (Slack and Hatch, 1967; Osborne and Sack, 2012).

The third pathway, the Crassulacean Acid Metabolism (CAM), also separates CO_2 absorption and carbon fixation but rather temporarily than spatially. In contrast to C_4 plants, the fixation of CO_2 by PEP-C in CAM plants occurs only during the night when stomata are open due to lower temperatures and therefore reduced transpiration. The synthesized malate is then stored in a vacuole. During the day, stomata are closed and the acid is transported out of the vacuole and decarboxylated to produce CO_2 so that the CBC can take place (Bonner and Bonner, 1948; Dodd et al., 2002; Sharkey, 2019). CAM plants in southern Africa are mainly succulents and occur widely in the Succulent Karoo biome and the Namib desert.

1.5 Epicuticular waxes
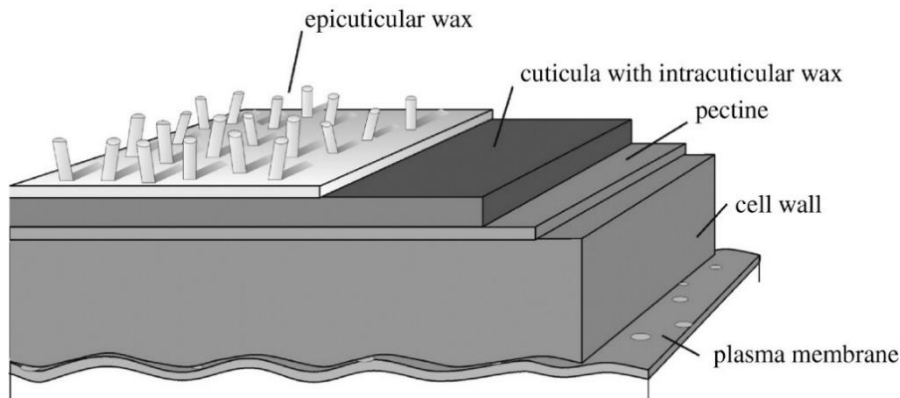
Figure 1-3 Simplified model of the stratification of the outermost layers of the plant epidermal cells. From Koch and Barthlott (2009).

Terrestrial higher plants synthesize waxes to protect all aerially exposed organs against harms like UV radiation, pathogens and water loss (Kolattukudy, 1976; Eglinton and Eglinton, 2008). These leaf waxes are located in the cuticula as intracuticular wax or outside the cuticula as epicuticular wax, where they form crystals (Figure 1-3; Koch and Ensikat, 2008). Epicuticular waxes mainly consist of *n*-alkanes, *n*-alkanols, fatty acids and wax esters (Eglinton and Hamilton, 1967; Kolattukudy, 1976). Epicuticular waxes are frequently washed or blown away and reproduced. The biosynthesis of leaf waxes is based on fatty acids. These are elongated in repetitive cycles with acetyl groups adding a C_2 unit each cycle. After elongation fatty acids can be transformed in two ways. One way is the acyl reduction pathway, which forms aldehydes and alkan-1-ols. Another way is the Decarbonylation Pathway which created alkanes secondary alcohols and ketones (Figure1-4; Kunst and Samuels, 2003; Shepherd, 2003). Plants produce wax components in different chain lengths. The distribution of chain length can vary by plant type and/or environmental conditions (Bush and McInerney, 2013). Plant derived fatty acids and alkan-1-ols are to a high extent even-chained, while alkanes and ketones are commonly odd-chained due to the decarbonylation (Kunst and Samuels, 2003; Shepherd and Wynne Griffiths, 2006; Koch and Ensikat, 2008).
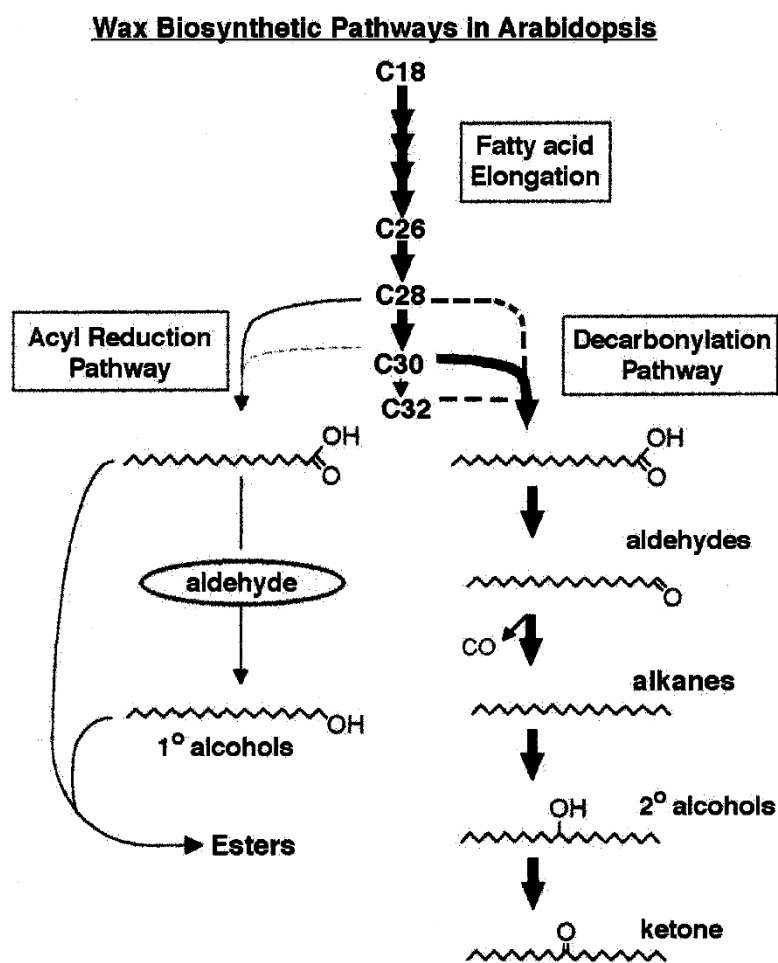
Figure 1-4 Proposed metabolic pathways for wax biosynthesis in Arabidopsis stems (from Kunst and Samuels, 2003).

1.6 Isotopic composition of leaf waxes

Differences in chain length of epicuticular waxes can provide information about the wax producing plants and the conditions they lived in. Furthermore, the carbon and hydrogen isotopic composition can give valuable insights on plant type and hydrology. Although it is not possible to distinguish stable isotopes of elements with low atomic numbers, they differ in physical properties due to their different masses. Consequently, molecules containing different stable isotopes may show different thermodynamic properties. The change of isotopic composition between two substances or two phases is known as fractionation (Bickert, 2006).

Fractionation can take place in processes like evaporation, condensation, diffusion and biogenic reactions. The ratio of different isotope species is expressed in δ-notation. By this, the isotope ratio is always compared to the isotope ratio of a standard according to the following equations (Hoefs, 2009):

$$\delta\ ^{13}C = \left(\frac{(^{13}C/^{12}C)_{sample}}{(^{13}C/^{12}C)_{VPDB}} - 1\right) \times 1000\ (‰)$$

$$\delta\ ^{2}H = \left(\frac{(^{2}H/^{1}H)_{sample}}{(^{2}H/^{1}H)_{VSMOW}} - 1\right) \times 1000\ (‰)$$

with VPDB being the standard for carbon isotopes (Vienne-Pee Dee Belemnite) and VSMOW being the standard for hydrogen isotopes (Vienna Standard Mean Ocean Water).

1.6.1 Carbon isotopes

The $\delta^{13}C$ values of leaf waxes depend on the photosynthetic pathways of the producing plant. During CO_2-fixation, ^{13}C gets depleted independent of the plant type. However, the carbon isotopic composition in plant matter strongly depends on the plant's carbon fixation pathway. While the carbon fractionation from atmospheric CO_2 in C_3 plants is about 18‰ it is only 6‰ in C_4 plants (Figure 1-5; Hoefs, 2009). The reason for this difference is, that the fractionation of PEP-C is lower compared to RuBisCo. The fractionation of CAM plants mainly varies with temperature (O'Leary, 1981).
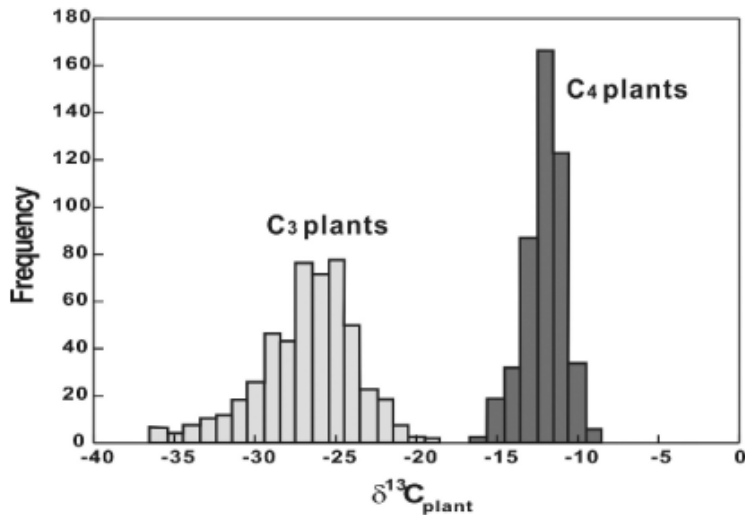
Figure 1-5. Histogram of δ13C-values of C3- and C4- plants (from Hoefs, 2009).

1.6.2 **Hydrogen isotopes**

While carbon isotopes are primarily influenced by the plants carbon fixation pathway, stable hydrogen isotopes in leaf waxes are influenced by multiple parameters. Soil water is the source for hydrogen used during photosynthesis. Whereas no apparent fractionation takes place during the uptake of soil water, deuterium is enriched by evapotranspiration and strongly depleted during biosynthesis (Hoefs, 2018). From these effects a net fractionation can be estimated (Figure 1-6; Feakins and Sessions, 2010; Sachse et al., 2012). Applying the net fractionation and considering evaporation of soil water, the hydrogen isotopic composition of precipitation (δD_p) can be reconstructed from δD determined in leaf waxes.
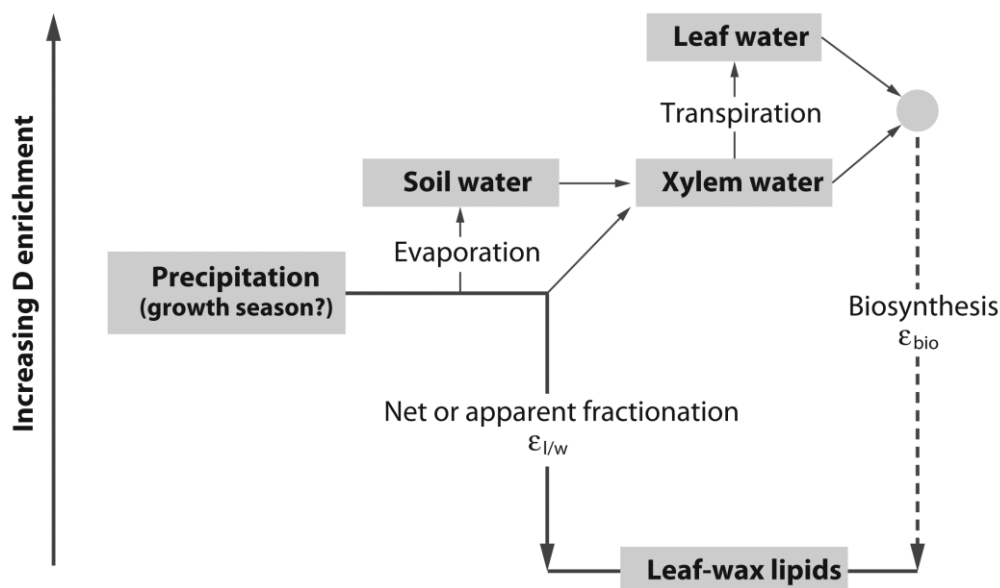
Figure 1-6. Conceptual diagram describing the hydrogen-isotopic relationships between precipitation and leaf-wax n-alkanes from terrestrial plants (from Hoefs (2018), after Sachse et al. (2012)).

δD_p decreases with increasing amount of precipitation (amount effect), higher latitude, higher altitude, increasing distance to coast (Figure 1-7; continental effect) and lower surface temperature (Dansgaard, 1964; Sachse et al., 2012). As a huge amount of deuterium depleted water was incorporated in ice masses during glacials, the isotopic composition of oceans in glacial states are enriched compared to inter-glacial states. Therefore, paleoclimatic reconstructions in the quaternary must also consider global ice volume changes (Schefuß et al., 2005; Collins et al., 2013).

Recognizing these effects, δD values of leaf wax *n*-alkanes can be used for reconstruction of precipitation amounts, altitude reliefs, evaporative conditions or humidity source, if the magnitude of the other effects can be estimated.
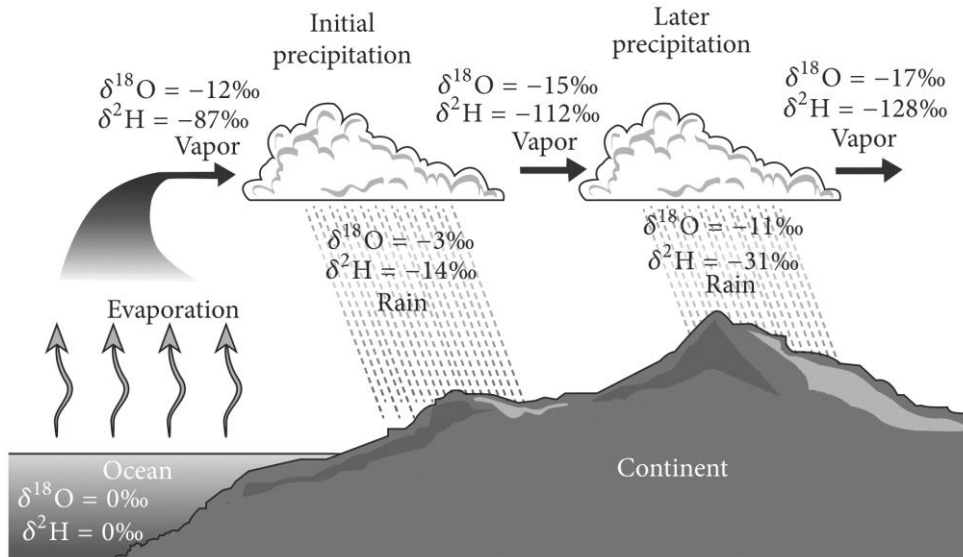
Figure 1-7. Schematic fractionation of oxygen and hydrogen isotopes in precipitation (from SAHRA (2021); based on Hoefs (2018) and Coplen et al. (2000).

1.7 Kalahari pans

Salt pans and pans are the terms used for playas in the Kalahari. Playas are drainless intracontinental closed depressions with a negative water balance, meaning that evaporation exceeds precipitation and fluvial input for more than half a year (Rosen, 1994). Pans are a common feature in the Kalahari Basin with varying sizes. Water in the pan can occur via precipitation, surface runoff, or groundwater inflow (Rosen, 1994; Shaw and Bryant, 2011). This usually happens during rainy season. In this time the pan can be inundated from some days up to a few weeks (Milewski et al., 2017). When the water evaporates, a crust is formed on top of the sediment. In salt pans this crust is formed from crystallized evaporites, mainly halite, gypsum, calcite and sepiolite (Figure 1-8; Milewski et al., 2017; Schüller et al., 2018). Otherwise, it is hardened pan sediment, fine-grained and often featuring dessication cracks. Sediment is transported into the pan either via dust input or surface runoff. For the latter the ratio between catchment area and pan size is probably a controlling factor (Schüller et al., 2018). When the pan is dry, sediment can be transported out of the pan and lead to deflation. Sediment loss can be the result of stable wind regimes or thermal uplifts

via vortices. Studies showed, that pans are an important source for dust emission (Eckardt and Kuring, 2005; Vickery et al., 2013; Nield et al., 2015). Effects which reduce sediment export can be residual moisture and a high level of capillary fringe (Rosen, 1994; Reynolds et al., 2007). Furthermore, the salt or clay crust can protect the sediment unless it is harmed by cracks or animal tracks (Milewski et al., 2017; Milewski et al., 2020). Many Kalahari pans feature lunette dunes on their lee side. The dunes are thought to consist of eroded pan sediment (Lancaster, 1978). Despite this, Telfer and Thomas (2006) showed, that lunette dunes from Witpan (South Africa) primarily consisted of reworked older lunette dunes and from adjacent linear dunes. Some pans are sparsely vegetated (Boocock and van Straten, 1962).
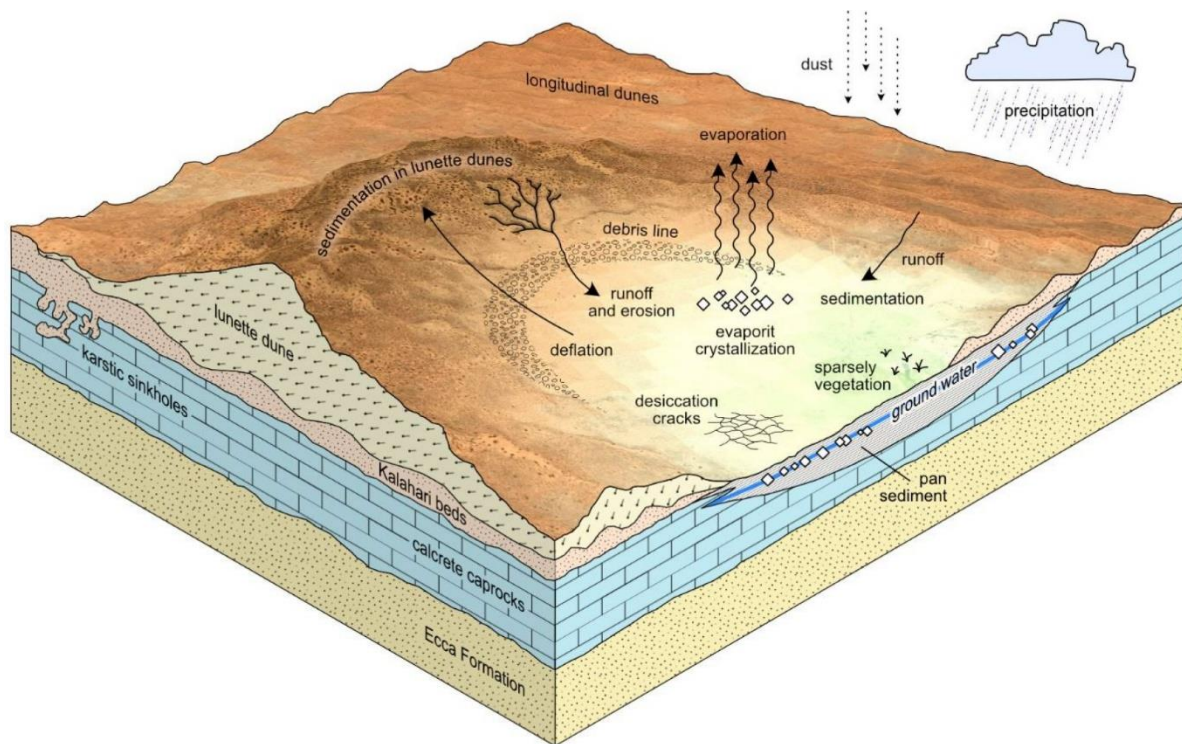
Figure 1-8 Model of a Kalahari pan with principle processes (From Schüller et al., 2022)

Pans can be formed by different processes. Some pans (e.g. in the Aminuis region) were originally part of a drainage system, which repeatedly got blocked by longitudinal Kalahari dunes during active phases. After that, pan formation started due to the low relief in the former river beds (Boocock and van Straten, 1962; Lancaster, 1986). Other pans (e.g. in the Koës region) were formed as karstic

sinkholes in calcretes, which occur at the southwestern rim of the Kalahari and form distinct drainage channels (Schüller et al., 2018, 2022).

The geological setting of the western and southwestern Kalahari, where pans occur, is dominated by sands and calcretes of the Tertiary Kalahari Group (Jones, 1980; Thomas and Shaw, 1990). The next sequence below mainly consist of shales and sandstones of the Permo-Carboniferous Dwyka Formation/Ecca Group, which are part of the Karoo supergroup (Lancaster, 1986; Thomas and Shaw, 1990).

1.8 Objectives of the thesis

The aim of this thesis was to investigate if Kalahari pans are suitable archives for reconstructions of environmental conditions and biocenosis using organic geochemical proxies and their potential to unravel intracontinental climate change since the Late Pleistocene. In detail, the following questions were addressed:

- Are leaf wax biomarkers detectable in pan sediments in magnitudes which allow proxy application and deductions on past conditions (Chapter 2)?
- What challenges unfold, when applying leaf wax proxies and stable isotopes? (Chapter 2 and Chapter 3)
- Are pan archives able to record abrupt climate change (Chapter 2 and Chapter 3)?
- How does the evolution of Late Quaternary environmental conditions, reconstructed from pan archives fit into the picture of present paleoclimate knowledge? (Chapter 2 and Chapter 3)
- Can we use pan archives to detect intraregional variations in environmental conditions and their changes (Chapter 4)?

1.9 Author's contributions

This thesis contains three first author manuscripts which are published in (chapter 2), submitted to (chapter 3) or in preparation (chapter 4) for international peer-reviewed journals. In this section a short summary of each chapter is given with a description of the authors contribution.

Chapter 2

The leaf wax biomarker record of a Namibian salt pan reveals enhanced summer rainfall during the Last Glacial-Interglacial Transition

Lukas Belz, Irka Schüller, Achim Wehrmann, Jürgen Köster, Heinz Wilkes

This paper describes a leaf wax biomarker study of Omongwa Pan in eastern Namibia. Bulk parameters, *n*-alkanes and their carbon and hydrogen isotopic composition, *n*-alkan-1-ols and fatty acids are used as proxies to reconstruct environmental and hydrologic conditions. The results show that pan sediments are well suited for the application of leaf wax biomarkers. The data indicate a wet phase during HS1 and dry conditions during the Holocene which was considered in the context of regional climate development.

Lukas Belz and Heinz Wilkes contributed to the study conception and design. All samples were collected in field campaigns by Lukas Belz together with all co-authors. Material preparation and data collection were performed by Lukas Belz and scientific assistants as well as laboratory assistants were also supervised by him. Results were interpreted by Lukas Belz, Jürgen Köster and Heinz Wilkes. The first draft of the manuscript was written by Lukas Belz and all co-authors commented on previous versions of the manuscript. All authors read and approved the final manuscript.

This chapter was published in *Palaeogeography, Palaeoclimatology, Palaeoecology* 2020, 543, 109561.

Chapter 3

Changes in southern Kalahari rainfall seasonality during the Last Glacial-Interglacial Transition and its impact on vegetation: A leaf wax study from pan sediments

Lukas Belz, Irka Schüller, Jürgen Köster, Andrea Vieth-Hillebrand, Achim Wehrmann, Heinz Wilkes

This chapter presents high-resolution bulk parameters, n-alkanes and the isotopic carbon and hydrogen compositions of sediments from Koës Pan in south-eastern Namibia. Results indicate the switch from winter rainfall to summer rainfall at the end of the last glacial, which impacts the validity of hydrogen isotopes on precipitation amount. The remarkable relative long chain *n*-alkane distribution depicts continuous high-resolved change which is discussed in context with comparable datasets.

Lukas Belz designed the study with suggestions from Jürgen Köster and Heinz Wilkes. All samples were collected in the field by Lukas Belz together with Irka Schüller, Achim Wehrmann, Heinz Wilkes and Jürgen Köster. Laboratory work and data collection were performed by Lukas Belz as well as scientific assistants and laboratory assistants, which were supervised by Lukas Belz. Andrea Vieth-Hillebrand provided the hydrogen isotope data. The first draft of the manuscript was written by Lukas Belz and all co-authors commented on previous versions of the manuscript.

This manuscript was submitted to *Journal of Quaternary Science*.

Chapter 4

Comparison of high-resolution leaf wax records from two Kalahari salt pans

Lukas Belz, Irka Schüller, Jürgen Köster, Achim Wehrmann, Heinz Wilkes

The final manuscript is a comparison of the results of Chapter 3 with new high-resolution n-alkane and carbon isotope data from Omongwa Pan since 17 ka BP with a focus on Late Pleistocene – Early Holocene processes. Results give evidence for similar climate conditions during the Late Pleistocene and a continuous shift to two different environmental states. The individuality and comparability of pan archives is discussed.

The study was conceived and designed by Lukas Belz. Heinz Wilkes contributed to the study conception. High resolution samples were collected in a field campaign by Lukas Belz together with Irka Schüller, Achim Wehrmann and Jürgen Köster. Material preparation and data collection were performed by Lukas Belz together with scientific assistants and laboratory assistants under his supervision. Results were interpreted by Lukas Belz. The manuscript was written by Lukas Belz and commented by Jürgen Köster.

This chapter provides preliminary alkane and carbon isotope results with need for additional experiments and data.

2. The leaf wax biomarker record of a Namibian salt pan reveals enhanced summer rainfall during the Last Glacial-Interglacial Transition

Lukas Belz[1,2], Irka Schüller[3], Achim Wehrmann[3], Jürgen Köster[1], Heinz Wilkes[1,2]

[1]Institute for Chemistry and Biology of the Marine Environment (ICBM), Carl von Ossietzky University, Oldenburg, 26111, Germany

[2]Helmholtz Centre Potsdam GFZ German Research Centre for Geosciences, Telegrafenberg, Potsdam, 14473, Germany

[3]Senckenberg am Meer, Marine Research Department, Wilhelmshaven, 26382, Germany

The leaf wax biomarker record of a Namibian salt pan reveals enhanced summer rainfall during the Last Glacial-Interglacial Transition

Abstract

Conventional continental geoarchives are rarely available in arid southern Africa. Therefore, paleoclimate data in this area are still patchy and late Quaternary climate development is only poorly understood. In the western Kalahari, salt pans (playas, ephemeral lakes) are common and can feature quasi-continuous sedimentation. This study presents the first climate-related biomarker record using sediments from the Omongwa Pan, a Kalahari salt pan located in eastern Namibia. Our approach to reconstruct vegetation and hydrology focuses on biogeochemical bulk parameters and plant wax-derived lipid biomarkers (n-alkanes, n-alkanols and fatty acids) and their compound-specific carbon and hydrogen isotopic compositions. The presented record reaches back to 27 ka BP. During the glacial, rather low δD values of n-alkanes and low sediment input exclude a strong influence of winter rainfall. n-Alkane and n-alkanol distributions and δ^{13}C values of n-hentriacontane (n-C$_{31}$) indicate a shift to a vegetation with a higher proportion of C$_4$ plants at the end of the Last Glacial Maximum until the end of Heinrich Stadial I (ca. 18-14.8 ka BP), which we interpret to indicate an abrupt excursion to a short wetter period likely to be caused by a temporary southward shift of the Intertropical Convergence Zone. Shifts in δD values of n-C$_{31}$ and plant wax parameters give evidence for changes to drier conditions during early Holocene. Comparison of this dataset with representative continental records from the region points to a major influence of summer rainfall at Omongwa Pan during the regarded time span and demonstrates the potential of southern African salt pans as archives for biomarker-based climate proxies.

2.1 Introduction

The climate dynamics in southern Africa following the Last Glacial Maximum (LGM, 21± 2 ka BP; Mix et al., 2001) are complex, due to its key position between the tropics and the temperate zone (Tyson et al., 1996; Chase et al., 2017). At this boundary the mixing of influences of the southern westerlies, the Intertropical

Convergence Zone (ITCZ) and adjacent convergent zones like the Congo Air Boundary (CAB) lead to a high variability of precipitation patterns over longer time scales (e.g. Cockcroft et al., 1987; Gasse et al., 2008; Burrough and Thomas, 2013; Chevalier and Chase, 2015). The southwestern edge of the summer rainfall zone (SRZ) is located in the west of continental southern Africa (Figure 2-1; Cockcroft et al., 1987; Nicholson, 2000; Chase and Meadows, 2007). Therefore, paleoenvironmental research in this area is important for a better understanding of the dynamics of summer rainfall in southwestern Africa.

A number of studies argue that during northern hemisphere cooling events affecting the Atlantic meridional overturning circulation like Heinrich Stadial 1 (HS1, ca. 18.0 – 15.5 ka BP; Labeyrie et al., 2003) and the Younger Dryas (YD, ca. 12.6 – 11.5 ka BP; Björck et al., 1998) the ITCZ was forced southward leading to increased precipitation in eastern southern Africa (Lancaster, 1979; van Zinderen Bakker, 1983; Dahl et al., 2005; Lewis et al., 2010; Schefuß et al., 2011). There is also evidence that large areas of East Africa and eastern South Africa were unaffected by this shift and were dry (Stager et al., 2011; Chevalier and Chase, 2015; Scott, 2016). Wet conditions during HS1 at Lake Ngami and signs of mega-lake condition in the Makgadikgadi basin (both Botswana) indicate the extent of the wet conditions in central southern Africa (Burrough et al., 2009; Cordova et al., 2017). Therefore, the question arises if the ITCZ shift affected also the western edge of summer rainfall and how environmental factors changed.

Existing terrestrial data records in southern Africa focus on lake deposits (e.g. Kristen et al., 2007; Kristen et al., 2010; Schmidt et al., 2014; Scott, 2016; Cordova et al., 2017) and reconstruction of lake shorelines (Thomas et al., 2003; Burrough et al., 2007; Burrough and Thomas, 2013), but the distribution of these archives in southwest Africa is scattered and patchy. Other reconstructions of climate conditions are based on hyrax middens (Chase et al., 2012 and refs therein), dunes (Chase, 2009; Hürkamp et al., 2011), fluvial deposits (Hürkamp et al., 2011; Ramisch et al., 2017) speleothems (Brook et al., 1996; Railsback et al., 2016), or aquifers (Stute and Talma, 1998). Most of these records only cover certain time spans or are discontinuous. A comparison of these different methods can lead to contradictory implications (Gasse et al., 2008; Burrough and Thomas, 2013).

Continental salt pans (playas) occur widespread in the western Kalahari (Lancaster, 1986). Recent studies of sediment proxies and microbial biomarkers in Kalahari pans in southern Africa show that such systems are suitable archives for the reconstruction of environmental conditions (Genderjahn et al., 2017; Genderjahn et al., 2018b; Schüller et al., 2018). Here we demonstrate that plant wax constituents (biomarkers) are well preserved in pan sediments, which opens the opportunity to use proxies based on these compounds for paleoenvironmental studies as well. Among these recently studied pans the Omongwa Pan, which is located in the present SRZ, is well suited to study summer rainfall dynamics, in particular due to its relatively high sedimentation rates (Schüller et al., 2018).

Long-chain n-alkanes, n-alkanols and n-fatty acids are constituents of cuticular plant waxes (Eglinton and Hamilton, 1967). The carbon number distribution of their homologues depends on vegetation type and/or environmental conditions (Rommerskirchen et al., 2006b; Vogts et al., 2009; Bush and McInerney, 2015; Herrmann et al., 2016). Most of higher plants can be divided into two different groups regarding their carbon assimilation pathways during photosynthesis, i.e. the Calvin-Benson cycle (C_3) and the Hatch-Slack cycle (C_4). The two pathways exhibit distinctive carbon isotope fractionation patterns during carbon assimilation (O'Leary, 1981). In southwest Africa grasses are mostly C_4 plants, while trees, shrubs and herbs are C_3 plants (Vogel et al., 1978; Ellis et al., 1980; Mucina and Rutherford, 2006; Vogts et al., 2009). On this basis, plant wax-derived compounds in sediments can be used to reconstruct the past vegetation assemblage. Furthermore, the isotopic composition of hydrogen in plant wax constituents allows an assessment of variations in hydrologic conditions such as the amount of precipitation, origin of water masses, and evaporative conditions (Sachse et al., 2012; Collins et al., 2013; Burdanowitz et al., 2018).

In this study we present the first paleoclimatic biomarker dataset from a Kalahari salt pan. We determined n-alkane, n-alkanol, and fatty acid compositions as well as compound-specific carbon and hydrogen isotope values of n-alkanes for sediments from the Omongwa Pan in the western Kalahari (Namibia). Additionally, we present the content of total organic carbon (TOC), its isotopic composition ($\delta^{13}C_O$), the content of total inorganic carbon (TIC), and isotopic

composition of carbon and oxygen in carbonates ($\delta^{13}C_C$, $\delta^{18}O_C$). We apply these data
to reconstruct past vegetation and ecology as well as hydrological changes, with a
focus on possible short-term changes during the Last Glacial-Interglacial
Transition. The record reaches back to 27 ka BP and provides insights into regional
changes as a response to global climate change. These interpretations are
compared to those derived from existing records for the southern African region in
order to investigate regional climatic interactions.
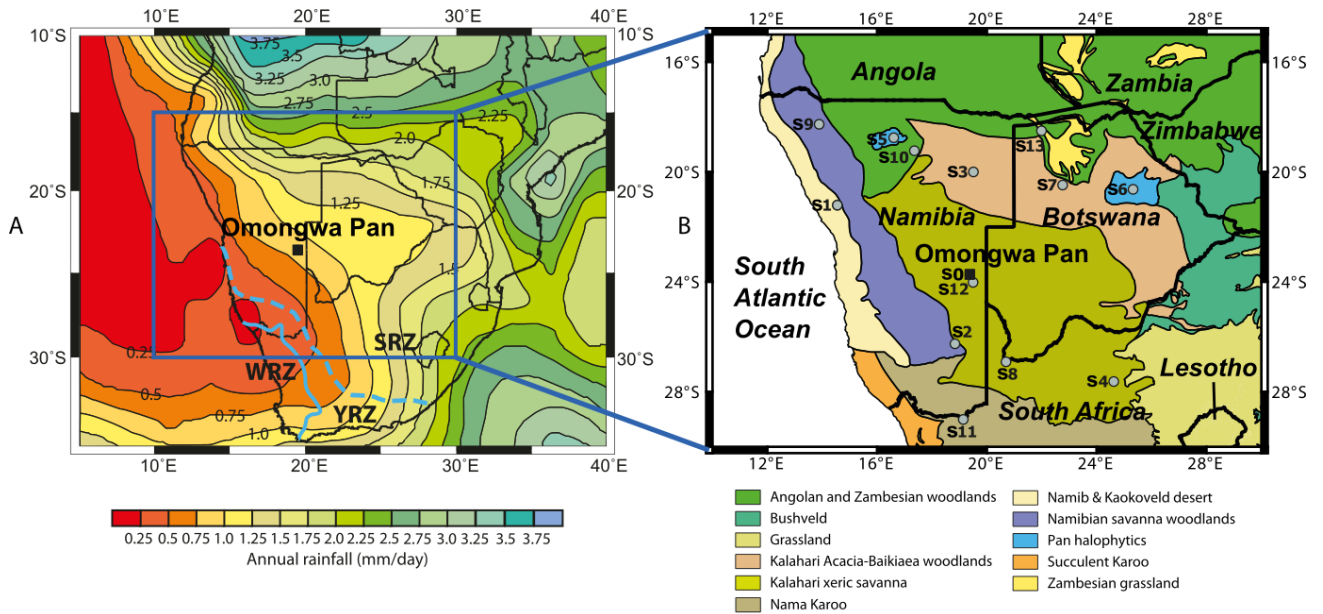
Figure 2-1 A. Map of southern Africa displaying modern annual rainfall distribution in mm/day.
CMAP Precipitation data provided by the NOAA/OAR/ESRL PSD, Boulder, Colorado, USA, from
their Web site at https://www.esrl.noaa.gov/psd/ (Xie and Arkin, 1997). The continuous blue line
indicates the boundary between winter (WRZ) and year round rainfall (YRZ) zones, the dashed blue
line marks the boundary between the YRZ and summer rainfall zone (SRZ) (data source: Chase and
Meadows, 2007). This map was created using Generic Mapping Tools (GMT; Wessel et al., 2013).
B. Map of southern African ecoregions (dataset simplified after Olson et al., 2001); with location of
Omongwa Pan (black square) and locations of other geoarchives discussed in the text (grey dots,
see Table 2-1 for site description).

2.2 Regional setting and site description

The occurrence of precipitation in southwestern Africa is strongly seasonal with
either winter or summer rainfall. During austral summer the ITCZ and the
connected CAB is shifted southward. This low-pressure trough attracts air masses

over the South Atlantic from the northwest, as part of the West African Monsoon (WAM), and air over the Indian Ocean from the east, thus transporting moisture up to the eastern boundary of the Namib Desert and causing summer rainfall (Nicholson, 2000). Precipitation is higher on the southern African east coast with a westward reduction (Tyson et al., 1996; Gasse et al., 2008). During the austral winter, the climate of central southern Africa is mainly dominated by semi-permanent subtropical anticyclones located between the austral Hadley and Ferrel cells, which generate stable and dry conditions (Tyson et al., 1996; Nicholson, 2000).

Table 2-1. Sites discussed in the text. The locations are shown in Figure 2-1.

Site		References	Latitude (°S)	Longitude (°E)
S1	Brandberg	Scott et al. (2004)	21.19	14.54
S2	Branddam East Pan	Schüller et al. (2018)	26.24	18.84
S3	Drotsky's Cave	Brook et al. (1996); Brook et al. (1998)	20.00	19.50
S4	Wonderwerk Cave	Chevalier and Chase (2015)	27.85	23.56
S5	Etosha Pan	Brook et al. (2013)	18.72	16.65
S6	Makgadikgadi basin	Shaw and Thomas (1996); Burrough et al. (2009)	20.62	25.36
S7	Lake Ngami	Burrough et al. (2007); Cordova et al. (2017)	20.48	22.76
S8	Molopo River	Hürkamp et al. (2011)	26.91	20.69
S9	Orumana Cave	Railsback et al. (2016)	18.26	13.89
S10	Otavi Mountain	Brook et al. (1999)	19.23	17.35
S11	Pella	Lim et al. (2016)	29.00	19.14
S12	Stampriet aquifer	Stute and Talma (1998)	24.00	19.50
S13	Tsodilo Hills	Thomas et al. (2003)	18.50	22.00

The Omongwa Pan studied here is located in the western Kalahari in the Aminuis Region. The size of the pan is 22 km², its catchment, based on local geomorphology, extends over 172 km² (Figure 2-2). The surrounding area is extensively utilized as rangeland. Modern local precipitation is about 250 mm/y, 90% thereof is falling during austral summer (Mees, 1999). Pan sediments primarily consist of quartz, feldspar, and to a minor degree illite and smectite. Furthermore, they contain evaporate minerals, mainly gypsum, halite, sepiolite and dolomite (Schüller et al., 2018). Sediment grain size is predominantly medium and coarse silt. In the analysed profile of Omongwa Pan, the finest grain composition occurs in a clayey layer at a depth of about 80 cm. The coarsest sediments at around 105 cm depth

contain fine and medium sand. During dry phases the pan is covered with a crust of salt minerals, mainly halite and gypsum crystals. A detailed sedimentological description can be found in Schüller et al. (2018).
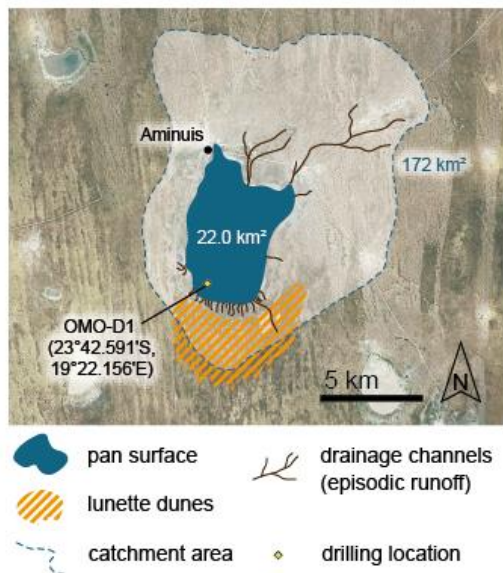
Figure 2-2 Omongwa Pan with spatial extension and size of the catchment area (modified after Schüller et al., 2018).

Only during rainy season water accumulates in the pan for short periods, which is accompanied by local run-off and sediment transfer from the catchment into the pan (several days to weeks). During flooding the salt crust on the surface is dissolved and it forms again when the water evaporates. Under dry conditions the crust hardens and seals the pan against dust emissions (Milewski et al., 2017). Nevertheless, deflation is an important sedimentological process of pans. Lunette dunes, a typical feature of salt pans, are located at the southern rim of Omongwa Pan (Figure 2-2). These dunes are usually considered as a result of pan deflation (Lancaster, 1978). Telfer and Thomas (2006) though showed that lunette dunes of Witpan, South Africa, mostly consist of reworked sediment of older lunette dunes. Recently, Schüller et al. (2018) have shown that the net sedimentation in Kalahari salt pans can be regarded as quasi-continuous, based on a dataset of 57 ^{14}C ages from five Kalahari pans.

The main limiting factor for vegetation in southern Africa is water availability. Important other factors are altitude, potential evaporation and minimum

temperature (Rutherford et al., 2006). The western Kalahari is a mix of the Xeric Savanna and Nama Karoo biomes (Figure 2-1B). Omongwa Pan is located in the Camelthorn Savanna close to the boundary with Mixed Tree and Shrub Savanna (Joubert et al., 2008). Important shrub and tree species in these ecoregions are *Senegallia mellifera, Vachellia erioloba,* graminoids including *Schmidtia pappophoroides, Stipagrostis uniplumis* and *Eragrostis rigidio* (Bester et al., 2003; Mucina and Rutherford, 2006). Both of these ecoregions are part of the Xeric Savanna Biome which ranges from eastern Namibia and southern Botswana to central South Africa (Figure 2-1B; Rutherford et al., 2006). Vegetation assemblages within the Namibian Xeric Savanna show a dynamic variability. Grass cover and shrub density vary and are influenced by factors like fire, frost, phases of distinctly lower or higher precipitation and shrub encroachment, which is often related to ranching but can also occur under natural conditions (Joubert et al., 2008).

2.3 Methods

2.3.1 Sampling and sample preparation

Samples were taken during dry season (October 2013 and September 2016) in the southwestern part of Omongwa Pan (23°42.6'S, 19°22.2'E). Samples of the upper 60 cm were taken from a profile pit. For elemental analyses pit samples were taken with 1 cm resolution; for extraction 5 cm intervals were sampled. Deeper samples were retrieved using an Edelman hand auger from Eijkelkamp. At 236 cm depth the base of the sedimentary infill was reached. In total, 17 cm were lost during sample recovery. Three parallel drillings were made at a distance of approximately 20 cm for sedimentological, microbiological, and biogeochemical analyses. Precision of drilling depth was checked by comparison of the depth of colour-distinguishable layers, showing an accuracy of ±1 cm. The ground water table was measured at a depth of 103 cm after drilling. All samples were wrapped in aluminium foil and then put in plastic bags on location and afterwards stored in glass vials at 4°C.

2.3.2 Age-depth model

For the sampled profile a calibrated age-depth model based on 14 calibrated ^{14}C ages was created using the Bacon 2.2 software package for R (Blaauw and Christen, 2011) and has been published by Schüller et al. (2018; Figure 2-3A). The whole core features a positive net sediment accumulation with an average sedimentation rate of 6.4±3.5 cm/ka. Low values (below 3 cm/ka) occur between 24.0 and 19.3 ka BP, in a period from 14.4 to 5.2 ka BP, and from 3.0 to 1.3 ka BP. High values (above 8 cm/ka) are displayed from 17.8 to 16.3 cm/ka and from 0.5 to 0.4 cm/ka (Figure 2-3B; Schüller et al., 2018). During the phases of low net accumulation, the core resolution can be impaired especially during the LGM and the early Holocene and proxies might be more affected by air-transported allochthonous material. However, no signs for a net deflation or a hiatus could be found in the sedimentological record (Schüller et al., 2018). Samples for biogeochemical analyses included in this study were examined to a depth of 110 cm and date back until 27.2 ka BP (Figure 2-3; Table 2-1).
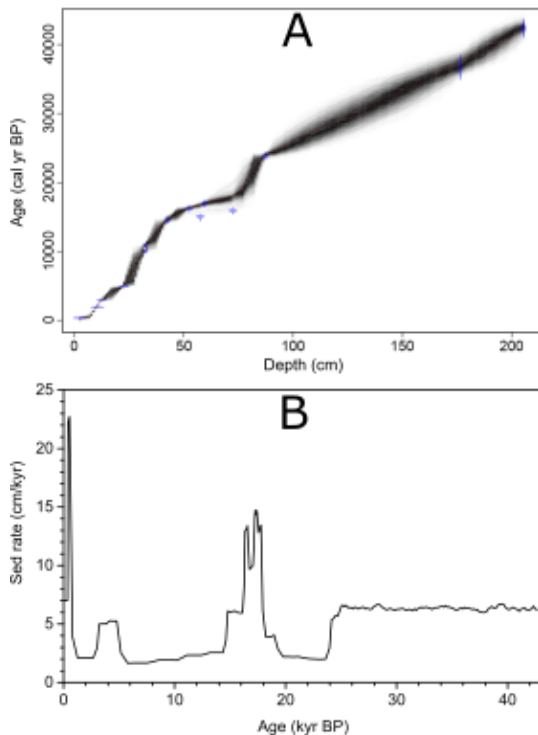
Figure 2-3 A. Age-depth model and B. sedimentation rate for the Omongwa Pan sediments (modifed after Schüller et al., 2018).

Table 2-2. Radiocarbon ages of the Omongwa Pan (Schüller et al., 2018).

Sample Depth (cm)	Age (cal ka BP)	95.4 % range (2sigma)
2-3	0.4	0.1
9-12	1.9	0.1
12-13	3.0	0.1
22-23	4.9	0.1
32-33	10.0	0.2
30-35	10.9	0.2
42-43	14.5	0.4
52-53	16.2	0.2
55-60	15.0	0.3
59-60	16.9	0.3
70-75	15.8	0.3
85-89	23.8	0.3
173-180	35.6	0.2
203-208	42.4	0.8

2.3.3 Elemental analysis and bulk stable isotopes

All sediment samples were freeze-dried and ground before analysis. Total carbon (TC) and total nitrogen (TN) contents were determined using a Euro EA3000 elemental analyser from EuroVector. Samples for TN and TC analyses were wrapped in tin capsules. For total organic carbon (TOC) measurements samples were decalcified in silver capsules by adding HCl (20 %) at 75°C. TIC was calculated as the difference of TC and TOC contents. Randomly selected 15 % of all samples were measured twice to confirm that the standard deviation was below 1 %.

For isotope analyses of bulk organic carbon ($\delta^{13}C_O$) samples were decalcified with HCl (7 %) at 80°C and weighed into tin capsules. Samples were measured using an elemental analyser (1108 from Carlo Erba) coupled to a MAT 252 isotope ratio mass spectrometer from Thermo Fisher Scientific. The calibration was performed using a certified isotope standard (IAEA CH-6 with a $\delta^{13}C$ value of −10.45 ‰). Instrument performance was checked using a sediment reference sample with a $\delta^{13}C_O$ value of −26.07 ‰ (IVA). The standard deviation for replicate analyses was ±0.5 ‰.

The stable isotope compositions of bulk carbonate ($\delta^{13}C_C$ and $\delta^{18}O_C$) were determined in continuous flow mode using a Finningan GasBench II with carbonate option, coupled to a DELTAplusXL mass spectrometer. From each sample, about ~300 µg were loaded into 10 ml Labco Exetainer vials. After flushing with He, phosphoric acid (100 %) was added to the samples and allowed to react for 60 min at 75°C, followed by the analytical procedure described by Spötl and Vennemann (2003). The carbon and oxygen isotope compositions are given relative to Vienna Peedee Belemnite (VPDB) standard. All isotope data are reported in the conventional delta notation. For calibration two international reference standards were used (NBS 19 with a $\delta^{13}C$ value of +2.0 ‰ and a $\delta^{18}O$ value of −2.2 ‰, and NBS 18 with a $\delta^{13}C$ value of −5 ‰ and a $\delta^{18}O$ value of −23.2 ‰) and proved with one internal standard (C1 with $\delta^{13}C$ +2.4 ‰, $\delta^{18}O$ −1.3 ‰). The standard deviation (1 sigma) for reference analyses was 0.1 ‰ for $\delta^{13}C_C$ and $\delta^{18}O_C$.

2.3.4 Lipid extraction and liquid chromatography

Lipids were extracted using an accelerated solvent extractor 200 from Dionex with a solvent mixture of dichloromethane and methanol (99/1) at 75°C and 50 bar for 20 min. The *n*-hexane-insoluble fraction was removed from the extract. The *n*-hexane-soluble fraction was separated by medium pressure liquid chromatography (MPLC) into aliphatic hydrocarbons, aromatic hydrocarbons and a fraction containing nitrogen, sulphur and oxygen (NSO) compounds (Radke et al., 1980). The NSO compound fraction was separated into carboxylic acids and neutral NSO compounds by means of column chromatography using potassium hydroxide-impregnated silica gel. 5α-Androstane, 5α-androstan-17-one, 5α-androstan-17β-ol, and erucic acid were added prior to MPLC as internal standards for quantification. *n*-Alcohols were derivatized to trimethylsilyl ethers using *N*-methyl-*N*-trimethylsilyl-trifluoroacetamide. Fatty acids were methylated using 14 % boron trifluoride in methanol, while heating at 70°C for 2 h.

2.3.5 Gas chromatography

Samples were analysed using a 6890 gas chromatograph (GC) from Agilent equipped with a Ultra 1 methyl siloxane fused silica capillary column (50 m × 200 μm, 0.33 μm film thickness), a cold injection system, and a flame ionization detector (FID). The carrier gas was helium at a flow rate of 1 ml/min. The initial temperature of the GC oven was 40°C held for 2 min, then heated at a rate of 5°C/min to 300°C and held for 65 min. The injector temperature was initially set to 40°C, increased to 300°C at a rate of 700°C/min and held at that temperature for 3 min. Identification of n-alkanes was achieved by comparison of retention times to those of reference standards. For quantification the FID signal was used. Plotted n-alkane concentrations of all samples were categorized visually with no regard to sample depth. Two distinct distribution patterns were recognized and the distinction confirmed by diverging geochemical parameters (see results, section 4.2). All samples were then attributed to the distribution patterns cluster I or cluster II.

2.3.6 Gas chromatography-mass spectrometry

Fatty acids and n-alkanols were identified and quantified using a gas chromatograph coupled to a mass spectrometer (GC-MS). Additionally, the n-alkane fractions of two samples were measured to check for possible co-eluents. Analyses were carried out using a Trace GC Ultra from Thermo Fisher Scientific equipped with a BPX5 fused silica capillary column (50 m x 220 μm, 0.25 μm film thickness) coupled to a DSQ mass spectrometer from Thermo Fisher Scientific. Carrier gas was helium at a constant flow rate of 1 ml/min. The initial temperature of the GC was 50°C held for 1 min, then heated at a rate of 3°C/min to 310°C and held for 30 min. The injector worked in splitless mode with an initial temperature of 50°C, heated to a maximum temperature of 300°C at a rate of 6°C/min and held for 10 min. Due to the presence of several co-eluents in the non-hydrocarbon fractions, which belong to homologous series of ketones and secondary alcohols, in most of the samples quantification by peak area in FID and total ion

chromatograms was not possible. Therefore, the peak areas of the $[M - 15]^+$ ion and the sum of the $[74]^+$ and $[87]^+$ ions were integrated to quantify n-alkanols and saturated n-fatty acids, respectively. The relative intensities of these ions in the mass spectra were determined for each homologue and used as a response factor when quantifying the individual wax constituents.

2.3.7 Gas chromatography-isotope ratio mass spectrometry

Compound-specific isotopic compositions were measured using a gas chromatograph 7890 from Agilent equipped with an Ultra 1 methyl siloxane fused silica column (50 m x 200 μm, 0.33 μm film thickness) coupled to a Delta V plus isotope ratio mass spectrometer from ThermoFisher Scientific. The temperature program of the GC oven was raised from 40°C (held for 2 min) to 300°C at a rate of 4°C/min. This temperature was held for 45 min. The injector was operated in split mode with a split ratio of 1:2 and 1:3 for the determination of carbon and hydrogen isotopes, respectively. Injection temperature was 280°C. Helium was used as the carrier gas at a flow rate of 1ml/min. All samples were measured in triplicate. Standard deviation was below 0.5 ‰ for carbon and below 5 ‰ for hydrogen for all samples. All results are given in delta notation in per mil vs. VPDB for carbon and Vienna Standard Mean Ocean Water (VSMOW) for hydrogen. As external standard for carbon isotope analysis a mixture containing n-alkanes with certified $\delta^{13}C$ values was used (Schimmelmann, USA; n-C_{15}, −30.2‰; n-C_{20}, −33.1‰; n-C_{25}, −28.2‰). As external standard for hydrogen isotope analysis a mixture containing n-alkanes with certified δD values was used (Schimmelmann, USA; n-C_{17}, −142.4‰; n-C_{19}, −118.0‰; n-C_{21}, −214.7‰; n-C_{23}, −48.8‰; n-C_{25}, −254.1‰).

For comparison of glacial and interglacial samples, δD values were corrected for the ice-volume effect. Enrichment of D was determined via $\delta^{18}O$ values using the global meteoric water line (Craig, 1961). Paleo-$\delta^{18}O$ values of seawater were estimated using the LR04 global benthic isotope stack (Lisiecki and Raymo, 2005).

2.4 Results

2.4.1 Bulk parameters

TOC contents vary between 0.2 and 1.4 % (Table 2-3). Elevated TOC concentrations (> 0.9 %) are found in samples from 1.2 to 1.9 ka BP and from 15.4 to 19.4 ka BP, except for one sample from 17.1 ka BP (Table 2-3). Concentrations below 0.5 % were observed in the surface sediment sample, at ages between 4.1 and 7.0 ka BP, from 10.0 to 10.9 ka BP and in samples older than 21.6 ka BP. TIC concentrations display a large variation between 0.2 % and 4.9 %, with low values (< 2 %) in samples younger than 15 ka BP and older than 23.6 ka BP (Figure 2-8C). The highest values (>4 %) occur in samples with ages between 16.1 ka BP and 19.4 ka BP. Isotope values of carbonate carbon ($\delta^{13}C_C$) and oxygen ($\delta^{18}O_C$) could be measured for samples with TIC concentrations above ca. 1.3 % only. Both parameters are significantly related (r^2 = 0.97). They show minimum values at 0.9 ka BP (−10.3 ‰ for $\delta^{13}C_C$ and −5.6 ‰ for $\delta^{18}O_C$) and high values above 0 ‰ at a time span ranging from 15.5 to 19.4 ka BP ($\delta^{13}C_C$) and from 15.5 to 21.6 ka BP ($\delta^{18}O_C$), respectively. Bulk organic carbon isotope values vary from $\delta^{13}C_O$ −19.4 to −16.1 ‰. Relatively low $\delta^{13}C_O$ values were found from 16.2 to 16.6 ka BP and from 17.1 to 18.1 ka BP; maximal values occur at 21.6 ka BP and 23.6 ka BP. Total nitrogen concentrations were measured but were below the threshold of 0.1 % required for reliable values.

The leaf wax biomarker record of a Namibian salt pan reveals enhanced summer rainfall during the Last Glacial-Interglacial Transition

Table 2-3. Data for organic and inorganic carbon and organic carbon isotope composition.

av. (cm)	Age (ka)	TOC (%)	$\delta^{13}C_O$ (‰)	TIC (%)
0.5	0.1	0.4	-17.3	0.3
1.5	0.2	0.6	-17.0	0.5
2.5	0.4	0.5	-17.8	0.4
3.5	0.7	0.7	-17.1	0.6
4.5	0.9	0.9	-17.0	0.8
5.5	1.2	1.0	-16.9	0.8
6.5	1.4	1.1	-17.0	0.8
7.5	1.7	1.0	-16.9	0.8
8.5	1.9	1.0	-17.1	0.7
9.5	2.2	0.9	-17.2	0.7
10.5	2.5	0.9	-17.2	0.7
11.5	2.7	0.8	-17.1	0.5
12.5	3.0	0.7	-17.4	0.4
13.5	3.2	0.7	-17.3	0.3
14.5	3.4	0.7	-17.2	0.2
15.5	3.6	0.8	-16.8	0.2
16.5	3.7	0.7	-16.1	0.2
17.5	3.9	0.5	-16.3	0.2
18.5	4.1	0.4	-17.7	0.2
19.5	4.3	0.4	-17.0	0.2
20.5	4.5	0.4	-16.9	0.2
21.5	4.7	0.4	-17.1	0.2
22.5	4.9	0.4	-16.7	0.2
23.5	5.4	0.4	-16.8	0.2
24.5	5.9	0.4	-17.0	0.2
25.5	6.4	0.4	-16.8	0.2
26.5	7.0	0.3	-17.0	0.4
27.5	7.5	0.5	-17.2	0.7
28.5	8.0	0.6	-17.3	1.1
29.5	8.5	0.5	-17.3	1.1
30.5	9.0	0.5	-17.2	1.0
31.5	9.5	0.5	-17.2	0.9
32.5	10.0	0.4	-17.5	0.9
33.5	10.5	0.4	-17.3	0.9
34.5	10.9	0.4	-17.0	0.8
35.5	11.4	0.5	-17.3	0.8
36.5	11.8	0.5	-17.2	1.0
37.5	12.3	0.5	-16.9	1.2
38.5	12.7	0.5	-16.7	1.2
39.5	13.2	0.5	-16.8	1.4
40.5	13.6	0.5	-16.9	1.4
41.5	14.1	0.5	-16.9	1.3
42.5	14.5	0.5	-16.8	1.4
43.5	14.7	0.5	-16.7	1.6
44.5	14.9	0.7	-16.7	1.8

Table 2-3 continued.

av. (cm)	Age (ka)	TOC (%)	$\delta^{13}C_O$ (‰)	TIC (%)
45.5	15.0	0.8	-16.6	2.2
46.5	15.2	0.9	-16.5	2.8
47.5	15.4	1.0	-16.3	3.2
48.5	15.5	1.1	-16.5	3.7
49.5	15.7	1.2	-16.8	3.9
50.5	15.9	1.0	-17.4	4.0
51.5	16.0	1.4	N/A	4.4
52.5	16.2	1.2	-18.7	4.2
53.5	16.3	1.2	-18.2	4.6
54.5	16.4	1.3	-19.1	4.5
55.5	16.5	1.3	-19.4	4.2
56.5	16.6	1.2	-18.3	4.4
57.5	16.7	1.2	-17.1	4.9
58.5	16.8	1.1	-17.3	4.8
59.5	16.9	1.2	-17.6	4.7
62.5	17.1	0.6	−18.0	4.0
69	17.6	1.3	−18.3	4.7
72.5	18.1	1.2	−18.0	4.4
77.5	19.4	1.2	−17.6	4.8
82.5	21.6	0.5	−16.0	2.5
87	23.6	0.2	−15.8	2.6
92	24.7	0.4	−16.6	1.5
97.5	25.6	0.2	−16.9	1.3
102.5	26.4	0.2	−16.8	1.0
107.5	27.2	0.3	−16.1	0.6

2.4.2 Distributions of *n*-alkanes, *n*-alkanols and *n*-alkanoic acids and lipid inventory

All samples contain *n*-alkanes with chain lengths from C_{17} to C_{35}, with an average total concentration of 1578±941 µg/g TOC. In general, the distributions show a significant odd-over-even predominance (OEP) with an average value of the carbon preference index (CPI_{27-33}) of 3.15, calculated according to Cooper and Bray (1963). For comparison of chain length distributions the average chain length (ACL_{27-35}) was calculated analogous to Meyers (2003). Long-chain *n*-alkanes (C_{27}-C_{33}) dominate in all samples. In this range *n*-C_{31} is always the most abundant homologue, with a maximum concentration of 639 µg/g TOC at an age of 8.4 ka BP.

ACL_{27-33} ranges from 29.6 to 30.7 (Table 2-4). Pristane and phytane were detected in trace amounts only.

The average n-alkan-1-ol concentration is higher compared to n-alkanes (2280±1955 µg/g TOC). n-Alkanol chain lengths range from C_{16} to C_{34} (Table 2-4). In general, the distributions show a distinct even-over-odd predominance (EOP; Figure 2-4B) with an ACL_{24-34} between 27.6 and 29.1. Besides long-chain n-alkan-1-ols, the neutral fractions of all samples include a wide variety of homologues series. These are mainly, but not limited to, alkan-2-ols, alkan-3-ols, and alkan-2-ones. Of these series, the latter one is most abundant with a total average concentration of 1581±798 µg/g TOC. Sterols were below detection limit. The total average concentration of n-alkanoic acids is 861±517 µg/g TOC. Chain lengths range from 14 to 32 carbon atoms, with an ACL_{16-32} of 21.9. In half of the samples, low concentrations or co-elutions with other compounds impeded the quantification of fatty acids.

All samples can be divided into two clusters with similar n-alkane, n-alkan-1-ol, and n-alkanoic acid distributions within each cluster (Figure 2-4), namely one cluster containing all samples younger than 15.5 ka BP and older than 19.4 ka BP (hereafter referred to as cluster I) and the other cluster comprising all samples within the time span from 15.5 to 19.4 ka (hereafter referred to as cluster II). Average n-alkane concentrations in cluster I are higher (1873±906 µ/g TOC) and OEP is less pronounced in comparison to cluster II. All samples in cluster I show a bimodal distribution with relatively high amounts of C_{17}-C_{24} n-alkane homologues. Among these mid-chain alkanes n-C_{21} is always the most prominent one. The relative abundances of odd long-chain n-alkanes decrease from n-C_{31} over n-C_{29}, n-C_{27}, n-C_{33} to n-C_{35}. In cluster II, n-alkane mean concentrations are lower (694±203 µg/g TOC) and only long-chain n-alkanes dominate, thus the bimodal distribution is absent. n-C_{31} is the most abundant homologue but, in contrast to cluster I, the relative abundance of n-C_{33} is higher than that of n-C_{29}. The average CPI_{26-34} and ACL_{27-33} are higher in samples of cluster II (6.62±0.5; 30.63±0.10) compared to those of cluster I (5.06±0.32; 29.85±0.14).

The leaf wax biomarker record of a Namibian salt pan reveals enhanced summer rainfall during the Last Glacial-Interglacial Transition

Table 2-4. Concentrations of n-alkanes, n-alkan-1-ols and n-alkanoic acids, ACL, CPI, $\delta^{13}C_{31}$, δD_{31} and ice volume corrected $\delta D_{31}IC$.

av. (cm)	Age (ka BP)	Σ-n- µg/g$_{TOC}$	Σ-n-Alkan-1- µg/g$_{TOC}$	Σ-n-Alkanoic µg/g$_{TOC}$	ACL (27-33)	ACL-OH (24-34)	ACL-COOH (16-32)	CPI (27-33)	CPI (19-23)	$\delta^{13}C_{31}$ (‰)	δD_{31} (‰)	δD_{31IC} (‰)
0.3	0.0	838	243	1534	29.9	28.8	20.4	5.1	1.5	−26.0	N/A	N/A
1.8	0.3	1330	924	843	29.9	28.7	22.1	5.3	1.6	−24.9	–	–
4.5	0.4	1539	1395	170	29.9	28.6	20.3	5.1	1.6	−24.6	–	–
7.5	0.9	3035	2245	N/A	29.7	28.4	N/A	5.0	1.5	−24.6	–	–
10.5	2.2	1893	1886	168	29.7	28.4	19.2	5.1	1.5	−24.9	–	–
13.5	3.2	1417	1452	571	29.6	28.5	21.9	5.2	1.6	−24.7	–	–
17.5	4.0	1807	2119	885	29.7	28.5	22.5	5.0	1.6	−25.7	–	–
23.0	5.7	1418	1002	N/A	29.7	28.9	N/A	5.3	1.6	−26.9	–	–
28.0	8.4	4086	9039	1333	29.8	28.3	22.3	5.0	1.7	−25.7	–	–
32.5	10.6	2230	2075	N/A	29.8	28.5	N/A	4.6	1.7	−25.8	–	–
37.5	12.8	3583	4589	1619	29.8	28.5	22.8	4.6	1.7	−27.6	–	–
43.0	14.6	2782	5291	307	30.1	28.7	21.5	4.7	1.7	−24.6	–	–
48.0	15.5	796	1811	618	30.4	28.7	23.6	5.2	1.7	−25.0	N/A	N/A
57.5	16.7	840	2328	N/A	30.6	28.8	N/A	6.4	1.7	−28.9	–	–
62.5	17.1	934	1856	1581	30.7	28.8	23.9	6.9	1.7	−24.6	–	–
69.0	17.6	391	792	704	30.7	28.1	22.7	7.6	1.6	−24.8	–	–
72.5	18.1	761	N/A	N/A	30.7	N/A	N/A	7.1	1.6	−24.5	–	–
77.5	19.4	444	861	N/A	30.7	28.3	N/A	6.5	1.6	−24.6	–	–
82.5	21.6	867	2136	N/A	30.1	29.1	N/A	4.5	1.5	−24.6	–	–
87.0	23.6	1247	N/A	N/A	30.0	N/A	N/A	4.7	1.6	−24.3	–	–
92.0	24.7	1153	N/A	N/A	29.8	N/A	N/A	5.3	2.0	−25.6	N/A	N/A
97.5	25.6	1806	N/A	N/A	29.9	N/A	N/A	5.6	2.0	−25.8	N/A	N/A
102.5	26.4	1699	2755	N/A	29.9	27.7	N/A	5.5	2.1	−25.6	–	–
107.5	27.2	984	806	N/A	29.9	27.6	N/A	5.5	2.0	−25.7	–	–

$ACL_{27-33} = (27 \times n\text{-}C_{27} + 29 \times n\text{-}C_{29} + 31 \times n\text{-}C_{31} + 33 \times n\text{-}C_{33}) / (n\text{-}C_{27} + n\text{-}C_{29} + n\text{-}C_{31} + n\text{-}C_{33})$

$ACL_{OH24-34} = (24 \times n\text{-}C_{24} + 26 \times n\text{-}C_{26} + 28 \times n\text{-}C_{28} + 30 \times n\text{-}C_{30} + 32 \times n\text{-}C_{32} + 34 \times n\text{-}C_{34}) / (n\text{-}C_{24} + n\text{-}C_{26} + n\text{-}C_{28} + n\text{-}C_{30} + n\text{-}C_{32} + n\text{-}C_{34})$

$ACL_{OOH16-32} = (16 \times n\text{-}C_{16} + 18 \times n\text{-}C_{18} + 20 \times n\text{-}C_{20} + 22 \times n\text{-}C_{22} + 24 \times n\text{-}C_{24} + 26 \times n\text{-}C_{26} + 28 \times n\text{-}C_{28} + 30 \times n\text{-}C_{30} + 32 \times n\text{-}C_{32} + 34 \times n\text{-}C_{34}) / (n\text{-}C_{16} + n\text{-}C_{18} + n\text{-}C_{20} + n\text{-}C_{22} + n\text{-}C_{24} + n\text{-}C_{26} + n\text{-}C_{28} + n\text{-}C_{30} + n\text{-}C_{32} + n\text{-}C_{34})$

$CPI_{27-33} = 0.5 \times ((n\text{-}C_{27} + n\text{-}C_{29} + n\text{-}C_{31} + n\text{-}C_{33}) / (n\text{-}C_{26} + n\text{-}C_{28} + n\text{-}C_{30} + n\text{-}C_{32}) + (n\text{-}C_{27} + n\text{-}C_{29} + n\text{-}C_{31} + n\text{-}C_{33}) / (n\text{-}C_{28} + n\text{-}C_{30} + n\text{-}C_{32} + n\text{-}C_{34}))$

$CPI_{19-23} = 0.5 \times ((n\text{-}C_{19} + n\text{-}C_{21} + n\text{-}C_{23}) / (n\text{-}C_{18} + n\text{-}C_{20} + n\text{-}C_{22}) + (n\text{-}C_{19} + n\text{-}C_{21} + n\text{-}C_{23}) / (n\text{-}C_{20} + n\text{-}C_{22} + n\text{-}C_{24}))$
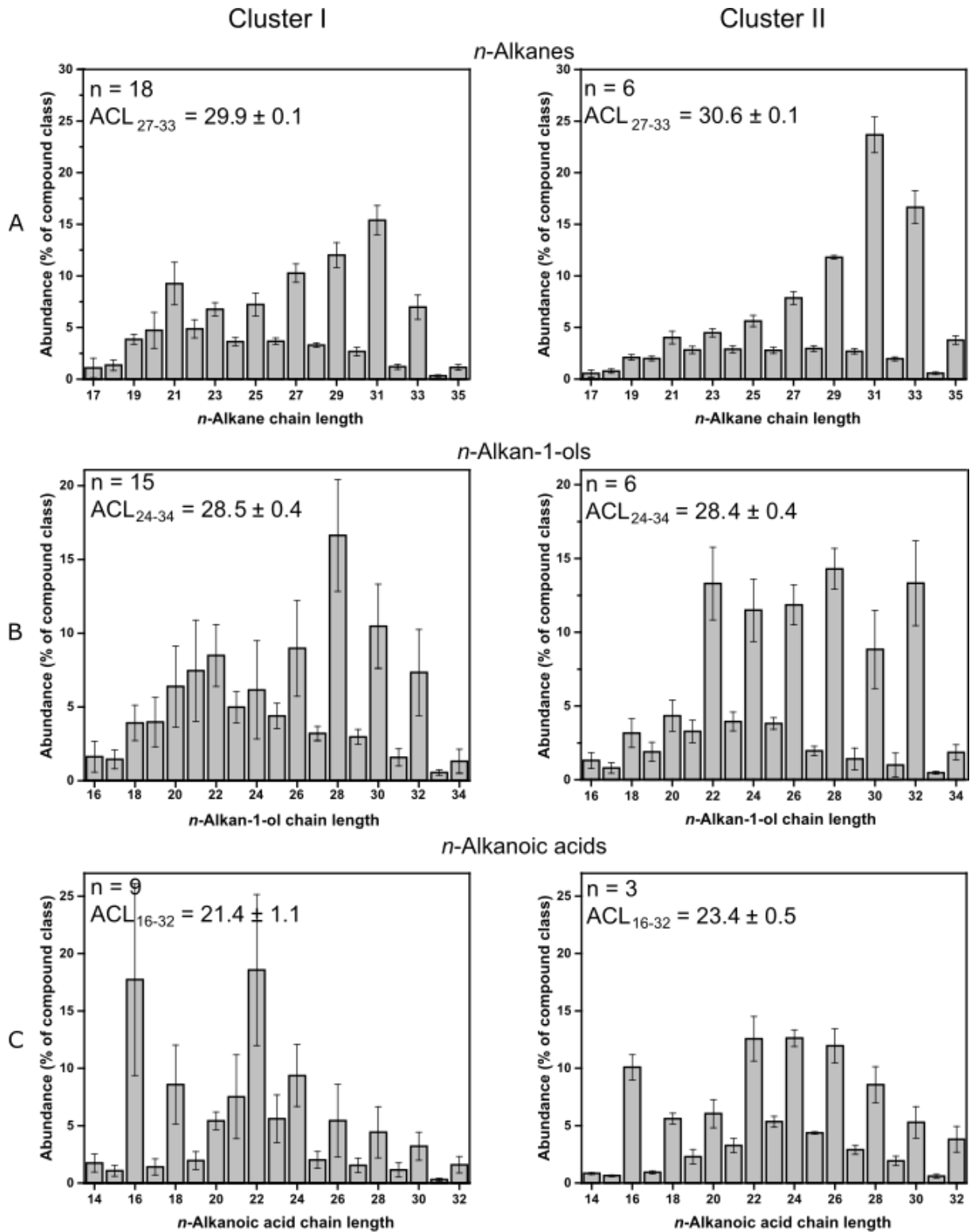
Figure 2-4 Relative chain length distributions and mean average chain lengths (ACL) of cluster I and cluster II for A. *n*-alkanes, B. *n*-alkan-1-ols and C. *n*-alkanoic acids.

n-Alkanols display higher mean concentrations in cluster I (2530 ± 2174 µg/g TOC) than in cluster II (1530 ± 602 µg/g TOC; Table 2-4). In analogy to the n-alkane distributions, cluster I shows a bimodal pattern with maxima at C_{22} and C_{28}, and a low EOP for C_{18}-C_{24} n-alkanols. The long-chain n-alkanols display a maximum at n-C_{28} followed by n-C_{30}, n-C_{32} and n-C_{26}. In Cluster II n-C_{22} to n-C_{32} alcohols show a relatively strong EOP with even homologues having comparable proportions ranging between 9.0 % (n-C_{30}) and 15.5 % (n-C_{32}).

The average concentration of n-alkanoic acids in cluster I (825 ± 537 µg/g TOC) is lower compared to cluster II (968 ± 435 µg/g TOC). In cluster I n-C_{16} and n-C_{22} homologues dominate, whereas long-chain acids are less abundant. In Cluster II n-C_{22}, n-C_{24} and n-C_{26} alkanoic acids are most abundant with similar relative amounts (Figure 2-4C). In general, the EOP is more pronounced in cluster I.
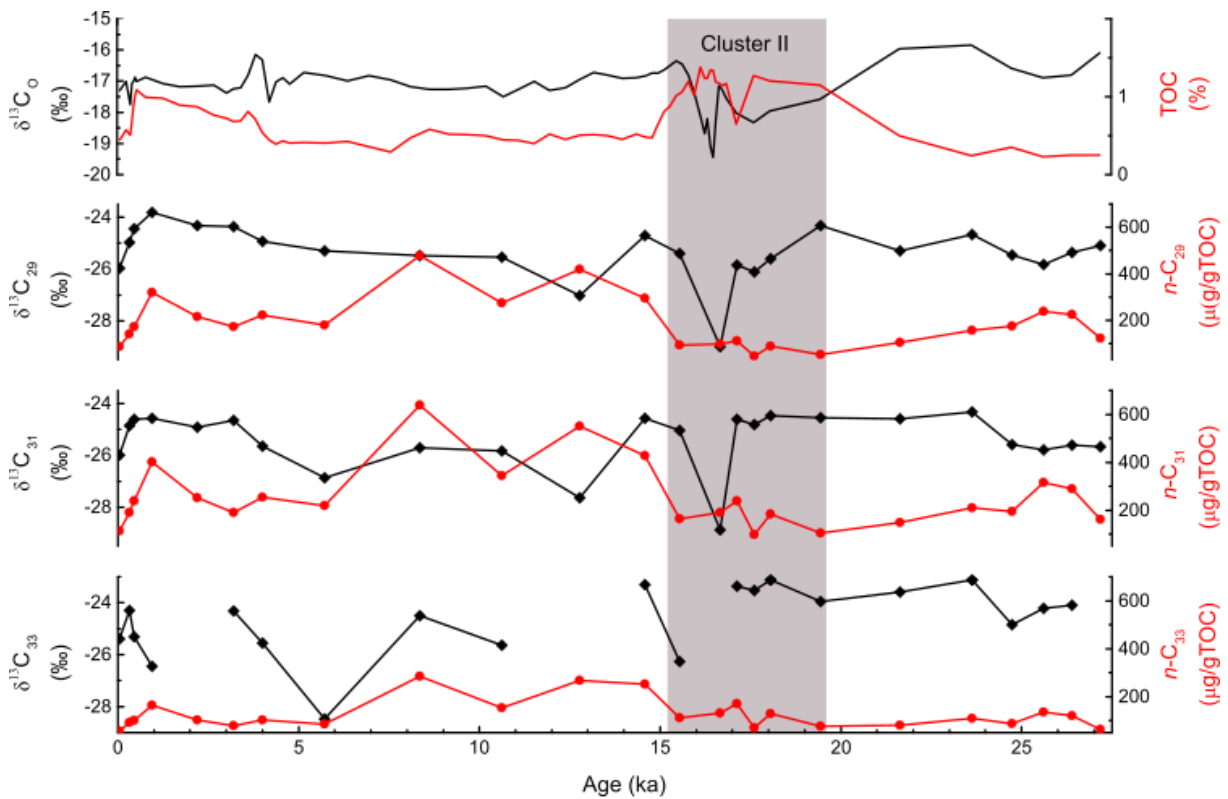
Figure 2-5 Concentrations (red circles) and compound-specific carbon isotope values of total organic carbon, n-C_{29}, n-C_{31} and n-C_{33} (black framed diamonds). Grey box marks samples with alkane pattern of cluster II.

2.4.3 **Stable carbon and hydrogen isotope values of *n*-alkanes**

The carbon isotopic composition of odd C_{21} to C_{33} *n*-alkanes varies from −29.0 ‰ to −22.0 ‰. $\delta^{13}C$ values for both clusters cover comparable ranges averaging at −24.6 and −25.0 ‰ in clusters I and II, respectively. Long-chain $\delta^{13}C$ values of *n*-alkanes C_{29} and C_{31} show comparable variation over time, while the variation of *n*-C_{33} is higher (Figure 2-5).
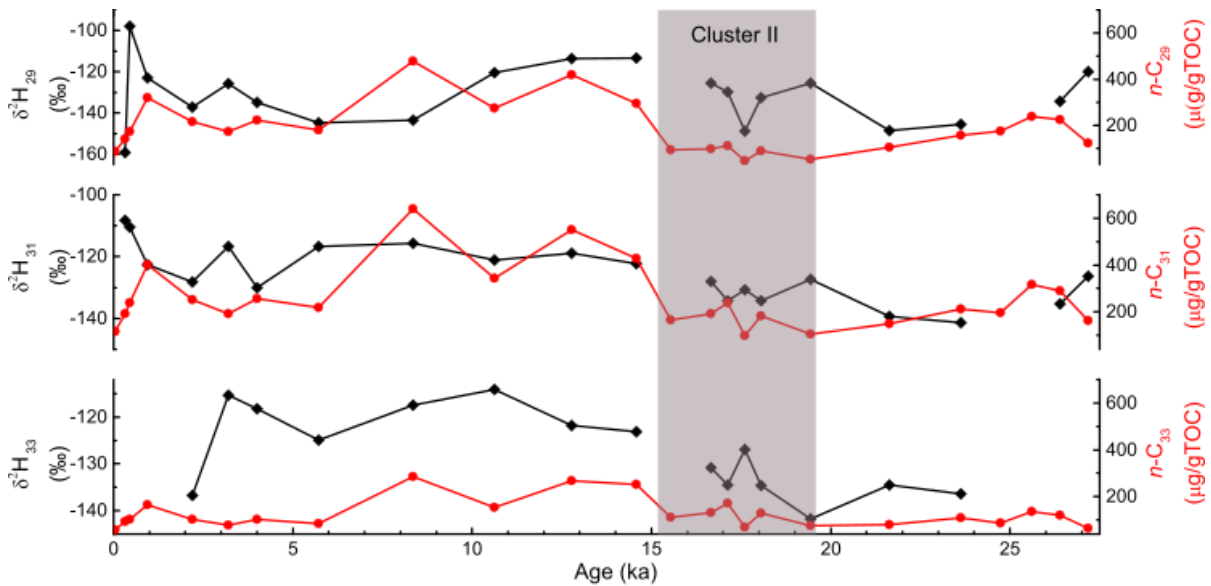
Figure 2-6 Concentrations (red circles) and compound-specific ice volume corrected hydrogen isotope values of *n*-C_{29}, *n*-C_{31} and *n*-C_{33} (black framed diamonds). Grey box marks samples with alkane pattern of cluster II.

For most intervals bulk organic and *n*-alkane carbon isotopic compositions show a relatively constant offset. There are two phases with diverging trends between both isotope records: The first one is the LGM when bulk values decrease while $\delta^{13}C_{31}$ stays constant; the second one occurs after 6 ka BP when the rise in compound-specific carbon isotope values is only reflected in a short peak around 4 ka BP by the bulk data (Figure 2-5).

The ice volume-corrected isotopic composition of hydrogen in odd C_{21}-C_{33} n-alkanes varies widely from −206 ‰ to −97 ‰. In case of C_{25}-C_{33} n-alkanes the values are in the same range in both clusters, but with a larger variation in cluster I. In general, $\delta D_{29\text{-}33}$ value show low values in samples older than 20 ka BP and high values between 15 and 5 ka BP (Figure 2-6).

2.5 Discussion

2.5.1 Significance of the biomarker record

In this paper we present the first plant wax biomarker record of a southern African salt pan. A summary of the proxy parameters used in this study and their paleoclimatic interpretation is provided in Table 2-5. The patterns of analysed long-chain lipids show the typical distribution of higher land plant material with a strong OEP for n-alkanes and EOP for n-alkanols and n-fatty acids. The CPI_{26-34} shows values >4, lies within the range of African plants from 3.3 to 30 and is comparable to soils of the Kalahari in South Africa (Vogts et al., 2009; Herrmann et al., 2016). The less pronounced OEP and the relatively high concentration of mid-chain n-alkanes shorter than n-C_{25} in samples featuring cluster I have not been reported for African plant material (Figure 2-4, Table 2-4; Rommerskirchen et al., 2006b; Vogts et al., 2009; Badewien et al., 2015b; Herrmann et al., 2016). However, leaf wax distributions with relatively high abundance of n-C_{25} have been documented for plants and sediments from the west coast of South Africa (Carr et al., 2014; Carr et al., 2015). Furthermore, roots of C_4 grasses and soils from central Queensland, Australia exhibited alkane distributions enriched in n-C_{14}-n-C_{20} homologues with EOP, suggesting that primary organic material does not necessarily have to feature a significant OEP (Kuhn et al., 2010).

Table 2-5. Proxy parameters used in this study.

Parameter	Interpretation	detailed description
sed. rate	sediment accumulation, fluvial input	Section 2.5.3
TOC	accumulation of biomass, vegetation density, fluvial input	Section 2.5.1
TIC, $\delta^{13}C_C$, $\delta^{18}O_C$	accumulation of carbonate, evaporation, precipitation amount	Section 2.5.3
ACL_{27-33}	higher values point to more grasses and/or drier conditions	Section 2.5.2
$\delta^{13}C_{org}$, $\delta^{13}C_{31}$	higher values point to more C_4 vegetation	Section 2.5.2
δD_{31}	reversed proxy for humidity, influenced by evaporation	Section 2.5.3
K/Al	fluvial input	Section 2.5.3

Having said this, degradation might still have played a role, which could mean, that the variation between both clusters might have been even bigger without degradation. It cannot be excluded, that the lower OEP in cluster I could be a sign for organic matter degradation. This would fit to the lower TOC values which occur in cluster I compared to cluster II, because degradation can be stronger if less organic carbon is available. Molecules with shorter carbon chains may be degraded faster than longer ones (Peters et al., 2005). Even if degradation had affected longer chain length to a large extent, this would probably shift the distribution of plant wax derived n-alkanes towards higher abundances of C_{33} and C_{35}. As these are less pronounced in cluster I compared to cluster II, while at the same time the relative abundance of n-C_{27} and n-C_{29} being increased it seems rather unlikely that the shift within long-chain n-alkanes is merely an effect of selective preservation.

2.5.2 Reconstruction of vegetation

Rommerskirchen et al. (2006b), Vogts et al. (2009) and Carr et al. (2014) created vegetation datasets for southern African plants, which are compared to the data of this study. n-Alkane distributions, ACL27-33 and n-alkanol ACL24-34 data from Omongwa Pan lie within the range of southern African savanna and grassland vegetation (Figure 2-7). Samples were also compared to data from soil samples originating from different South African biomes (Herrmann et al., 2016). In samples belonging to cluster I ACL27-33 is slightly lower (29.85±0.14) compared to average savanna soil samples (31±0.4), while Cluster II samples have a similar chain length (30.63±0.10). The long-chain distribution of cluster I is relatively similar to the average pattern from the Fynbos biome typical for the southwestern tip of South Africa, while cluster II compares best to the samples from the Nama Karoo biome (Herrmann et al., 2016). However, the variability in soil n-alkane distributions within the biomes is very high, which strongly limits the comparability (Herrmann et al., 2016).
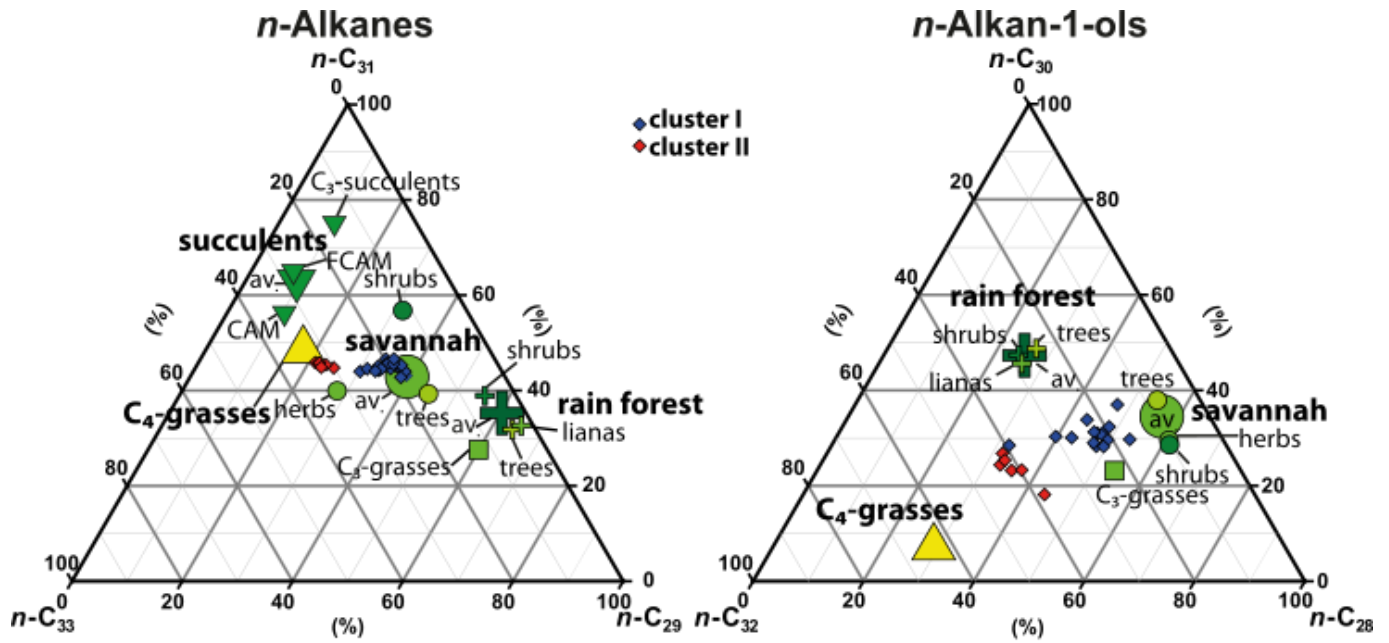
Figure 2-7 Ternary diagrams of A. n-C_{29}, n-C_{31} and n-C_{33} alkanes; B. n-C_{28}, n-C_{30} and n-C_{32} alkanols of clusters I (blue diamonds) and II (red diamonds). Average values are displayed for C_4 grasses (up-triangle Rommerskirchen et al., 2006b), C_3 grasses (square; Rommerskirchen et al., 2006b) succulents (down-triangle; Carr et al., 2014), C_3 savanna (circle) and rain forest (cross) vegetation (Vogts et al., 2009).

As the most abundant n-alkane in leaf waxes of African C_3 and C_4 plants is n-C_{31}, $\delta^{13}C_{31}$ values are thus considered to best indicate changes in the vegetation assemblage (Rommerskirchen et al., 2006b; Vogts et al., 2009; Badewien et al., 2015b). As end members of $\delta^{13}C_{31}$ values we use –35.7±2.8 (C_3-plants) and –22,1±2.1 (C_4-plants) according to Badewien et al. (2015a). The range of $\delta^{13}C_{31}$ values observed indicates that C_4 plants have played an important role in the local vegetation assemblage over the whole time-span under scrutiny. It has been shown that C_3 plants produce higher amounts of n-alkanes than C_4 plants (Garcin et al., 2014). Therefore, the occurrence of C_4 plants could even be underestimated due to an unrepresentative lowering of $\delta^{13}C_{31}$ values in sediments by the contribution from C_3 plants.
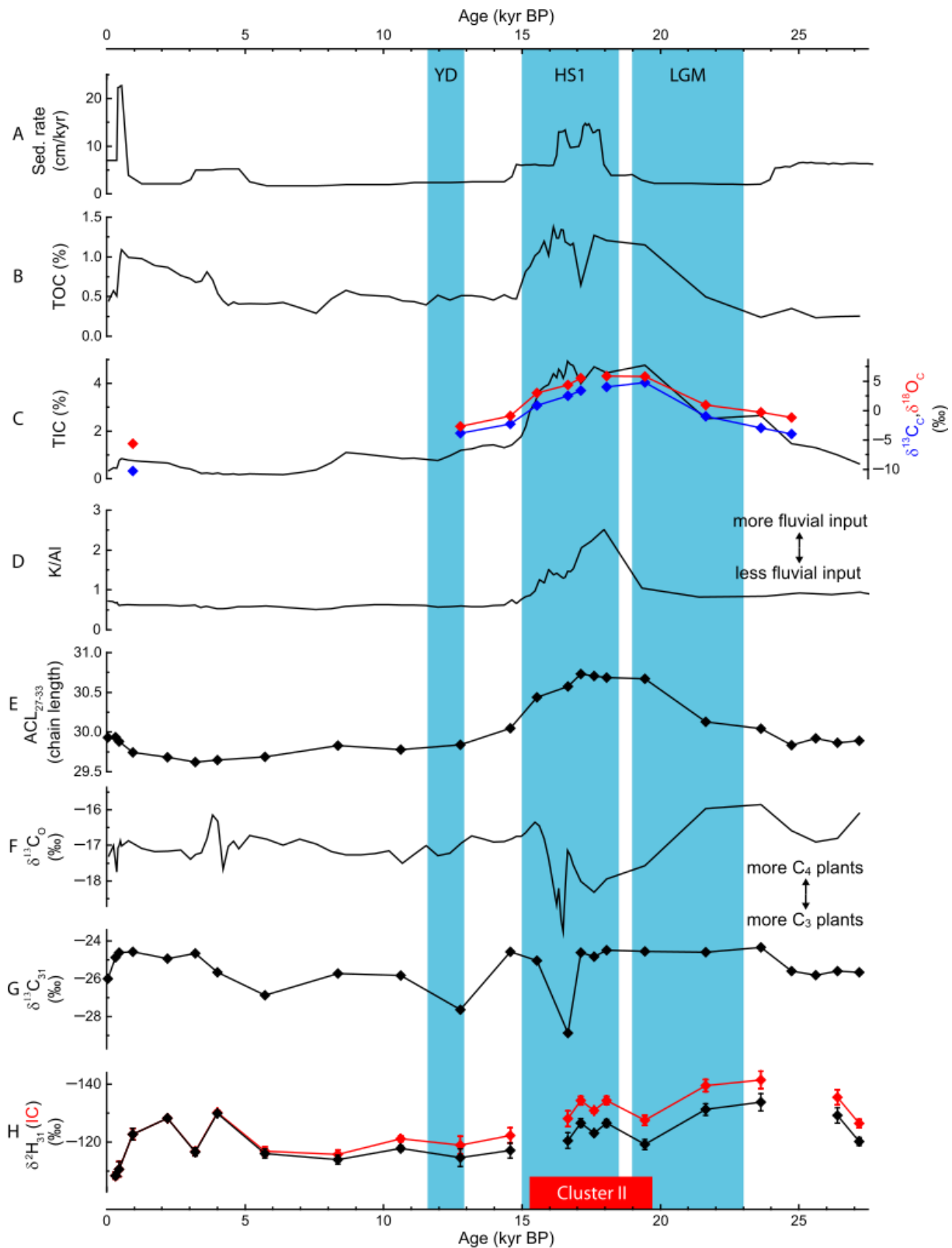
Figure 2-8 Bulk, molecular and isotopic parameters of Omongwa Pan. A. sedimentation rate, B. TOC, C. TIC, D. K/Al ratio (Schüller et al., 2018), E. ACL27-33, F. $\delta^{13}C_O$; G. $\delta^{13}C_{31}$, H. δD_{31} (black) and δD_{31} corrected for ice volume effect (red). Red area marks time span featuring Cluster II. Blue areas mark Last Glacial Maximum (LGM), Heinrich Stadial 1 (HS1) and Younger Dryas (YD).

46

The important role of C_4 plants is also evident when the relative distributions of the major long-chain n-alkanes and n-alkanols are compared to average data of the vegetation datasets (Figure 2-7). The chain length distribution displays a clear difference between clusters I and II. Samples of cluster II, featuring a higher concentration of wax constituents of longer chain lengths, display a distribution more similar to C_4 grasses and possibly indicate a higher relative amount of C_4 vegetation (Rommerskirchen et al., 2006b), than those from cluster I. Regarding alkanoic acids n-C_{22} has been found to be the most pronounced homologue in C_3 plants, while C_4 plants have a maximum at n-C_{24} (Wiesenberg et al., 2004). Therefore, the chain lengths distribution of n-alkanoic acids supports that the C_4 content in cluster II is higher (Figure 2-4). Bush and McInerney (2013) provided evidence that the chain length of leaf wax compounds can also be influenced by environmental factors, so that the chain length distribution of the same species can change with temperature and water availability. They attributed a shift to longer chain lengths within the same species to drier conditions. In general, the vegetation assemblage at Omongwa Pan since the Pleistocene was rather stable. Most evidence for vegetational changes were found for HS1. The variation in chain length distributions points to environmental change and/or increase of C_4 vegetation, although carbon isotope values stay stable since the LGM, with the exception of one sample with an age of ca. 17 ka BP.

2.5.3 Reconstruction of hydrology

Bulk organic and inorganic carbon isotopes do not correlate over the core (Figure 2-8). A positive correlation might either origin from the incorporation of inorganic carbon into OM by primary production within the pan or by occurrence of biogenic carbonates. Microbial biomarkers and DNA analyses of Omongwa Pan sediments suggest only a very low abundance of cyanobacteria which limits incorporation of biogenic inorganic carbon into OM. (Genderjahn et al., 2018b). Furthermore, the carbonate carbon and oxygen isotopes with values close to 0 suggest a mineralogic origin of inorganic carbon (Wacey et al., 2007). In lakes, elevated carbonate contents and high $\delta^{13}C_C$ and $\delta^{18}O_C$ values usually are clear indicators for arid and

highly evaporative conditions (Leng and Marshall, 2004). Between 20 and 16 ka BP TIC content, $\delta^{13}C_C$, and $\delta^{18}O_C$ of Omongwa Pan are at their highest values (Figure 2-8). During this period annual temperatures in southern Africa were up to 5-6°C cooler than today resulting in a lower potential evapotranspiration (PET; Scott, 1982; Stute and Talma, 1998; Truc et al., 2013; Chevalier and Chase, 2015, 2016). This highlights that these values cannot simply be regarded as sign for stronger evaporation. As stated in section 2.2 Omongwa Pan is inundated over short periods only under recent conditions. If the pan would have been flooded year-round during the time span between 20 and 16 ka, TIC and carbonate isotopes should reflect lower evaporation. Therefore, we assume that precipitation was higher than before, but still lower than PET, leading to repeated events of full evaporation during rainy season and thus carbonate accumulation accompanied by enrichment of ^{13}C and ^{18}O (Rosen, 1994; Roy et al., 2008). Also, the sedimentation rate of Omongwa Pan, deduced from the age model, is used as another proxy for precipitation (Figure 2-8A). Assuming, that most sediment input occurs by local run-off and that wind driven deflation is enhanced during dry phases, high sedimentation rates indicate increased precipitation (Schüller et al., 2018).

The fractionation of hydrogen isotopes between the precipitation (δD_p) and leaf wax lipids in sediments is complex and depends on many variables like vegetation assemblage, evapotranspiration and catchment size (Sachse et al., 2012). Herrmann et al. (2017) found a significant correlation between δD_{wax} in soils and δD_p of the same area of the southern African SRZ. However, in more arid parts of the savanna biome high evapotranspiration leads to D enrichment, which excludes quantitative precipitation reconstructions (Herrmann et al., 2017). Therefore, as long as PET is stable, δD_{31} values represent relative changes in δD_p. Within the Omongwa Pan record, the phase with low δD_{31} values is mainly before 15 ka BP and its trends do not really correlate to sedimentation rate or TIC content (Figure 2-8C, H). The low PET during this phase compared to the rest of the record leads to less enriched values and complicates comparison of δD_{31} values before and after HS1. Changes in C_3/C_4 ratio can also affect δD_{31} (Sachse et al., 2012; Collins et al.,

2014), however, considering the only minor changes of carbon isotopes through the record of the Omongwa pan such an influence can probably be neglected.

2.5.4 Climatic conditions at the Omongwa Pan during the last 27 ka

2.5.4.1 Until Last Glacial Maximum

Data from Omongwa Pan samples older than LGM indicate relatively dry conditions. The moderate sedimentation rate, low TIC and TOC contents and a low K/Al ratio mark limited fluvial input (Figure 2-8D; Schüller et al., 2018). The influence of summer rainfall in the southwestern part of southern Africa before the LGM (between 27 and 23 ka BP) is difficult to grasp. There are lacustrine conditions at Etosha Pan (S5) and Tsodilo Hills (S13) and lake high stands in the Magadikgadi basin (S6; Figure 2-9; Thomas et al., 2003; Burrough et al., 2009; Brook et al., 2013) marking increased moisture, which possibly originates from the WAM and which is transported to central Kalahari sites from Angolan highlands (Burrough et al., 2009; Cordova et al., 2017). On the contrary, there is a gap in the record from Lake Ngami (S7) and signs for wet conditions at Drotsky's Cave (S3) speleothem records are lacking (Brook et al., 1996; Brook et al., 1998; Burrough et al., 2007). The proxies point to slightly less dry conditions at Omongwa Pan compared to the LGM that followed, where the catchment might have been affected by this "wetter phase" to some extent.

Data from the LGM at Omongwa Pan have to be looked upon with caution. The low sedimentation rate originating from low fluvial input or possible minor deflation impairs the resolution and might distort age control. The LGM is represented by two samples only. Given that the δD_{31} values are reduced by low evapotranspiration, the low sedimentation or even lightly wind driven deflation and the low organic and inorganic carbon content, the environmental conditions between 24 and 21 ka BP were probably rather dry and the stable high $n\text{-}C_{31}$ carbon isotope values do not reveal vegetation changes. Towards the late LGM there are significant changes, but the sample in the late LGM lies at the end of a phase with a low sedimentation rate and is possibly a displaced sign of the HS1

onset. Several studies found indications for a northward shift of winter rain into the Kalahari leading to wetter conditions from ca. 24 to 18 ka BP (e.g.van Zinderen Bakker, 1983; Cockcroft et al., 1987; Chase and Meadows, 2007; Gasse et al., 2008; Stone, 2014). Evidence for a supposed further intensification of winter rainfall into the southwestern Kalahari during the LGM is provided by the coexistence of high fluvial and aeolian input into Branddam East Pan (S2; Schüller et al., 2018), increased river activity of the Molopo (S8; Hürkamp et al., 2011) and significantly higher oxygen isotope values in the Stampriet aquifer (S12; Stute and Talma, 1998). In contrast relatively dry conditions during the LGM occurred in the southern Namib at Pella (S11; Lim et al., 2016).

The occurrence of winter rainfall at Omongwa Pan is rather unlikely. Due to the continental effect, moisture can be expected to have led to a significant enrichment in δD_{31} if it came from the Atlantic Ocean, where modern winter rainfall originates, rather than from the more distant Indian Ocean (Rozanski et al., 1993). Thus, the lack of a positive hydrogen isotope signal at Omongwa Pan and the above-mentioned rather dry climate conditions contradict winter rainfall at Omongwa Pan. Fittingly, speleothem sites north of Omongwa Pan, like Drotsky's Cave (S3) and at the Otavi Mountains (S10) do not show signs of increased precipitation or more humid conditions (Figure 2-9; Brook et al., 1996; Brook et al., 1998; Brook et al., 1999). At the same time there is no lake record at the Tsodilo Hills paleo-lake (S13) after 23 ka BP (Thomas et al., 2003). Therefore, the northernmost boundary of winter rainfall during the LGM must have been located to the south between Omongwa Pan and Branddam East Pan (S2, Figure 2-1).
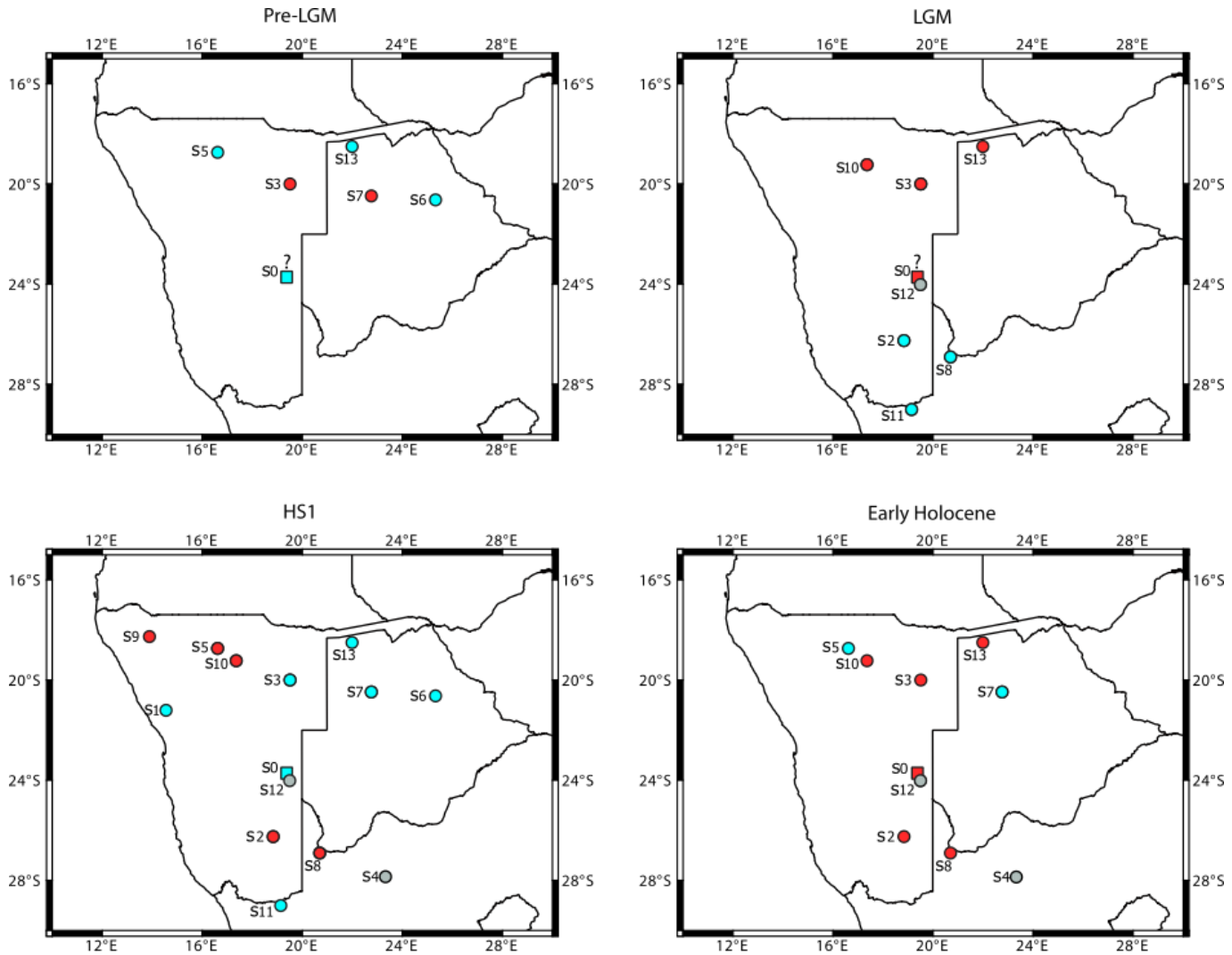
Figure 2-9 Overview of relatively dry (red) and wet (blue) conditions compared
to present at chosen locations in southern Africa, before LGM, during LGM,
during HS1 and during early Holocene. Site references are stated in Table 1.
Detailed descriptions of sites conditions are given in the text.

2.5.4.2 Last Glacial-Interglacial Transition

From the end of the LGM until late HS1 (19.5 until 15.5 ka BP) the *n*-alkane, *n*-
alkanol and fatty acid distributions at Omongwa Pan switch to the pattern of
cluster II (Figure 2-8). Four out of the six samples, which comprise this cluster, are
from a short period between 18.1 and 16.7 ka BP. This is an argument towards an
abrupt environmental excursion, leading from rather dry conditions with low
sedimentation or even a short phase of net deflation, to a period of high

sedimentation and enhanced organic input into the pan (Figure 2-8A). This excursion is characterized by a rather wet environment, indicated by high TIC content and elevated $\delta^{13}C_C$ and $\delta^{18}O_C$ values. A high K/Al ratio points to high fluvial input (Figure 2-8D; Schüller et al., 2018).

During LGIT δD values are slightly increased relative to LGM conditions (Figure 2-8). The effect of reduced PET is hard to estimate. According to Stute and Talma (1998) a sharp increase of temperature at the Stampriet aquifer (S12) occurred around 16 ka BP whereas the increase at Wonderwerk Cave (S4) started slightly earlier, around 17 ka BP (Brook et al., 2010). The Stampriet aquifer was, in contrast to Omongwa Pan, affected by winter rainfall and cool airmasses during LGM (Stute and Talma, 1998). Therefore, it seems likely that temperatures at Omongwa Pan rose earlier parallel to the rise at Wonderwerk Cave. Consequently, PET was higher during late HS1 than during LGM and δD values are higher than before, while non-organic proxies indicate more humid conditions. The change in vegetation might mainly be related to vegetation density. Within the Namibian savanna biome, vegetation can switch between dense and open grassy states (Joubert et al., 2008). The shift towards C_4 is accompanied by an increase in TOC content, which shows an enhanced accumulation of organic material in the catchment of the salt pan. This can be attributed to a change towards a denser grassy cover in the pan catchment as a result of more intense summer rainfall. Grass biomass increases with precipitation (February et al., 2013; Berry and Kulmatiski, 2017). At the end of HS1, TIC, $\delta^{13}C_C$, and $\delta^{18}O_C$ decrease strongly and lower K/Al ratios and sedimentation rate indicate lesser flooding events and fluvial input. The rise of δD_{31} values is probably caused by further increasing PET as well as dryer conditions indicated by other proxies (Figure 2-8). *n*-Alkane, *n*-alkanol and *n*-fatty acid distributions change back to the pattern of cluster I. $\delta^{13}C_{31}$ data show a clear decrease, revealing a higher proportion of C_3 plant material.

In the central and western Kalahari several sites provide evidence for wetter conditions during HS1. Speleothems at Drotsky's Cave (S3) and the paleo-lake at the Tsodilo Hills (S13) feature increased local rainfall northeast of Omongwa Pan (Brook et al., 1996; Brook et al., 1998; Thomas et al., 2003). Further east, Lake Ngami (S7) shows highest lake levels and a mega paleo-lake in the Makgadikgadi

basin was flooded during HS1(S6; Figure 2-9; Burrough et al., 2007; Burrough et al., 2009; Cordova et al., 2017). Both lakes are connected with the Okavango delta and, apart of local rainfall, water in the lake system mainly originates from Angolan highlands, where precipitation is influenced by WAM (Burrough and Thomas, 2013). Direct effects of WAM on the western Kalahari during HS1 are unlikely as no evidence for wetter conditions was found at sites located to the northwest at the Etosha Pan (S5), Otavi Mountain Cave (S10) and Orumana Cave (S9; Brook et al., 1999; Brook et al., 2013; Railsback et al., 2016). Sites south of Omongwa Pan show trends towards drier conditions: at Branddam East Pan (S2) fluvial input decreases after 18 ka BP (Schüller et al., 2018) and flooding incidents in the Molopo River (S8) decline (Hürkamp et al., 2011). In western Namibia at Brandberg (S1) conditions were slightly wetter than today or evaporation was lower (Scott et al., 2004; Scott et al., 2018). At Pella (S11), aridity decreases during HS1 with rising temperatures (Lim et al., 2016). From this follows that the source of moisture at Omongwa Pan must originate in intensified summer rainfall. A southward shift of the ITCZ in southern Africa during HS1 and the YD has been assumed (Lancaster, 1979; Singarayer and Burrough, 2015). This is supported by data from sediments deposited close to the Zambezi River mouth (Schefuß et al., 2011).

For the YD there are no indications for ITCZ changes and accompanying enhanced summer precipitation at Omongwa Pan. However, the record is limited to one data point only. While at Drotsky's Cave local rainfall is again higher (Figure 2-9; Brook et al., 1996; Brook et al., 1998), there is a significant decrease in rainfall at Lake Ngami and lower lake stands in the Makgadikgadi basin (Burrough et al., 2007; Burrough et al., 2009; Cordova et al., 2017). This suggests, the intensity of the shift must have been weaker and reached the centre of southern Africa only in parts. This agrees with data from the eastern coast where the precipitation during YD was less pronounced than during HS1 (Schefuß et al., 2011).

2.5.4.3 Holocene

The sedimentation rate at Omongwa Pan was very low for most of the Holocene (Figure 2-8A) which may restrict the accuracy of the age-depth relation. The decreasing compound-specific $\delta^{13}C$ values demonstrate a shift towards C_3 vegetation. The slightly enhanced TOC and TIC values around 10-8 ka BP are not reflected in other data and possibly result from only minor changes in climate conditions. Geochemical parameters in samples from the Late Holocene older than 4 ka BP are constant. The following rise of TOC almost to HS1 level, a slight rise of sedimentation rate and the decrease of δD values indicate higher water availability. On the contrary, TIC rises only to a small extent and sedimentation rate and K/Al ratios at Omongwa Pan show almost no fluvial input during the entire Holocene (Figure 2-8C, D; Schüller et al., 2018). Changes could thus be possibly better explained by less evaporative conditions than higher precipitation. Reduced evaporation could result from reduced temperatures, which were reconstructed for Stampriet aquifer (S12) and Wonderwerk Cave (S4; Stute and Talma, 1998; Brook et al., 2010). Although $\delta^{13}C_{31}$ values are elevated between 4 and 0.5 ka BP suggesting more C_4 vegetation, there are no changes in *n*-alkane distribution, and $\delta^{13}C_O$ data shows a short-termed peak between 5 and 4 ka BP only.

Available Holocene climate data reveal a high spatial and temporal variability in central southern Africa (Burrough and Thomas, 2013). Northeast of Omongwa Pan, sites not influenced by the Okavango are dry during the early Holocene (S3; Figure 2-9; Brook et al., 1996; Brook et al., 1998; Thomas et al., 2003). Stromatolites at Etosha Pan1 (S5) indicate a prolonged phase of lacustrine conditions from 8-6.6 ka BP (Brook et al., 2013). These wet conditions did not reach the Kalahari as the cenotes in the Otavi Mountains (S10) are not affected (Brook et al., 1999). The dry conditions at Omongwa Pan in the early Holocene are consistent with dry conditions at surrounding sites (Schüller et al., 2018), and at Wonderwerk Cave (S4, Scott and Thackeray, 2015; Ecker et al., 2018). Changes in the late Holocene (< 4 ka BP) at Omongwa Pan correspond to wet conditions at Drotsky's Cave, Wonderwerk Cave and at Lake Ngami (Brook et al., 1996; Brook et al., 1998; Brook et al., 2015; Scott and Thackeray, 2015; Cordova et al., 2017;

Ecker et al., 2018). In conclusion, the climate of Omongwa Pan since the Late Pleistocene strongly depends on the expansion and the precipitation intensity of summer rainfall.

2.6 Conclusions

In this study, we present the first climate-related biomarker and isotope record from a salt pan in the western Kalahari. We show that plant wax-derived biomarkers are well-preserved in the pan sediments. Our results provide the following major insights into the regional climatic variations: a short wet phase due to a southward shift of the ITCZ during HS1 was accompanied by a significant change in vegetation. A comparable event during the YD is not reflected in the record of Omongwa Pan. The northward shift of the austral westerlies transporting moisture did not reach the catchment area of Omongwa Pan during the LGM. This highlights the importance to investigate pans located in southern Namibia in order to more precisely identify the maximum northward extent of winter rainfall. Overall it turns out that salt pans can be useful archives for deciphering the pronounced spatial climate variability in southern Africa. This is important to fill gaps with respect to intracontinental climate processes and to identify boundary shifts in an area where lacustrine archives are absent.

Acknowledgments

3. Changes in southern Kalahari rainfall seasonality during the Last Glacial-Interglacial Transition and its impact on vegetation: A leaf wax study from salt pan sediments

Lukas Belz[1], Irka Schüller[2], Jürgen Köster[1], Andrea Vieth-Hillebrand[3], Achim Wehrmann[2], Heinz Wilkes[1]

[1]Institute for Chemistry and Biology of the Marine Environment (ICBM), Carl von Ossietzky University, Oldenburg, 26111, Germany

[2]Senckenberg am Meer, Marine Research Department, Wilhelmshaven, 26382, Germany

[3]Helmholtz Centre Potsdam GFZ German Research Centre for Geosciences, Telegrafenberg, Potsdam, 14473, Germany

Abstract

Variation in rainfall seasonality is an important factor in continental southern African climate. Studies showed a shift from winter towards summer rainfall in the southwestern Kalahari after the Last Glacial Maximum, which must have had an impact on environmental conditions. Here we present high-resolution leaf wax biomarker data (*n*-alkanes) from Koës Pan (Namibia) and their compound-specific carbon and hydrogen isotopic compositions since 19.9 ka BP. *n*-Alkane distribution, average chain length (ACL) and carbon isotopes show abrupt changes around 17.5 ka BP pointing to lasting dryer and/or warmer conditions, probably linked to a seasonal rainfall shift. In our interpretation the abrupt change is a result of changing growing seasons and adapting vegetation. This development is not visible in δD_{31} values which are probably affected by changes of the continental effect. Over most parts of the record, the relative distribution of *n*-C_{29}, *n*-C_{31} and *n*-C_{33} displays two different phases of continuous, linear sequences indicating high-resolved change in vegetation and environmental conditions. The results highlight the sensitivity of long chain *n*-alkanes and reveal weaknesses of well-established molecular proxies like the ACL, which can sometimes lack details within a data set with the consequence that valuable paleoclimatic information might get overlooked.

3.1 Introduction

One focus in continental climate reconstruction of the western parts of southern Africa is the dynamic of seasonal rainfall (Cockcroft et al., 1987; Nicholson, 2000; Chase and Meadows, 2007; Gasse et al., 2008; Chase et al., 2017). The centre of southern Africa mainly features summer rainfall caused by humid airmasses originating from the Indian Ocean, which are attracted by two throughs, the Intertropical Convergence Zone (ITCZ) and the connected Congo Air Boundary (CAB).

The southwestern part conceives precipitation during austral winter from the Atlantic Ocean as a part of the southern west wind zone (Tyson et al., 1996;

Nicholson, 2000, 2009). Many studies described a northward extension of winter rainfall during the last glacial maximum (LGM) and its retreat afterwards (e.g. van Zinderen Bakker, 1983; Cockcroft et al., 1987; Chase and Meadows, 2007; Stone, 2014). This expansion is thought to be caused by a glacial accumulation of Antarctic sea ice that pushed the austral westerlies further northward (Gersonde et al., 2005). Other studies found evidence for enhanced summer rainfall in central southern Africa during cold pulses in the northern hemisphere at the end of the last glacial, like Heinrich Stadial 1 (HS1). This is explained by a southward shift of ITCZ and CAB.

Different sedimentary archives and proxies have been used to reconstruct hydrologic conditions in the mainly semi-arid southern Africa: speleothems (Brook et al., 1998; Railsback et al., 2016), fluvial deposits (Hürkamp et al., 2011; Ramisch et al., 2017), pan sediments (Schüller et al., 2018), pollen and nitrogen isotopes from hyrax middens (e.g. Chase et al., 2012; Lim et al., 2016), aquifers (Stute and Talma, 1998) and hydrogen isotopes from leaf wax n-alkanes (i.e. δD_{31} or δD_{wax}) taken from lake (Schmidt et al., 2014; Tabares et al., 2020), marine (Collins et al., 2013; Vogts et al., 2016; Burdanowitz et al., 2018) or pan deposits (Belz et al., 2020) and hyrax middens (Chase et al., 2019).

Leaf wax δD correlates to the isotopic composition of precipitation (δD_p) which is largely controlled by the rain fall intensity (amount effect). Other important factors are the temperature effect, the global ice volume effect, the altitude effect and the continental effect. The continental effect leads to more depleted δD_p values with increasing distance that moisture travelled over land (Dansgaard, 1964; Sachse et al., 2012; Collins et al., 2013; Herrmann et al., 2017). Furthermore, the hydrogen isotope composition of leaf wax n-alkanes is influenced by evapotranspiration, vegetation assemblage and catchment size (Risi et al., 2008; Garcin et al., 2012; Sachse et al., 2012). The change of rain season from winter rainfall to summer rainfall would affect δD values obviously by a change of growing season from winter to summer. This applies especially for grasses and plants with shallow roots. Due to increased temperatures during summer, the plants had to cope with higher water loss via enhanced potential evapotranspiration (PET). Furthermore would this change be accompanied by a switch of humidity source (Stute and

Talma, 1998). With summer rain coming from the Indian Ocean, the continental effect must be higher in summer rain than in winter rain, which is coming from the much closer Atlantic Ocean (Figure 3-1C). Besides hydrogen isotopes, the chain-length distribution of leaf wax derived long-chain n-alkanes can give insights into the vegetation assemblage. The carbon number distribution of n-alkane homologues depends on vegetation type and/or environmental conditions (Rommerskirchen et al., 2006b; Vogts et al., 2009; Badewien et al., 2015b; Bush and McInerney, 2015; Herrmann et al., 2016). The carbon isotopic composition of leaf waxes depends largely on the carbon assimilation pathways employed in photosynthesis. The Calvin-Benson cycle (C_3) and the Hatch-Slack cycle (C_4) are the two most important pathways (Vogel et al., 1978; O'Leary, 1981). C_4 plants in southwestern Africa are mainly savanna grasses displaying a distinguishable lower isotope fractionation during CO_2 assimilation compared to C_3 plants (Vogel et al., 1978; Mucina and Rutherford, 2006; Vogts et al., 2009; Badewien et al., 2015b). Magill et al. (2019) introduced the Leaf Wax Isotopic Spread (LEWIS) proxy, which reflects species richness, as well as the $^{31}f_{woody}$, a tool to estimate woody plant coverage based on $\delta^{13}C_{31}$.

Recently, studies have shown that pans (playas) which occur widespread in the Kalahari can be useful environmental archives (Schüller et al., 2022). Most of the studied pans showed a quasi-continuous sedimentation, which allows the application of inorganic as well as organic geochemical and microbial proxies for environmental and climatic reconstruction (Genderjahn et al., 2017; Genderjahn et al., 2018a; Genderjahn et al., 2018b; Schüller et al., 2018; Belz et al., 2020).

In this study, we present organic geochemical data for pan sediments from Koës Pan in the southwestern Kalahari (Namibia). We determined proxies derived from n-alkane compositions and their compound-specific carbon and hydrogen isotope values. Additionally, we present the content of total organic carbon (TOC), its isotopic composition ($\delta^{13}C_{org}$) and the content of total inorganic carbon (TIC). We apply these data to reconstruct past vegetation and ecology as well as hydrological conditions, with a focus on rainfall regime changes during the Last Glacial-Interglacial Transition. The record reaches back to 19.9 ka BP and provides insights into regional changes as a response to global climate change.
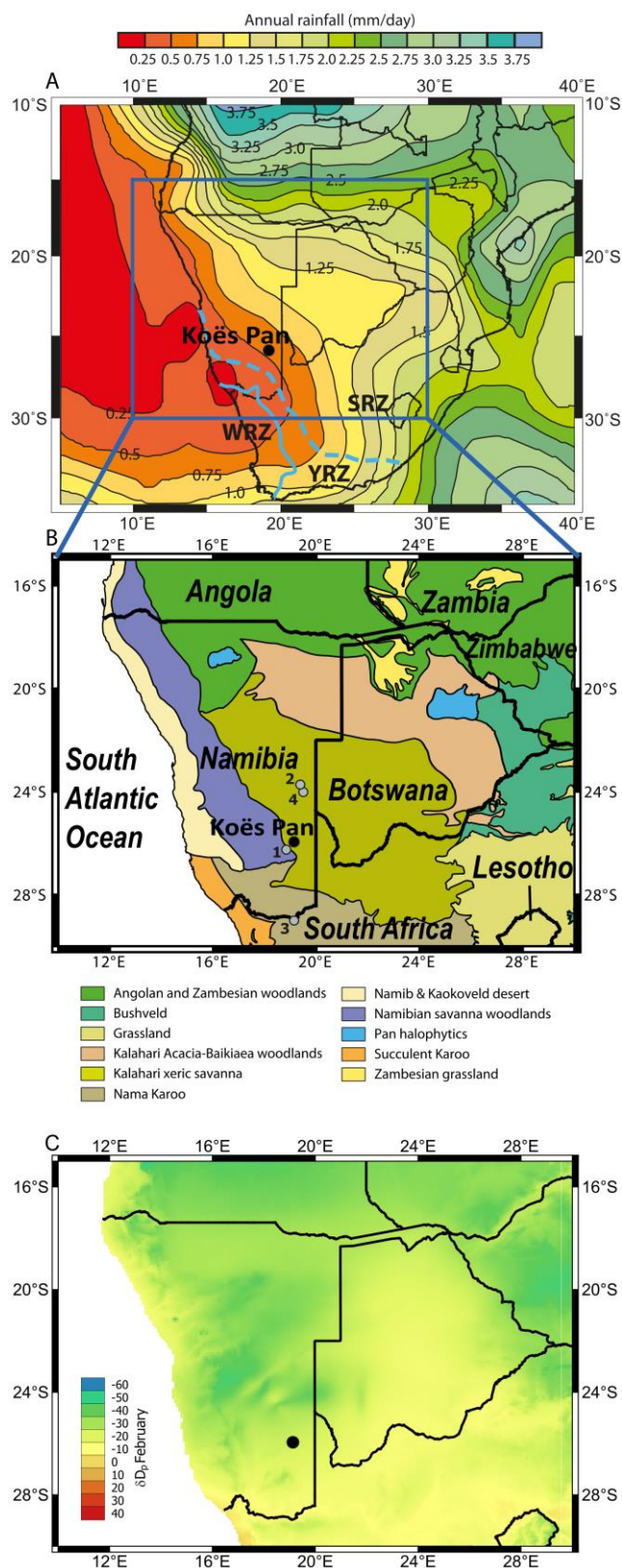
Figure 3-1. A. Map of southern Africa displaying modern annual rainfall distribution in mm/day. CMAP Precipitation data provided by the NOAA/OAR/ESRL PSD, Boulder, Colorado, USA, from their Web site at https://www.esrl.noaa.gov/psd/ (Xie and Arkin, 1997). The continuous blue line indicates the boundary between winter (WRZ) and year-round rainfall (YRZ) zones, the dashed blue

line marks the boundary between the YRZ and summer rainfall zone (SRZ; data source: Chase and Meadows, 2007). The blue square marks the section of Figure 1B. This map was created using Generic Mapping Tools (GMT; Wessel et al., 2013) Changed after (Belz et al., 2020). B. Map of southern African ecoregions (dataset simplified after Olson et al., 2001); with location of Koës Pan (black circle) and locations of other geoarchives discussed in the text (grey dots): 1 Branddam East Pan (Schüller et al., 2018), 2 Omongwa Pan (Belz et al., 2020), 3 Pella (Lim et al., 2016), 4 Stampriet aquifer (Stute and Talma, 1998) changed after (Belz et al., 2020). C. Map with interpolated hydrogen isotopes of precipitation δD_p in February, the month with most precipitation at Koës Pan (Bowen et al., 2005; Bowen, 2021).

3.2 Regional setting and site description

Modern climate conditions in the western Kalahari vary strongly with seasons. During austral summer, the ITCZ and the CAB shift southward, attracting air masses and moisture from the Indian Ocean (Nicholson, 2000). The amount of precipitation decreases westward (Tyson et al., 1996; Gasse et al., 2008). In the western Kalahari dry conditions dominate during winter. This is caused by semi-permanent subtropical anticyclones (Tyson et al., 1996; Nicholson, 2000). In South Africa and the southernmost parts of Namibia precipitation occurs mainly during winter. This winter rainfall is caused by moisture transported by northward shifted westerlies with a northward decreasing amount of precipitation. Under modern conditions this precipitation does not reach the Namibian Kalahari (Cockcroft et al., 1987; Tyson et al., 1996; Nicholson, 2000; Chase and Meadows, 2007).

The studied Koës Pan is located at the southwestern margin of the Kalahari close to the village of Koës in the ǁKaras Region. The size of the pan is 11.3 km², its catchment, based on local geomorphology, extends over 218 km² and features prominent flow structures (Figure 3-2; Schüller et al., 2018). Vegetation surrounding the pan is dominated by shrubs and grasses. Shrub density is enhanced closer to the pan shore. The surrounding area is utilized as rangeland. Average annual precipitation is about 174 mm, 85 % thereof fall between December and April peaking in February (climate-data.org, 2020). The pan is

embedded in calcretes and sands of the Paleogene Kalahari group (Lancaster, 1986). Sediments are dominated by medium to coarse silts with a mean grain size of 52.5 µm. Koës Pan sediments mainly consist of quartz, feldspar, and to a minor degree illite and smectite. They also contain evaporate minerals, mainly gypsum, halite, sepiolite and dolomite (Schüller et al., 2018). A more detailed description of pan sedimentology can be found in Schüller et al. (2018). During dry phases, the pan surface consists of an even crust with desiccation cracks. During the rainy season water accumulates in the pan for short periods (several days to weeks). This is accompanied by sediment transfer from the catchment into the pan. Under dry conditions the crust hardens and seals the pan against considerable dust emissions (Milewski et al., 2017). However, Koës Pan features lunette dunes at the southeastern rim of the pan (Figure 3-2). These dunes are usually considered to be caused by pan deflation processes but can also consist of reworked lunette dunes (Lancaster, 1978; Telfer and Thomas, 2006). A recent study which dated sediments from five Kalahari pans, showed that almost all analysed pans feature a continuous net accumulation of sediment (Schüller et al., 2018; Schüller and Wehrmann, 2018).
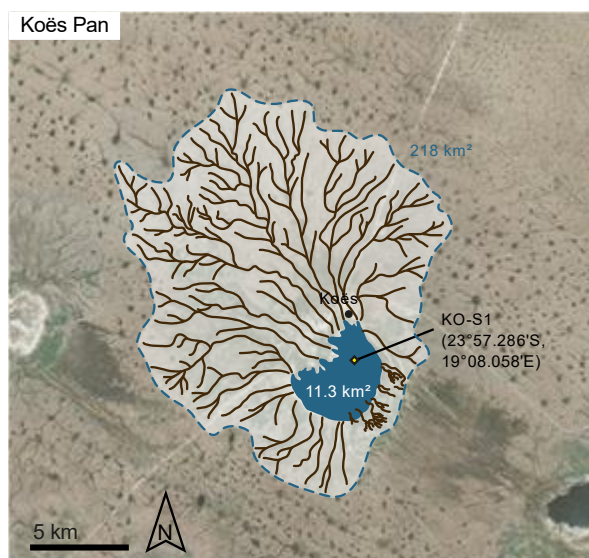
Figure 3-2. Koës Pan with spatial extension and size of the catchment area (modified after Schüller et al., 2018).

The vegetation in southeastern Namibia consists mainly of Xeric Savanna and Nama Karoo biome (Figure 3-1B). Koës Pan is located within the Xeric Savanna Biome close to the Nama Karoo in the Dwarf Shrub Savanna ecoregion and close to the boundary to the Mixed Tree and Shrub Savanna (Rutherford et al., 2005; Rutherford et al., 2006). While the latter of these two ecoregions is completely part of the Xeric Savanna biome, the Dwarf Shrub Savanna also overlaps with the Nama Karoo and Namibian Savanna Woodlands. Important shrub and tree species in these ecoregions are *Senegallia mellifera*, *Vachellia erioloba* and *Requienia sphaerosperma*, graminoids include *Schmidtia kalahariensis*, *Stipagrostis ciliata* and *Stipagrostis uniplumis* (Bester et al., 2003; Rutherford et al., 2005; Mucina and Rutherford, 2006).

Vegetation assemblage in southern Africa is variable and controlled by water availability, altitude, evaporation, and minimum temperature (Rutherford et al., 2006). Grass cover and shrub density are influenced by factors like wildfire, frost and phases of lower or higher precipitation (Joubert et al., 2008; Tabares et al., 2020).

3.3 Methods

3.3.1 Sampling and sample preparation

Sampling took place during dry season (September 2016) in the northern part of Koës Pan (Figure 3-2, 23°57.286'S, 19°08.058'E). Samples were gathered from a small profile pit. The bottom of the pit was reached at a depth of 77 cm where a sandstone basement was found. The sample of the hard surface crust comprises the uppermost 4 cm. All other sediments until a depth of 72 cm below surface were sampled in 1 cm intervals. The groundwater table was not reached. After recovery, samples for organic geochemistry analyses were wrapped in aluminium foil and then put in plastic bags on location. For longer storage, samples were transferred to glass vials and kept at 4°C.
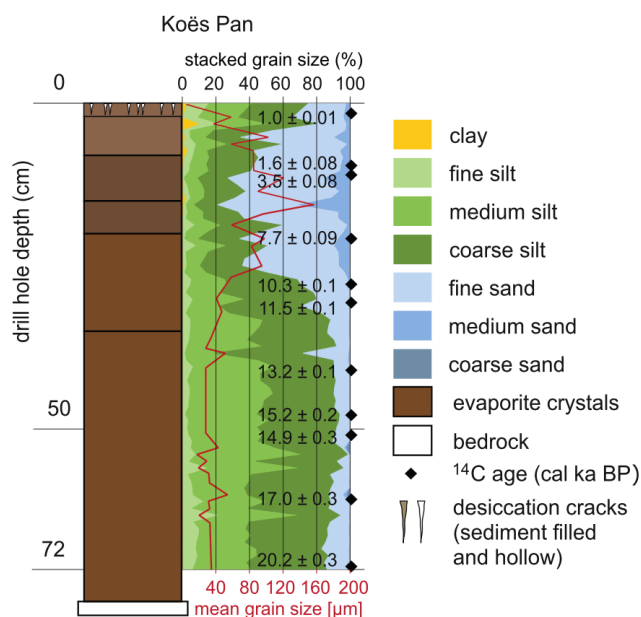
Figure 3-3. Sediment profile of Koës Pan with calibrated ^{14}C ages, stacked grain size distribution and mean grain size (red line). Sediment colours were taken according to the Munsell soil colour chart (modified after Schüller et al., 2018).

3.3.2   Age-depth model

An age depth relation model of the profile has been established in an earlier study (Figure 3-3; Schüller et al., 2018), based on 11 calibrated ^{14}C ages using the Bacon 2.2 software package for R (Figure 3-4; Blaauw and Christen, 2011). The pan features a continuous net sediment accumulation and displays no signs for hiatuses. The oldest sample dates back until 19.9 ka BP (Schüller and Wehrmann, 2018).
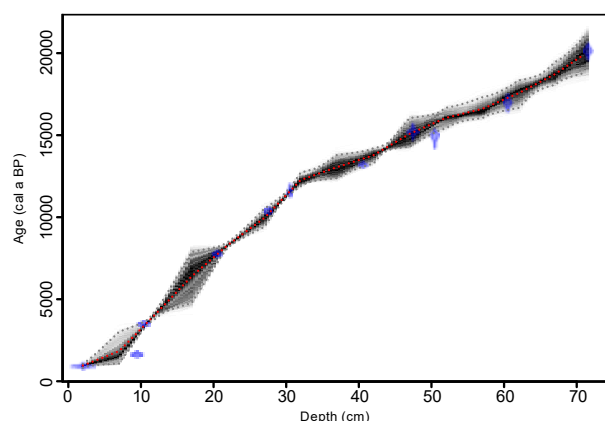
Figure 3-4. Age-depth model for Koës Pan sediments (modifed after Schüller et al., 2018).

3.3.3 Elemental analysis and bulk stable isotopes

Before analyses, samples were freeze-dried and homogenized. For determination of total carbon (TC) and total nitrogen (TN) contents samples were wrapped in tin capsules and analysed using a Vario El Cube elemental analyser from Elementar. For TIC analyses samples were treated with perchloric acid (2N) and CO_2 was measured using a carbon-sulfur-determinator C/S 580 from Eltra. TOC was calculated as the difference of TC and TIC contents.

For bulk $\delta^{13}C_{org}$ analyses samples were decalcified using HCl (2 mol/l), dried afterwards at 80°C and wrapped in tin capsules. Measurements were performed using an elemental analyser (1108 from Carlo Erba) coupled to a MAT 252 isotope ratio mass spectrometer from Thermo Fisher Scientific. For calibration, a certified isotope standard (IAEA CH-6 with a $\delta^{13}C$ value of −10.45‰) was used. Instrument performance was checked using a sediment reference sample with a $\delta^{13}C_{org}$ value of −26.07‰ (IVA), see also Belz et al. (2020). All samples were measured at least twice. The standard deviation for replicate analyses was ± 0.5‰.

3.3.4 Lipid extraction and liquid chromatography

Lipid extraction was done using a SpeedExtractor from Büchi with a solvent mixture of dichloromethane and methanol (9/1) at 70°C and 70 bar. *n*-Hexane-insoluble components were removed by filtration over $NaSO_4$ after adding a 40 times excess of *n*-hexane. Squalane was added as internal standard for quantification. The extract was separated into aliphatic hydrocarbons, aromatic hydrocarbons and a fraction containing nitrogen, sulphur and oxygen (NSO) compounds by medium pressure liquid chromatography (MPLC; Radke et al., 1980).

3.3.5 Gas chromatography

The saturated hydrocarbon fractions were analysed using a 6890 gas chromatograph (GC) from Agilent equipped with a high temperature capillary column (J&W DB-5HT, 30 m × 25 mm, 0.1 µm film thickness), a cold injection system, and a flame ionization detector (FID). The carrier gas was helium. The injector temperature was initially set to 60°C, increased to 350°C at a rate of 600°C/min and held at that temperature for 1 min. The initial temperature of the GC oven was 60°C held for 2 min, then heated at a rate of 3°C/min to 350°C and held for 15 min. *n*-Alkanes were identified by comparison of retention times to those of reference standards. For quantification of individual compounds, the FID signal was used relative to that of the internal standard. All samples were extracted and analysed in a random sequence.

3.3.6 Gas chromatography-isotope ratio mass spectrometry

Compound-specific carbon isotope compositions were measured using an Agilent 6890 gas chromatograph coupled to a MAT 253 isotope ratio mass spectrometer from Thermo Fisher scientific. GC conditions were analogous to those described in section 3.5 except the temperature programme. Injector temperature started at 60°C, increased to 305°C at a rate of 600°C/min and then held for 2 min. The initial temperature of the GC oven was 60°C held for 2 min, then heated at a rate of 3°C/min to 300°C and held for 18 min. Compound-specific hydrogen isotope compositions were measured using an Agilent 7890 gas chromatograph coupled to a Delta V plus isotope ratio mass spectrometer from Thermo Fisher Scientific. Conditions were as described in Belz et al. (2020). All samples were analysed at least in duplicate, hydrogen isotopes in triplicate. Results are given in delta notation in per mil vs. Vienna Pee Dee Belemnite (VPDB) for carbon and Vienna Standard Mean Ocean Water (VSMOW) for hydrogen.

δD values were corrected for the ice-volume effect for comparison of glacial vs. interglacial samples analogous to Belz et al. (2020). Enrichment of δD was deduced via $\delta^{18}O$ values using the global meteoric water line (Craig, 1961). Palaeo-$\delta^{18}O$

values of seawater were estimated using the LR04 global benthic isotope stack (Lisiecki and Raymo, 2005).

3.4 Results

3.4.1 Bulk parameters

The TOC content is constantly low and varies between 0.05 and 0.19 % with an average of 0.11 ± 0.03 % (Table 3-1). Rather elevated TOC concentrations ($\geq$ 0.12 %) are found in samples from 1.6 to 3.9 ka BP, at 8.5 ka BP and from 14.7 to 19.2 ka BP (Figure 3-5E). Low concentrations (≤ 0.09 %) are observed in samples within a time span from 5.7 to 13.4 ka BP. TIC concentrations vary between 0.1 % and 1.1 %, with an average of 0.18 ± 0.3 %. Relatively low values (< 0.9 %) occur in samples younger than 12.3 ka BP with a minimum between 3.4 and 7.0 ka BP (Table 3-1). Older samples show elevated TIC contents $\geq$ 0.9 % (Figure 3-5B). Bulk organic carbon isotope values vary from -19.0 to -16.9 ‰ over most parts of the core (Table 3-1). There are two sections with lower $\delta^{13}C_{org}$ values < -20.0 ‰ (from 6.6 to 7.7 ka BP and from 13.9 to 17.9 ka BP) with a minimum value of -21.1 ‰ at 15.7 ka BP (Figure 3-5F). Total nitrogen concentrations have been analysed but are below the threshold required for reliable values (0.05 %).

3.4.2 Distributions of *n*-alkanes

All samples contain *n*-alkanes with chain lengths from C_{19} to C_{35} with an average total concentration of 9502±4508 µg/g TOC. Distributions show a significant odd-over-even predominance which is visible in the average value of the carbon preference index (CPI_{27-33}) of 9.15±1.00 (Figure 3-9B; Cooper and Bray, 1963):

$$CPI_{27-33} = 0.5 \times \left(\frac{[n\text{-}C_{27}] + [n\text{-}C_{29}] + [n\text{-}C_{31}] + [n\text{-}C_{33}]}{[n\text{-}C_{26}] + [n\text{-}C_{28}] + [n\text{-}C_{30}] + [n\text{-}C_{32}]} \right) + 0.5 \times \left(\frac{[n\text{-}C_{27}] + [n\text{-}C_{29}] + [n\text{-}C_{31}] + [n\text{-}C_{33}]}{[n\text{-}C_{28}] + [n\text{-}C_{30}] + [n\text{-}C_{32}] + [n\text{-}C_{34}]} \right)$$

For comparison the average chain length (ACL$_{27-33}$) was calculated for the same carbon number range (Meyers, 2003):

$$ACL_{27-33} = \frac{27 \times [n\text{-}C_{27}] + 29 \times [n\text{-}C_{29}] + 31 \times [n\text{-}C_{31}] + 33 \times [n\text{-}C_{33}]}{[n\text{-}C_{27}] + [n\text{-}C_{29}] + [n\text{-}C_{31}] + [n\text{-}C_{33}]}$$
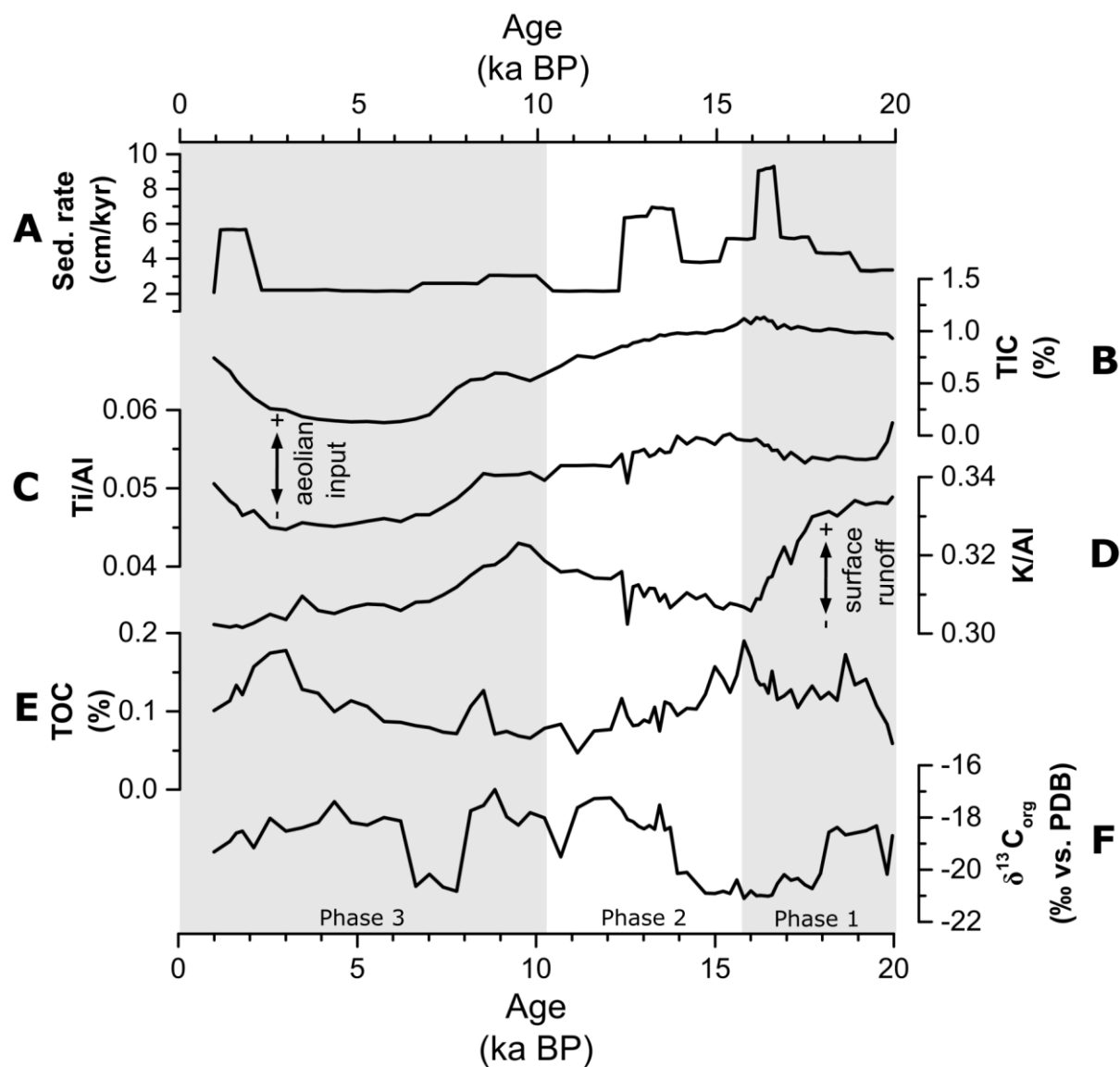
Figure 3-5. Bulk parameters of Koës Pan. A. sedimentation rate, B. TIC, C. Ti/Al ratio (Schüller and Wehrmann, 2018) TIC, D. K/Al ratio (Schüller and Wehrmann, 2018), E. TOC, F. δ^{13}C$_{org}$. Grey and white background indicate Phases 1, 2 and 3 which are described in detail in the text.

Table 3-1. Bulk parameters of Koës Pan.

av. Depth (cm)	Age (ka)	TOC (%)	$\delta^{13}C_{org}$ (‰)	TIC (%)
2	1.0	0.10	-19.32	0.74
4.5	1.4	0.11	-18.92	0.62
5.5	1.6	0.13	-18.59	0.53
6.5	1.8	0.12	-18.52	0.46
7.5	2.1	0.16	-19.15	0.36
8.5	2.5	0.17	-18.03	0.26
9.5	3.0	0.18	-18.53	0.24
10.5	3.4	0.13	-18.39	0.18
11.5	3.9	0.12	-18.19	0.16
12.5	4.3	0.10	-17.40	0.14
13.5	4.8	0.11	-18.19	0.13
14.5	5.2	0.11	-18.30	0.13
15.5	5.7	0.09	-18.00	0.12
16.5	6.2	0.09	-18.13	0.13
17.5	6.6	0.08	-20.63	0.16
18.5	7.0	0.08	-20.17	0.20
19.5	7.4	0.07	-20.67	0.33
20.5	7.7	0.07	-20.83	0.45
21.5	8.1	0.11	-17.74	0.53
22.5	8.5	0.13	-17.53	0.54
23.5	8.8	0.07	-16.92	0.60
24.5	9.1	0.07	-17.96	0.60
25.5	9.5	0.07	-18.29	0.56
26.5	9.8	0.07	-17.82	0.52
27.5	10.2	0.08	-18.01	0.59
28.5	10.7	0.08	-19.51	0.67
29.5	11.1	0.05	-17.63	0.76
30.5	11.6	0.07	-17.27	0.75
31.5	12.0	0.08	-17.25	0.81
32.5	12.3	0.12	-17.68	0.85
33.5	12.5	0.09	-18.08	0.86
34.5	12.7	0.08	-18.16	0.89
35.5	12.8	0.08	-18.33	0.90
36.5	13.0	0.09	-18.44	0.92
37.5	13.1	0.09	-18.31	0.91
38.5	13.3	0.11	-18.45	0.93
39.5	13.4	0.08	-17.51	0.96
40.5	13.6	0.11	-18.48	0.96
41.5	13.7	0.11	-18.37	0.97
42.5	13.9	0.09	-20.15	0.98
43.5	14.2	0.10	-20.10	0.98
44.5	14.4	0.10		0.99
45.5	14.7	0.12	-20.90	0.98
46.5	15.0	0.16	-20.91	1.00
47.5	15.2	0.14	-20.83	1.01

Table 3-1 continued.

av. Depth	Age	TOC	$\delta^{13}C_{org}$	TIC
(cm)	(ka)	(%)	(‰)	(%)
47.5	15.2	0.14	-20.83	1.01
48.5	15.4	0.12	-20.91	1.04
49.5	15.6	0.15	-20.38	1.06
50.5	15.8	0.19	-21.10	1.12
51.5	16.0	0.17	-20.81	1.07
52.5	16.1	0.14	-21.00	1.13
53.5	16.2	0.13	-20.99	1.12
54.5	16.3	0.13		1.14
55.5	16.4	0.12	-21.01	1.10
56.5	16.5	0.15	-20.97	1.10
57.5	16.7	0.12	-20.54	1.02
58.5	16.9	0.12	-20.19	1.06
59.5	17.1	0.13	-20.41	1.02
60.5	17.3	0.10	-20.33	1.05
61.5	17.5	0.12	-20.58	1.03
62.5	17.7	0.13	-20.72	1.01
63.5	17.9	0.12	-20.14	1.00
64.5	18.1	0.12	-18.56	1.02
65.5	18.4	0.11	-18.37	1.02
66.5	18.6	0.17	-18.66	1.00
67.5	18.9	0.13		0.99
68.5	19.2	0.14	-18.50	0.99
69.5	19.5	0.11	-18.31	0.98
70.5	19.8	0.08	-20.17	0.98
71.5	19.9	0.06	-18.69	0.93

ACL_{27-33} ranges from 30.3 to 31.2 (Figure 3-9A). In all samples long chain n-alkanes (C_{27}-C_{33}) dominate, with n-C_{31} being always the most abundant homologue with an average concentration of 3375±1466 µg/g TOC (Table 3-2, Figure 3-7). All long chain homologues are higher in concentration in samples older than 8 ka and lower in younger samples (Figure 3-7A). n-Alkane distributions in all samples show a stable pattern n-C_{31} > n-C_{33} > n-C_{29} > n-C_{27} (Figure 3-6). Despite this stable pattern there is a distinctive variation in relative concentrations between the intervals from 1-10.2 ka BP (Phase 3), 10.7-15.6 ka BP (Phase 2) and 15.8-19.9 ka BP (Phase 1): the youngest phase displays the highest relative concentration of n-C_{31} which is above 40% in all samples (Figure 3-6). Both the youngest and the middle phases feature concentrations of n-C_{33} which are about twice compared to n-C_{29}, while concentration of both homologues is about equal in Phase 1. To highlight

relative changes between the homologues n-C$_{29}$ and n-C$_{33}$ a ratio was calculated modified after Carr et al. (2014):

$$\text{Norm33} = \frac{[n\text{-C}_{33}]}{[n\text{-C}_{29}] + [n\text{-C}_{33}]}$$

Norm33 values range from 0.40 to 0.72 (Table 2). There is a strong shift from higher values (above 0.55, from the youngest sample until 16.6 ka BP) to lower values (below 0.55, between 16.7 and 19,9 ka BP; Figure 3-9C).

The relative abundances of n-C$_{29}$, n-C$_{31}$ and n-C$_{33}$ are displayed in a ternary diagram (**Figure 3-8**B). Within each of the three phases defined above, values have a steady development (**Figure 3-8**B). While in Phase 3, samples form a cluster with a diffuse distribution, the plot illustrates 2 legs of linear variation change over time from 19.9 until 10.7 ka BP. This is recognised in Phase 1 by a decrease of the relative abundance of n-C$_{29}$ and n-C$_{31}$ while n-C$_{33}$ rises. In Phase 2 a continuous increase of n-C$_{31}$, a steady concentration of n-C$_{29}$ and a lowering content of n-C$_{33}$ follows.

3.4.3 Stable carbon and hydrogen isotope values of n-alkanes

The carbon isotopic composition of long chain n-alkanes (C$_{27}$ to C$_{33}$) displays δ^{13}C values from –25.5 ‰ to –21.6 ‰. In samples younger than 16 ka BP, n-alkanes with chain lengths C$_{29}$ – C$_{33}$ lie generally in the same range with lowest values for δ^{13}C$_{31}$. Older samples display higher δ^{13}C values for n-C$_{33}$, medium values for n-C$_{31}$ and lower values for n-C$_{29}$ (Fig. 6B). To estimate species richness and woody cover LEWIS$_{29\text{-}33}$ and $^{31}f_{\text{woody}}$ indices were calculated according to Magill et al. (2019):

$$\text{LEWIS}_{29\text{-}33} = \max|\delta^{13}\text{C}_{29\text{-}33}| - \min|\delta^{13}\text{C}_{29\text{-}33}|$$

$$^{31}f_{\text{woody}} = \{\sin(-1.8353 - 0.0838 * {}^{13}\text{C}_{31})\}^2$$
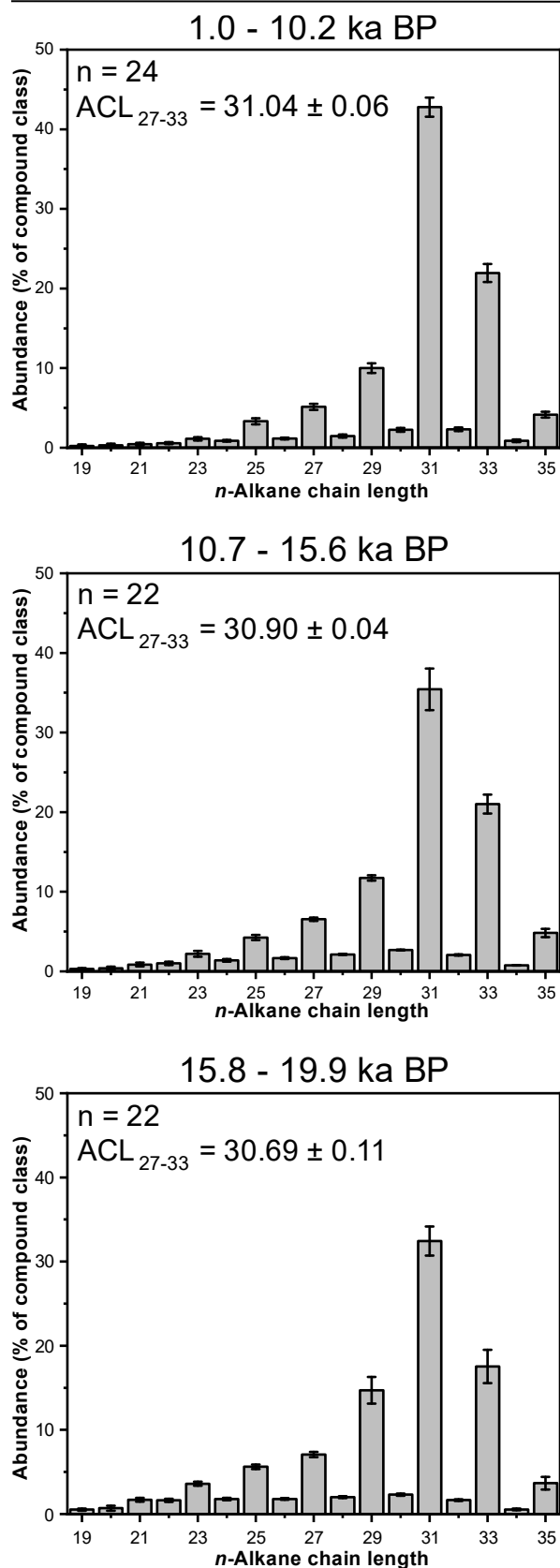
Figure 3-6. Relative chain length distributions of n-alkanes and mean average chain lengths (ACL$_{27\text{-}33}$) of samples from the timespans: A. 1.0-10.2 ka BP, B. 10.7-15.6 ka BP, C. 15.8-19.9 ka BP

.

Table 3-2. Leaf wax proxies in Koës Pan sediment samples.

av. Depth (cm)	Age (ka)	Σ-n-Alkanes (C$_{17-35}$) µg/g$_{TOC}$	ACL (27-33)	Norm33	CPI (27-33)	$\delta^{13}C_{31}$ (‰)	LEWIS (29-33)	$^{31}f_{woody}$	δD_{31} (‰)	δD_{31IC} (‰)
2	1.0	1228.6	31.1	0.69	10.5	-25.5	1.29	0.08	-165.8	-165.8
4.5	1.4	2187.1	31.2	0.73	11.6				-158.2	-158.2
5.5	1.6	1814.5	31.1	0.71	11.2				-162.1	-162.1
6.5	1.8	1491.8	31.0	0.67	11.7	-24.9	0.58	0.08	-180.4	-180.4
7.5	2.1	1890.0	31.1	0.71	11.8				-170.5	-170.5
8.5	2.5	1910.6	31.1	0.70	12.7				-164.6	-164.8
9.5	3.0	1754.9	31.1	0.71	13.2	-25.0	1.16	0.09	-168.1	-168.3
10.5	3.4	2178.2	31.1	0.70	11.9				-166.6	-166.8
11.5	3.9	3083.1	31.1	0.71	11.9				-165.8	-166.0
12.5	4.3	3211.4	31.1	0.71	12.3	-24.9	1.15	0.08	-138.1	-138.3
13.5	4.8	2656.9	31.1	0.70	12.0				-161.9	-162.2
14.5	5.2	2806.8	31.0	0.69	11.5	-25.1	0.92	0.09	-160.8	-161.1
15.5	5.7	3374.6	31.1	0.71	12.2				-164.1	-164.6
16.5	6.2	3092.9	31.0	0.69	11.6				-163.3	-163.8
17.5	6.6	3725.2	31.0	0.68	12.3	-24.6	0.88	0.07	-163.4	-164.1
18.5	7.0	5114.9	31.0	0.68	7.9				-169.0	-169.8
19.5	7.4	4052.8	30.9	0.63	11.5				-153.1	-154.0
20.5	7.7	5723.0	31.0	0.66	11.3	-24.8	1.08	0.08	-152.7	-153.7
21.5	8.1	4390.4	31.0	0.66	11.0	-24.3	0.65	0.06	-147.8	-149.0
22.5	8.5									
23.5	8.8	8910.8	31.0	0.67	11.2	-24.8	0.84	0.08	-149.0	-150.6
24.5	9.1	9530.6	31.0	0.68	11.0				-145.6	-147.5
25.5	9.5	10982.3	31.1	0.68	10.8				-153.4	-155.6
26.5	9.8	9950.9	31.0	0.66	10.4	-25.1	1.12	0.09	-146.2	-148.7
27.5	10.2	10715.4	31.0	0.66	10.3	-24.5	0.78	0.07	-145.8	-148.7
28.5	10.7	8268.6	30.9	0.62	9.6	-24.8	0.94	0.08	-152.8	-156.0

Table 3-2 continued.

av. Depth (cm)	Age (ka)	Σ-n-Alkanes (C$_{17-35}$) µg/g$_{TOC}$	ACL (27-33)	Norm33	CPI (27-33)	$\delta^{13}C_{31}$ (‰)	LEWIS (29-33)	$^{31}f_{woody}$	δD_{31} (‰)	δD_{31IC} (‰)
29.5	11.1	15287.9	30.8	0.60	9.4				-148.3	-151.9
30.5	11.6	11306.3	30.9	0.64	9.9	-24.8	0.98	0.08	-147.4	-151.6
31.5	12.0	9519.6	30.8	0.61	9.4				-144.5	-149.3
32.5	12.3	11404.0	30.8	0.61	9.5	-24.5	0.98	0.07	-148.3	-153.3
33.5	12.5	11278.0	30.9	0.64	9.7	-24.6	0.84	0.07	-146.2	-151.4
34.5	12.7	12312.1	30.9	0.63	9.5	-24.5	0.86	0.06	-147.5	-152.9
35.5	12.8	12195.5	30.8	0.62	9.1	-24.3	0.70	0.06	-146.2	-151.7
36.5	13.0	12213.5	30.9	0.64	9.3					
37.5	13.1	13666.9	30.9	0.64	9.1	-24.3	1.10	0.06	-146.6	-152.3
38.5	13.3	10586.8	30.9	0.64	9.0					
39.5	13.4	16052.7	30.9	0.65	9.1					
40.5	13.6	10901.8	30.9	0.64	9.3	-24.5	1.18	0.06	-151.2	-157.4
41.5	13.7	9431.9	30.9	0.66	9.2				-141.0	-147.3
42.5	13.9	10184.3	30.9	0.65	9.2					
43.5	14.2	13846.8	30.9	0.66	9.1	-24.1	0.80	0.05	-145.7	-152.5
44.5	14.4	15987.7	31.0	0.67	9.1					
45.5	14.7	11694.9	30.9	0.66	9.0				-148.6	-155.9
46.5	15.0	8861.6	31.0	0.66	9.0	-24.1	0.93	0.05	-132.6	-140.2
47.5	15.2	10733.0	30.9	0.66	8.9	-24.1	0.51	0.05	-138.4	-146.1
48.5	15.4	12932.4	30.9	0.66	8.9	-24.1	0.91	0.06	-132.4	-140.1
49.5	15.6	11601.2	30.9	0.66	8.9	-24.3				
50.5	15.8	9044.5	30.9	0.65	8.8					
51.5	16.0	10931.7	30.9	0.65	9.0	-24.5	0.52	0.07	-140.5	-148.4
52.5	16.1	11749.8	30.9	0.63	9.0				-159.7	-167.6
53.5	16.2	15101.5	30.8	0.61	9.0	-23.9	0.92	0.04	-154.7	-162.6

Table 3-2 continued.

av. Depth	Age	Σ-*n*-Alkanes (C$_{17-35}$)	ACL	Norm33	CPI	δ^{13}C$_{31}$	LEWIS	$^{31}f_{woody}$	δD$_{31}$	δD$_{31IC}$
(cm)	(ka)	μg/g$_{TOC}$	(27-33)		(27-33)	(‰)	(29-33)		(‰)	(‰)
54.5	16.3	14212.0	30.8	0.62	9.1	-23.7	1.09	0.04	-144.5	-152.5
55.5	16.4	12731.8	30.8	0.59	9.4	-24.2	1.00	0.05	-135.3	-143.3
56.5	16.5	10859.1	30.7	0.58	9.6	-24.6	1.91	0.07	-135.8	-143.8
57.5	16.7	14797.7	30.6	0.52	9.9	-24.0	2.23	0.05	-136.5	-144.5
58.5	16.9	14309.0	30.6	0.52	10.0				-135.9	-143.9
59.5	17.1	12765.9	30.6	0.53	10.3					
60.5	17.3	15191.0	30.6	0.51	10.4	-24.3	2.45	0.06	-131.7	-139.8
61.5	17.5	13192.8	30.6	0.52	10.5					
62.5	17.7	11537.3	30.6	0.51	10.7					
63.5	17.9	14457.4	30.6	0.51	10.7	-24.1	2.62	0.05	-138.4	-146.6
64.5	18.1	12853.8	30.6	0.50	10.8				-131.9	-140.1
65.5	18.4	14488.3	30.6	0.51	10.8					
66.5	18.6	9569.2	30.6	0.50	10.7	-24.2	2.55	0.05	-135.8	-144.1
67.5	18.9	12022.2	30.6	0.50	10.9					
68.5	19.2	9881.2	30.6	0.50	10.9	-24.2	2.62	0.05	-136.7	-145.1
69.5	19.5	14209.5	30.6	0.50	11.1	-24.9			-132.6	-140.9
70.5	19.8	15049.0	30.6	0.50	11.0				-134.1	-142.5
71.5	19.9	14232.7	30.6	0.48	10.9		1.74	0.08	-164.0	-172.4

LEWIS$_{29\text{-}33}$ values display a range from 0.51 to 2.62 (Table 3-2). In samples younger than 16.5 ka BP values stay well below 1.3, while all values of older samples are above 1.9 except the oldest sample (1.7). Values of $^{31}f_{woody}$ vary from 3.59% to 9.19%, with high values in samples younger than 10 ka BP and a slightly decreasing trend with rising age (Table 3-2). The measured hydrogen isotopic composition of long chain n-alkanes (C$_{27}$ to C$_{33}$) varies from –220.6‰ to –131.7‰. There is a general trend towards higher values from younger to older samples for all n-alkane homologues analyzed, except for one low outlier at 19.9 ka and one high outlier at 4.3 ka (Figure 3-7C). The ice corrected δD_{31} values follow this trend in three relatively stable levels from 1 to 7 ka BP (average –164.2±8.2‰), 7 to 14.7 ka BP (average –152.0±2.8‰) and from 15.0 to 20.0 ka BP (average –147.6±9.3‰).

3.5 Discussion

3.5.1 Reconstruction of environmental conditions

3.5.1.1 Aeolian input vs. surface runoff

In general, TOC contents in samples from Koës Pan are all lower compared to samples of the 250 km northward located Omongwa Pan, which has TOC contents varying from 0.2 % to 1.4 % with an average of 0.7 %. The ranges of TIC in samples from Omongwa Pan is larger (0.2 % - 4.9 %) and the average (1.7 %) is almost 10 times higher compared to samples of this study (Belz et al., 2020). This is also the case for sedimentation rate, K/Al and Ti/Al values (Schüller et al., 2018; Schüller and Wehrmann, 2018). These differences also oppose the catchment/pan size ratio which is 7.8 for Omongwa Pan and 19.3 for Koës Pan, and therefore point to an average lower net input of material at Koës Pan (Schüller et al., 2018).

Elevated values of sedimentation rate at Koës Pan correlate with low K/Al values and relatively high Ti/Al values (Figure 3-5; Schüller and Wehrmann, 2018). This can point to a relatively minor role of surface runoff in the pan though variations in TI/Al and K/Al ratios are very low over the whole record.

The content of inorganic carbon in playa sediments is usually controlled by groundwater discharge, surface runoff or detrital input of carbonate (Rosen, 1994;

Roy et al., 2008). Belz et al. (2020) regarded increased TIC contents as result of repeated evaporation events in Omongwa Pan and therefore as an indicator for surface runoff. In Koës Pan sediments, however, the TIC values correlate remarkably with Ti/Al values, which are regarded as a proxy for aeolian input (Figure 3-5; Niedermeyer et al., 2009; Weldeab et al., 2013; Clift et al., 2014; Schüller et al., 2018). In contrast to Omongwa Pan, Koës Pan does not feature carbonates directly at the pan rim which is reflected in distinctively lower TIC values (Genderjahn et al., 2018b; Belz et al., 2020). The carbonate content in Koës Pan likely originates from aeolian input of carbonate dust eroded from local calcretes.

3.5.1.2 Changes in vegetation

n-Alkane distributions in Koës Pan sediments, as reflected by ACL and CPI values, are in the same range as those of Omongwa Pan sediments from the Kalahari and soil samples from Savanna, Fynbos and Nama Karoo biomes (Herrmann et al., 2016; Belz et al., 2020) and from southern African plants (Rommerskirchen et al., 2006b; Vogts et al., 2009; Carr et al., 2014). Longer chain lengths of n-alkanes within the same species have been attributed to dryer and or warmer conditions (Bush and McInerney, 2013). Other interpretations attribute n-C_{29} more to trees and n-C_{33} more to grasses (Howard et al., 2018).

The variation of relative distribution between n-C_{29}, n-C_{31} and n-C_{33} as depicted in Figure 3-8B is quite extraordinary. Ternary diagrams of relative long chain n-alkane concentrations are displayed in several studies, especially to assess sediment paleorecords (e.g. Schwark et al., 2002; Zhang et al., 2006; Jambrina-Enríquez et al., 2016; Belz et al., 2020), transects of soils or sediments (Rommerskirchen et al., 2003; Rommerskirchen et al., 2006a; Bush and McInerney, 2015; Herrmann et al., 2016) or plant samples (Bush and McInerney, 2013; Lemma et al., 2019). They are commonly used to picture a division or overlapping of samples, from one or several locations/plant types. Comparison of plants or soils often show a strong scattering of similar samples and a large overlapping of different sources (Bush and McInerney, 2015; Herrmann et al., 2016). Even in diagrams from one archive, where samples scatter less, clusters

tend to largely overlap (Schwark et al., 2002; Zhang et al., 2006; Jambrina-Enríquez et al., 2016) or show separated clusters (Belz et al., 2020). In the data from Koës Pan, the variation of relative distribution between n-C$_{29}$, n-C$_{31}$ and n-C$_{33}$ is relatively small compared to biome soil samples (Figure 3-8A). Yet, during Phase 1 and Phase 2, samples do not cluster and overlap only slightly with samples of similar ages but follow almost linear trends marking continuous change. This is only visible due to the high sub-millennial resolution of the record and underlines the uniqueness of the Koës Pan record.

At the beginning of Phase 1 n-alkane distribution compares best with soil samples from the Fynbos biome (Herrmann et al., 2016). Some studies proposed an intracontinental extension of the coastal Fynbos biome during the northward expanded winter rainfall (Chase and Meadows, 2007; Shi et al., 1998, 2000). Despite this, a record at Pella indicated that the expansion of Fynbos did not reach the southern border of Namibia (Lim et al., 2016). However, the alkane distribution could possibly point to a comparable vegetation assemblage and/or environmental conditions to the area of the modern Fynbos biome, which is dominated by colder temperatures and where precipitation occurs mainly during winter month.

The steady shift towards a higher fraction of n-C$_{33}$ and the rise of the ACL in Phase 1 can be attributed to drier and/or warmer conditions during growing season. Shifts in the C$_3$/C$_4$ ratio as a cause for these changes are rather unlikely, as compound-specific carbon isotopes variations are minor only (Figure 3-7B). This does not exclude other changes within the vegetation assemblage as causing factors though. This could indicate an approximation towards the Savanna biome. The further development during Phase 2 and Phase 3 corresponds most to soil samples from the Nama Karoo Biome (Figure 3-8A; Herrmann et al., 2016). A shift from the Savanna towards Nama Karoo biome would reflect a change towards dryer conditions (Rutherford et al., 2006). Northward expansions of the Nama Karoo Biome have been associated with cooler conditions or with seasonal moisture shifts, which lowered the proportions of relative summer rain and total rainfall (Scott and Nyakale, 2002; Mucina and Rutherford, 2006). Nevertheless, the soil samples used for this comparison originate from biomes with huge sizes and

variations of environmental conditions within them. There is also a rather large

overlapping of biomes (Herrmann et al., 2016).
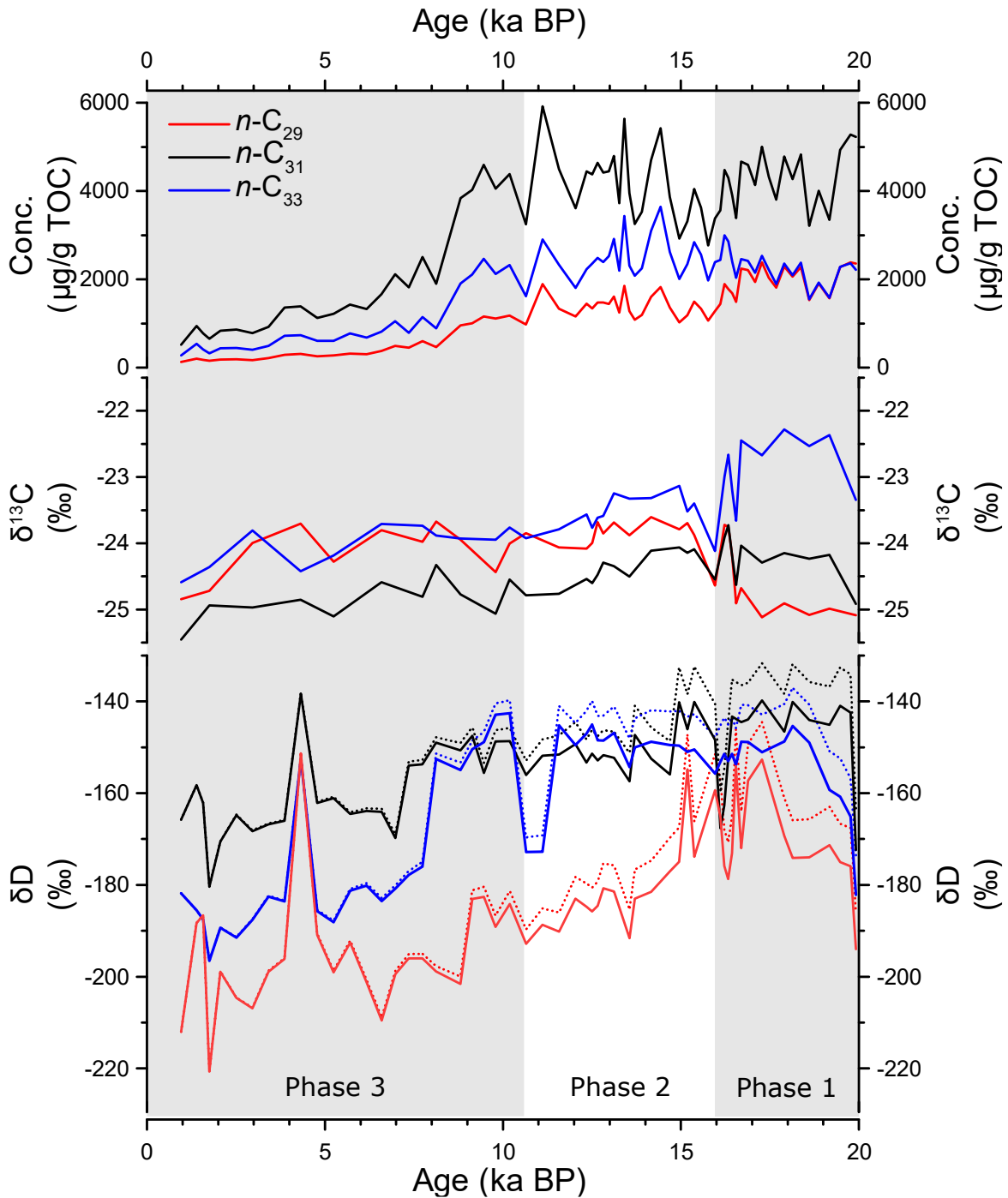
Figure 3-7. Isotopic parameters of Koës Pan n-alkanes. A. Concentrations of n-C$_{29}$, n-C$_{31}$ and n-C$_{33}$, B. Compound-specific carbon isotope values of n-C$_{29}$, n-C$_{31}$ and n-C$_{33}$. C. Compound-specific hydrogen isotope values of n-C$_{29}$, n-C$_{31}$ and n-C$_{33}$, without (dotted line) and with ice volume correction (line). Grey and white background indicate Phases 1, 2 and 3 which are described in detail in the text.

The continuous change in relative distribution between n-C_{29}, n-C_{31} and n-C_{33} in samples before 11 ka BP displays a much greater variation than the ACL_{27-33} record can reveal (Figure 3-8B, Figure 3-9A). The variation in Phase 1 before 17 ka BP is not visible in the ACL_{27-33} at all, the continuous shift over Phase 2 only to a minor extent. Only the abrupt change in the latter half of Phase 1 between 17 and 16 ka BP is visible as a larger increase. This highlights the limits of a numerical parameter like the ACL, where variations of individual n-alkane homologues can be hidden in the calculated average.

Compared to average compound-specific $\delta^{13}C$ values of sediments from Omongwa Pan (25.1 ‰-21,6 ‰), which also lies in the Savanna biome, average values from Koës Pan are higher indicating a higher influence of C_4 plants. In leaf waxes of southern African C_3 and C_4 plants the most abundant n-alkane is n-C_{31}. Thus, $\delta^{13}C_{31}$ values are best suited to identify changes in the vegetation assemblage (Rommerskirchen et al., 2006b; Vogts et al., 2009; Badewien et al., 2015b).

In general, the variation of $\delta^{13}C_{31}$ values is so low, that there is no sign for major shifts regarding the C_3/C_4 ratio over the studied period (Figure 3-9D). Despite this, there are visible changes in $\delta^{13}C_{29}$ and $\delta^{13}C_{33}$ during Phase 1 indicating a change in conditions (Figure 3-7B). We conclude that the contribution of C_3 plants to n-C_{33} must have been slightly higher after 16 ka BP indicating possibly dryer conditions during growing season leading to lower values of $\delta^{13}C_{33}$. Another factor which can be an explanation for the increase of $\delta^{13}C_{29}$ values after 16 ka BP could be a lower ^{13}C fractionation of C_3 plants, which is reported for dryer and warmer conditions in Africa due to stomata closure (Garcin et al., 2014). A shift at the same time is visible in the $LEWIS_{29-33}$ values, with a strong decrease possibly marking a drop in species richness. The steady trend of $^{31}f_{woody}$ values from 19 to 15 ka BP and the slow continuous rise of values after 15 ka with low variation does not reflect shifts visible in other plant wax proxies. Bulk carbon isotopes display largely independent variations compared to compound-specific $\delta^{13}C$ values (Figure 3-5).
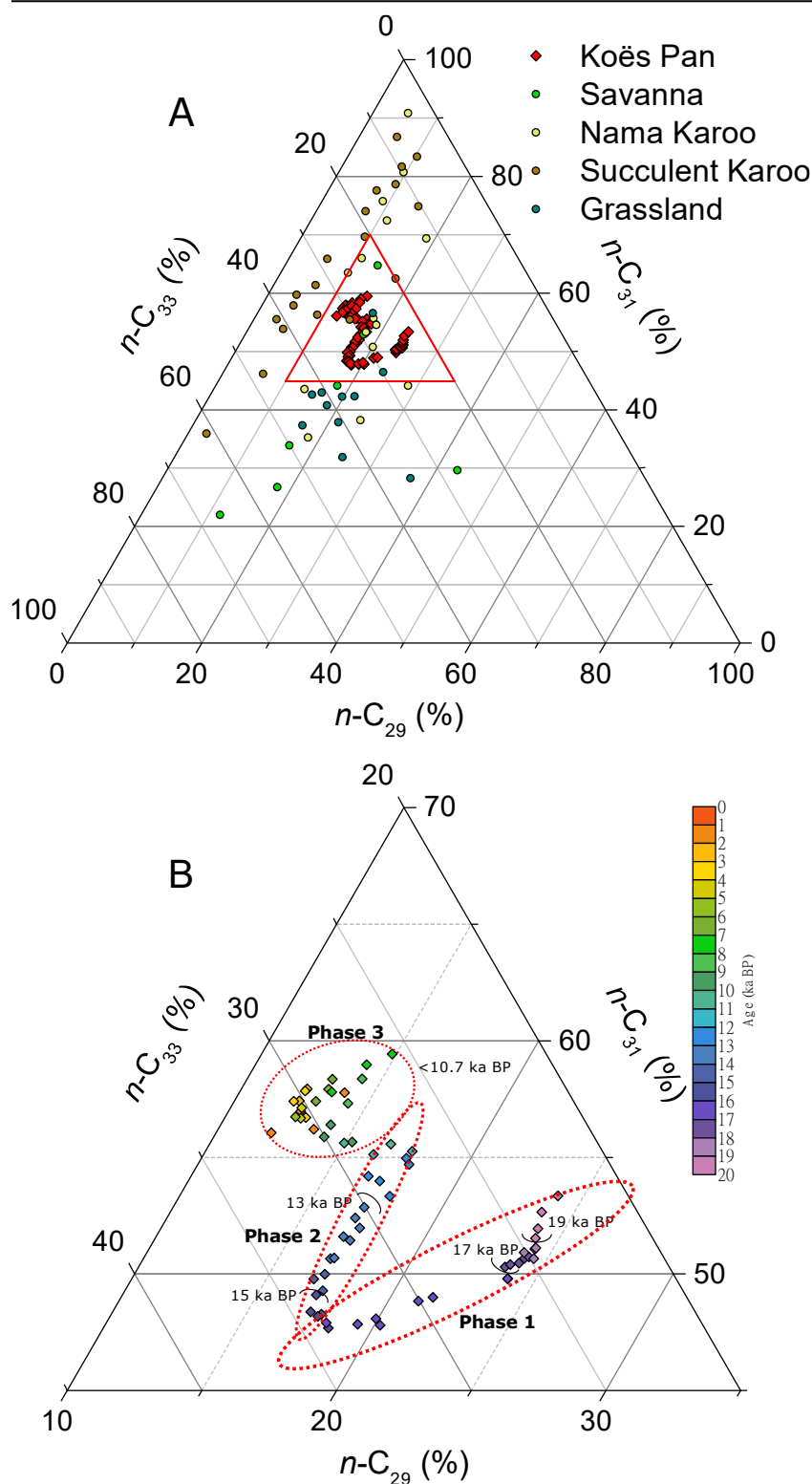
Figure 3-8. Relative distribution of long chain n-alkanes. A. Ternary diagram of *n*-C$_{29}$, *n*-C$_{31}$ and *n*-C$_{33}$ alkanes from Koës Pan (diamonds) and from South African soil samples (circles; Herrmann et al., 2016), red triangle marks section of B. Detailed section of ternary diagram of *n*-C$_{29}$, *n*-C$_{31}$ and *n*-C$_{33}$ alkanes from Koës Pan, sample colour indicates sediment age, red dotted circles depict Phases 1, 2 and 3 which are described in detail in the text.

3.5.1.3 Reconstruction of hydrology

Important factors, which influence δD_{31} are vegetation assemblage, evapotranspiration and catchment size (Sachse et al., 2012; Collins et al., 2013; Herrmann et al., 2017). Large changes in the vegetation assemblage, especially the C_3/C_4 ratio, which might have affected δD_{31} values (Sachse et al., 2012; Collins et al., 2014) are not indicated considering the rather low variation of $\delta^{13}C_{31}$ values. PET however, did change. Until 17.5 ka BP annual temperatures in southern Africa were up to 5-6 °C cooler than today resulting in a lower PET (Figure 3-9; Scott, 1982; Stute and Talma, 1998; Truc et al., 2013; Chevalier and Chase, 2015, 2016; Lim et al., 2016). The following rise of temperature and PET must have positively influenced δD_{31} over the next few thousand years. However, even after correcting for ice-volume effects the δD_{31} does not rise but decreases stepwise after 15.0 ka BP, though K/Al ratios depict a change to much lower surface runoff at the same time. The missing factor which leads to high values during the LGM could be the continental effect (Stute and Talma, 1998; Sachse et al., 2012). The depletion in deuterium is higher with increasing distance the humidity travelled from ocean to the locality of precipitation. Summer rainfall, therefore, leads to depleted δD_p of summer rain in eastern Namibia due to its origin in the Indian Ocean (Figure 3-1C). A change in rainfall regimes towards summer rain would therefore affect the δD_{31} towards lower δD_{31} values. A change to summer rain would also transfer growing season of many species to summer, leading to higher temperatures during growing season, which heightens PET effects on wax isotopes.

3.5.2 Implications for the reconstruction of climatic conditions at Koës Pan for the last 20 ka

From the late LGM until 17 ka BP high K/Al values point to high input by surface runoff, while Ti/Al and TIC content mark high aeolian input at the same time (Figure 3-5; Schüller and Wehrmann, 2018). This indicates wind driven precipitation (frontal) rather than convectional driven precipitation (showers) and points towards winter rainfall during the LGM at Koës Pan, which corresponds to

similar data from the nearby Branddam Pan and the Stampriet aquifer (Stute and Talma, 1998; Schüller et al., 2018). High K/Al values mark relatively wet conditions. LEWIS$_{29\text{-}33}$ values possibly indicate highest species richness of the vegetation during the period studied here.

Around 17 ka BP winter rain ceases at Branddam Pan (Schüller et al., 2018). About the same time many proxies at Koës Pan indicate abrupt changes and thus provide evidence for rain season shift. K/AL values indicate less wet conditions, chain length parameters, especially ACL and relative distribution of n-C$_{29}$, n-C$_{31}$ and n-C$_{33}$ and δ^{13}C$_{29}$ and δ^{13}C$_{33}$ change drastically and point to dryer and/or warmer conditions during growing season and LEWIS$_{29\text{-}33}$ potentially displays a drop of species richness. A short dynamic transition phase from about 17 to 15 ka BP of temporary overlapping winter and summer rainfall is indicated by variable δ^{13}C values of n-C$_{29}$, n-C$_{31}$ and n-C$_{33}$ and by short drops of hydrogen isotope ratios (Figure 3-7).
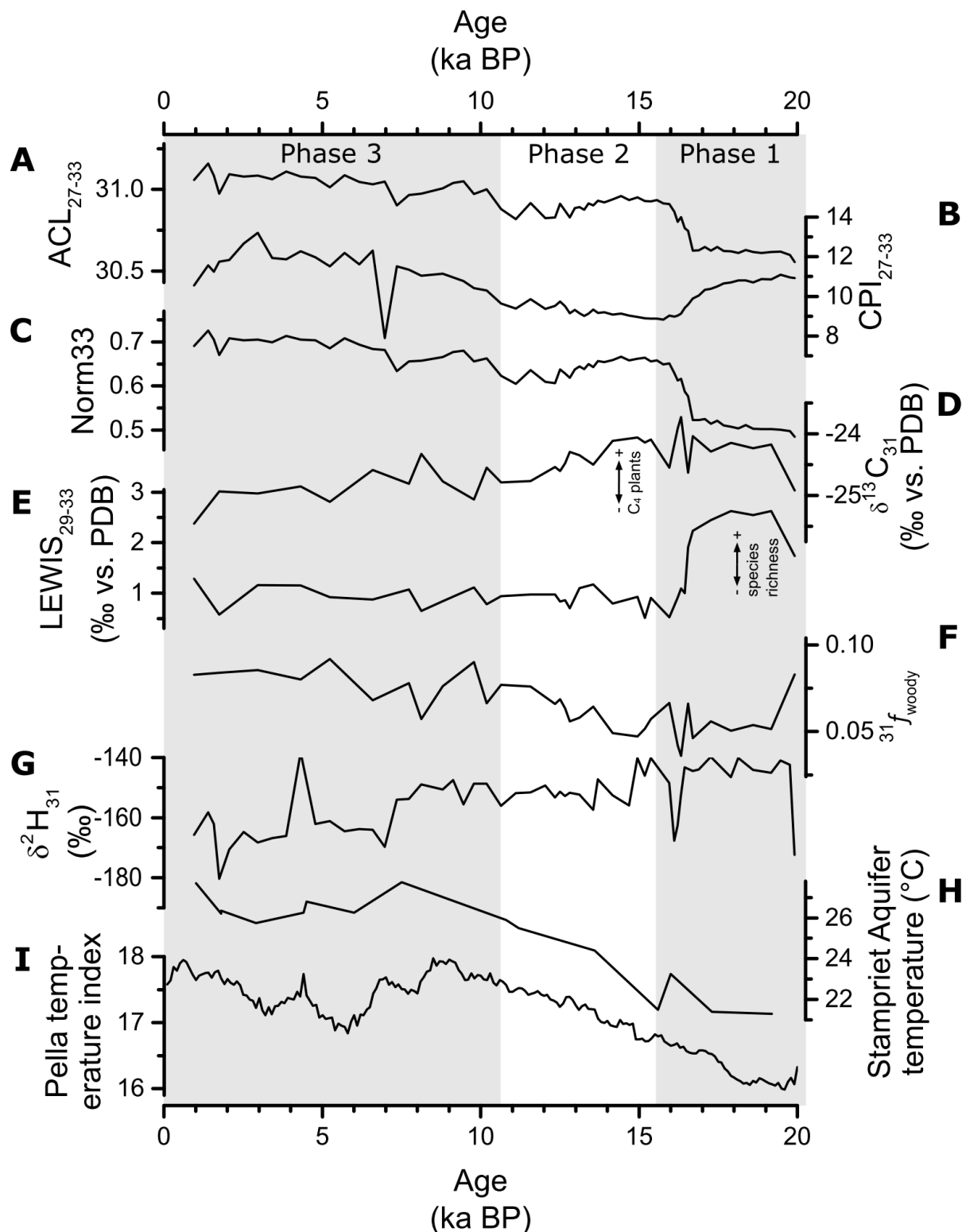
Figure 3-9. Leaf wax parameters of Koës Pan sediments. A. $ACL_{27\,33}$, B. CPI_{27-33}, C. Norm33, D. $\delta^{13}C_{31}$, E. $LEWIS_{29-33}$, F. $^{31}f_{woody}$, G. δD_{31} corrected for ice volume effect, H. Paleotemperature reconstruction from Stampriet Aquifer (Stute and Talma, 1998), I. Pella temperature Index (Lim et al., 2016). Grey and white background indicate Phases 1, 2 and 3 which are described in detail in the text.

Paleotemperature records from the region (Figure 3-9H and I; Stute and Talma, 1998; Lim et al., 2016) show a phase of continuous warming from 17 to 9 ka. The stepwise, rapid changes in plant wax indices suggest that they are rather caused by a shift of growing season and precipitation regime than just by elevated temperatures. Today at Keetmanshoop, which is close to Koës Pan, the difference of average maximum temperatures between July and January is about 14°C (climate-data.org, 2020). Though this gradient must have been lower during glacial conditions, it is obvious, that seasonal temperature and PET gradients were higher than long-term average temperature changes. After these changes, most proxies indicate relatively stable conditions. Despite this, the change of trends in relative chain lengths distribution from Phase 1 to Phase 2 marks a continuous transition of plant wax assemblage that might indicate a change from a more Savanna Biome-like vegetation towards a more Nama Karoo vegetation probably caused by a different environmental forcing than before which is not reflected in other pan records from the region (Schüller et al., 2018; Belz et al., 2020). The increase of temperatures towards the Holocene which increased PET, is completely invisible in the δD_{31} values record nor is the temperature and PET rise which would be expected by a change in growing season (Figure 3-9G). Furthermore, sedimentation rate and K/Al values do not indicate increased moisture until slight increases around 10 ka BP (Schüller and Wehrmann, 2018). We conclude, that an important factor for keeping the hydrogen isotopes stable and lower than before is the change of moisture origin following the change from winter to summer rainfall.

Most proxies show little variation throughout the Holocene at Koës Pan. High ACL and $Norm_{33}$ values and in general low K/Al values indicate rather dry conditions. There is a change in relative distribution of n-C_{29}, n-C_{31} and n-C_{33} towards Phase 3 which is characterized by high relative abundance of n-C_{31}. The samples do note indicate any continuous trend anymore and cluster, suggesting rather an absence of greater environmental changes within the Holocene. Dry conditions in the early Holocene are furthermore visible at many sites throughout the region (Brook et al., 1996; Brook et al., 1998; Thomas et al., 2003; Hürkamp et al., 2011; Burrough and Thomas, 2013; Belz et al., 2020). Slightly elevated K/Al values from 10 to 8 ka BP which are accompanied by slightly increased TIC and to a lesser extent by Ti/Al

values marking increased aeolian transport are not reflected in ACL, carbon or hydrogen isotopes, thus probably indicating no fundamental environmental changes. The low δD_{31} values after 7 ka BP are also not correlating with any proxy which could mark higher water availability or increased precipitation.

3.6 Conclusions

In this study we investigated the influences of a change in rainfall seasonality on vegetation, environment and its impact on paleoclimatic proxies by analysing climate-diagnostic leaf wax biomarkers and their isotopes in sediments from a pan in the western Kalahari. The results show a temporary increase in rain and a rather abrupt and lasting shift in many leaf wax-based proxies at the end of the LGM which go along with the parallel change from winter to summer rainfall.

However, while carbon isotopes show only little variation in the ratio between C_3 and C_4 vegetation, the changes in relative *n*-alkane distribution in phases point to continuous changing environmental forcing, probably mostly caused by a shift in growing season. This forcing possibly resulted as well in changes of the biome as in a changing leaf wax composition. The steady subtle change of the relative distribution of *n*-C_{29}, *n*-C_{31} and *n*-C_{33} mark the high sensitivity of *n*-alkane distribution if variations of individual *n*-alkane homologues are considered and underlines the limitation of integrating proxies like ACL which obscure these variations. This sensitivity also proofs the value of high-resolution sampling of pan sediments which made variations visible in sub-millennia scale.

The hydrogen isotope record must have been influenced by the switch of humidity source and changes in evaporation due to changed growing season. Any conclusion from it on the amount of precipitation or water availability in this phase might be heavily biased. Studies using leaf wax hydrogen isotopes from sites in the region which underwent variations in rainfall seasonality should always consider this. The discrepancy between bulk and compound-specific carbon isotope values highlights that the carbon cycle within pans and their catchments is not

understood yet and not all proxies that are used in lacustrine environments can be adapted to pan sediments.

Acknowledgements

4. Comparison high-resolution leaf wax records from two Kalahari salt pans

Lukas Belz[1], Irka Schüller[2], Achim Wehrmann[2], Jürgen Köster[1], Heinz Wilkes[1]

[1]Institute for Chemistry and Biology of the Marine Environment (ICBM), Carl von Ossietzky University, Oldenburg, 26111, Germany

[2]Senckenberg am Meer, Marine Research Department, Wilhelmshaven, 26382, Germany

This chapter provides preliminary alkane and carbon isotope results with need for additional experiments and data.

Abstract

Southern African pans (playas) have been used as environmental archives for local continental data in recent studies. This study compares proxies derived from *n*-alkane compositions and their compound-specific carbon isotope values of two Kalahari pan sediment records. We present new high-resolution data from Omongwa Pan, Namibia, reaching back to 18.0 ka BP. Relatively wet conditions caused by different mechanisms at both pans during the last glacial-interglacial transition lead to comparable yet distinguishable geochemical records. Results also point to a Holocene northward expansion of the Nama Karoo biome, which did not reach Omongwa Pan. We introduce the Norm^{13}C$_{33}$ index as a potential proxy for evaporative conditions. Overall, pans allow a reconstruction of local conditions which is important to identify links and boundaries of intracontinental changes of climate.

4.1 Introduction

Kalahari pans (playas) are drainless depressions, with a wide distribution in central southern Africa. Recent studies revealed the potential of sediments from pans for paleoenvironmental reconstructions (Genderjahn et al., 2017; Genderjahn et al., 2018b; Schüller et al., 2018; Belz et al., 2020; Belz et al., submitted). Pans can present a valuable source for local continental paleo-environmental data in the arid Kalahari where common archives are scarce. However, unlike marine archives which are often integrating terrestrial signals from a large source area, the catchment of pans can be rather small. The small catchments can give insights on intra continental dynamics and boundaries of regional climate development. On the other hand, similar to records from lakes, this can possibly lead to misinterpretation and confusion between regional and supra-regional effects. Local effects like geologic or environmental settings can also play an important role (Roberts et al., 2016; Schüller et al., 2018).
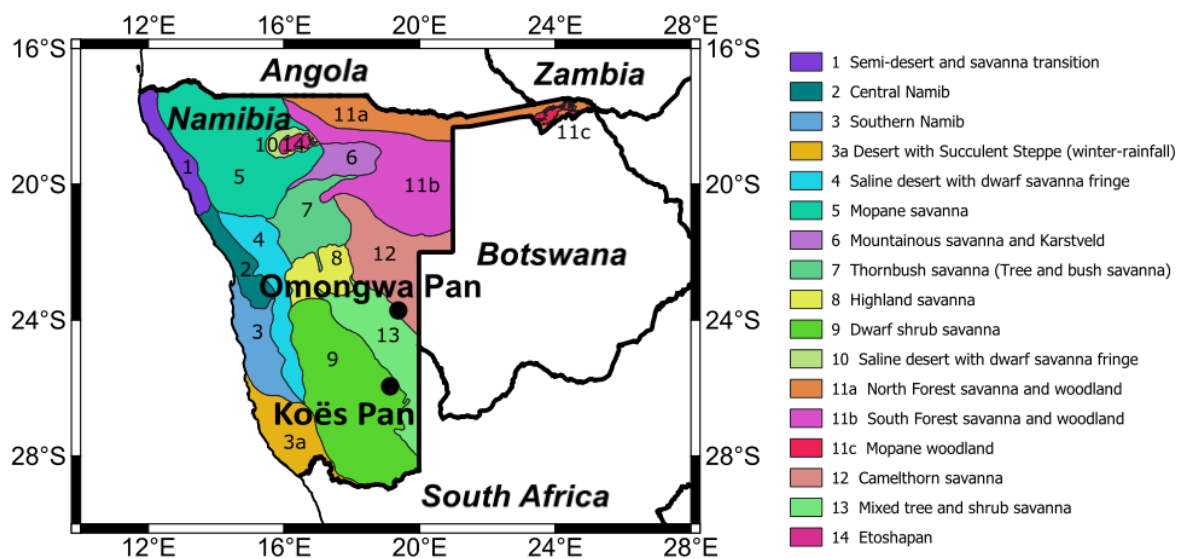
Figure 4-1 Map with Nambian ecoregions (data source: Rutherford et al., 2005). Locations of Omongwa Pan and Koes Pan are marked as black dots

In this study, we compare data from sediments of two Kalahari pans. We present new high-resolution data from pan sediments from Omongwa Pan in comparison to an existing record of Koës Pan, both located in the western Kalahari (Namibia; Belz et al., submitted). We determined *n*-alkane composition derived proxies and their compound-specific carbon isotope values. We compare this data to reconstruct differences in vegetation and ecology during the late Pleistocene and during different phases of the Holocene. We furthermore evaluate the benefit of the high-resolution record from Omongwa Pan in comparison with an older less resolved record (Belz et al., 2020).

4.2 Site description
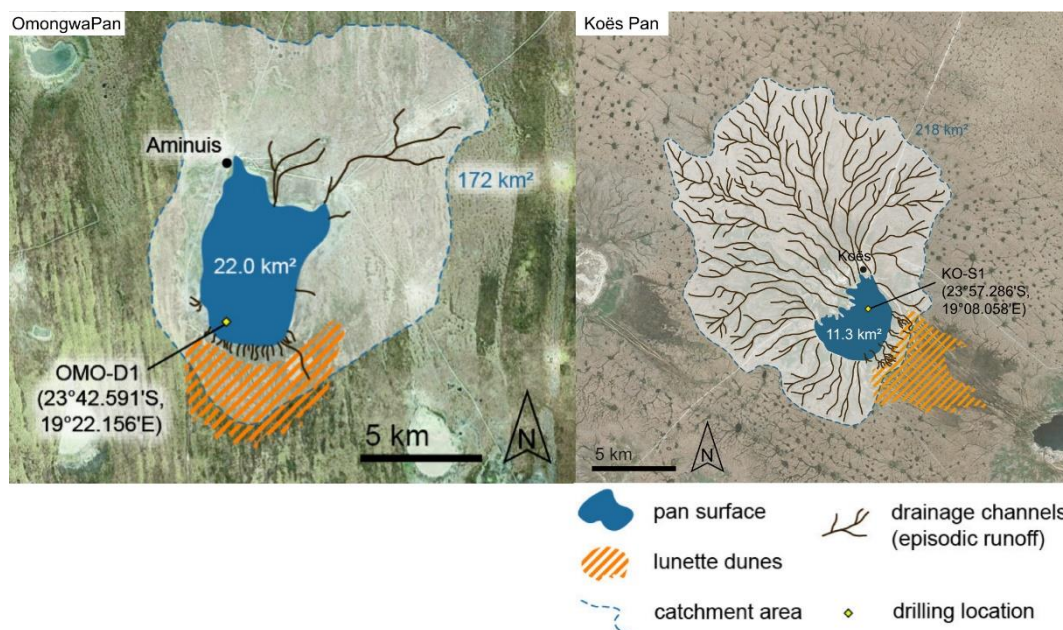
Figure 4-2 Omongwa and Koë Pan with spatial extension and size of the catchment area (modified after Schüller et al., 2018).

The two pans used for this comparison are Omongwa Pan and Koës Pan Omongwa Pan is located in the western Kalahari in the Aminuis Region. Koës Pan (located ca. 250 km south from Omongwa Pan) is situated close to the village of Koës in the ‖Karas Region (Figure 4-1). The size of Omongwa Pan is about twice of that of Koës Pan. The catchment of Koës Pan is slightly larger and features distinctive flow structures. At the leeward rim of both pans lunette dunes can be found (Figure 4-2; Schüller et al., 2018). Both pans are embedded in sands and calcretes of the Paleogene Kalahari group (Lancaster, 1986). At Omongwa Pan carbonates (stromatolites) were found directly at the rim of the pan (Genderjahn et al., 2018b).

Pan sediment mineralogy is similar and sediments of both pans contain evaporates, mainly halite and gypsum. Grain size in both pans is dominated by medium to coarse silts. Under dry conditions Omongwa Pan features a crust of salt minerals (mainly halite and gypsum) while the surface of Koës Pan consist of hardened clay (Schüller et al., 2018). A detailed geologic description and

mineralogic data of both pans have already been published (Schüller et al., 2018; Schüller and Wehrmann, 2018).

At both pans vegetation is dominated by shrubs and grasses. Shrub density is enhanced closer to the pan shore. The surrounding area is utilized as rangeland. Both pans are located within the Xeric Savanna biome, but Koës Pan is close to the border of the Nama Karoo(Rutherford et al., 2006). Within the biome Omongwa Pan is located in the Camelthorn Savanna ecoregion and Koës Pan in the Dwarf Shrub Savanna ecoregion (Figure 4-1; Rutherford et al., 2005; Rutherford et al., 2006). A detailed description of the local vegetation can be found elsewhere (Rutherford et al., 2005; Belz et al., 2020; Belz et al., submitted).

Modern environmental conditions at both pans are determined by a strong seasonality of precipitation, with a rainy season in summer and dry winters. The humidity of summer rain in the Kalahari originates in the Indian Ocean and decreases southwestward (Tyson et al., 1996; Gasse et al., 2008; Nicholson, 2009). Average annual precipitation is about 250 mm at Omongwa Pan and 174 mm at Koës (Mees, 1999; climate-data.org, 2020).

During the last glacial–interglacial transition (LGIT) the area around Omongwa Pan exhibit wet conditions probably caused by a southward shift of the intertropical convergence zone (ITCZ) during Heinrich Stadial 1 (HS1; Lancaster, 1979; van Zinderen Bakker, 1983; Dahl et al., 2005; Lewis et al., 2010; Schefuß et al., 2011; Belz et al., 2020). Until 16 ka BP the more southern located Koës Pan was influenced by northward shifted winter rainfall since the Last Glacial (van Zinderen Bakker, 1983; e.g. Cockcroft et al., 1987; Chase and Meadows, 2007; Stone, 2014; Schüller et al., 2018; Belz et al., submitted). During the early Holocene climate in the western Kalahari changed to dry stable conditions with two short wet phases around 10 ka BP and 4 ka BP in Northern Namibia and Botswana (Burrough and Thomas, 2013 and references therein).

4.3 Methods

4.3.1 Sampling and sample preparation

All samples were taken during dry season (September 2016) in the southwestern part of Omongwa Pan (23°42.6'S, 19°22.2'E). Samples were gathered from a profile pit located adjacent to the profile pit from October 2013 (Belz et al., 2020). The pit was sampled in 1 cm intervals. The deepest samples are from a depth of 60 cm below ground. Groundwater table was not reached. Samples were wrapped in aluminium foil and then put in plastic bags on location and stored in glass vials at 4°C afterwards, see also Belz et al. (2020).

4.3.2 Age-depth model

Age depth relation of the profile has been established for Omongwa Pan in an earlier study using a model based on the Bacon 2.2 software package for R (Blaauw and Christen, 2011), based on 14 calibrated ^{14}C ages (Schüller et al., 2018; Belz et al., 2020). The pan features a continuous net sediment accumulation and displays no clear signs for hiatuses. The oldest sample of this dataset dates back to 16.9 ka BP (Schüller and Wehrmann, 2018).

4.3.3 Lipid extraction and liquid chromatography

All samples were freeze-dried and homogenized. Lipid extraction was done using an SpeedExtractor from Büchi with a solvent mixture of dichloromethane and methanol (9/1) at 70°C and 70 bar. n-Hexane-insoluble components were removed by filtration over $NaSO_4$. Squalane was added as internal standard for quantification. The extract was separated into aliphatic hydrocarbons, aromatic hydrocarbons and a fraction containing nitrogen, sulphur and oxygen (NSO) compounds by medium pressure liquid chromatography (MPLC; Radke et al., 1980). A detailed description of extraction can be found elsewhere (Belz et al., submitted).

4.3.4 Gas chromatography

The hydrocarbon fraction was analysed using a 6890 gas chromatograph (GC) from Agilent equipped with a high temperature column (J&W DB-5HT, 30 m × 25 mm, 0.1 μm film thickness), a cold injection system, and a flame ionization detector (FID). The carrier gas was helium. The injector temperature was initially set to 60°C, increased to 350°C at a rate of 600°C/min and held at that temperature for 1 min. The initial temperature of the GC oven was 60°C held for 2 min, then heated at a rate of 3°C/min to 350°C and held for 15 min. n-Alkanes were identified by comparison of retention times to those of reference standards. For quantification signal intensity of FID signal was used relative to internal standard.

4.3.5 Gas chromatography-isotope ratio mass spectrometry

Compound specific isotopic compositions of carbon were measured using a gas chromatograph 6890 from Agilent coupled to a MAT 253 isotope ratio mass spectrometer from Thermo Fisher scientific. GC conditions were analogue to section 3.4 except for the temperature programme. Injector temperature started at 60°C, increased to 305°C at a rate of 10°C/min and was held at that temperature for 2 min. The initial temperature of the GC oven was 60°C held for 2 min, then heated at a rate of 3°C/min to 300°C and held for 18 min.

4.3.6 Calculated proxies

To estimate the ratio between odd and even n-alkanes, CPI values were calculated according to Cooper and Bray (1963):

$$\text{CPI}_{27\text{-}33} = 0.5 * \left(\frac{n\text{-}C_{27} + n\text{-}C_{29} + n\text{-}C_{31} + n\text{-}C_{33}}{n\text{-}C_{26} + n\text{-}C_{28} + n\text{-}C_{30} + n\text{-}C_{32}} \right) + \left(\frac{n\text{-}C_{27} + n\text{-}C_{29} + n\text{-}C_{31} + n\text{-}C_{33}}{n\text{-}C_{28} + n\text{-}C_{30} + n\text{-}C_{32} + n\text{-}C_{34}} \right)$$

The average chain length of n-alkanes ($\text{ACL}_{27\text{-}33}$) was calculated analogous to Meyers (2003):

$$\text{ACL}_{27\text{-}33} = \frac{27*n\text{-}C_{27} + 29*n\text{-}C_{29} + 31*n\text{-}C_{31} + 33*n\text{-}C_{33}}{n\text{-}C_{27} + n\text{-}C_{29} + n\text{-}C_{31} + n\text{-}C_{33}}$$

To indicate changes in the relative concentration of homologues $n\text{-}C_{29}$ and $n\text{-}C_{33}$ the Norm33 index was calculatedaccording to (Herrmann et al., 2016):

$$\text{Norm33} = \frac{n\text{-}C_{33}}{n\text{-}C_{29} + n\text{-}C_{33}}$$

For comparison of species richness and woody cover, the following proxies were calculated after Magill et al. (2019):

$$\text{LEWIS}_{29\text{-}33} = \max|\delta^{13}C_{29\text{-}33}| - \min|\delta^{13}C_{29\text{-}33}|$$

$$^{31}f_{\text{woody}} = \{\sin(-1.8353 - 0.0838 * {}^{13}C_{31})\}^2$$

For a more precise comparison of $\delta^{13}C_{29}$ and $\delta^{13}C_{33}$ we calculate the $\text{Norm}^{13}C_{33}$ ratio as follows:

$$\text{Norm}^{13}C_{33} = \frac{\delta^{13}C_{33}}{\delta^{13}C_{29} + \delta^{13}C_{33}}$$

4.4 Results

This section contains the results for samples from Omongwa Pan. Koës Pan results have been described in (Belz et al., submitted).

4.4.1 Distribution of *n*-alkanes

In all samples from Omongwa Pan, n-alkanes with chain length from C_{17} to C_{35} can be detected. Average total concentration of n-alkanes is 3307±1148 µg/g TOC. Total n-alkane concentration is highest at 9.2 and 12.8 ka BP (Table 4-1). Low values (below 2500 µg/g TOC) are found in all samples before 15 ka BP. Samples exhibit a prominent odd-over-even predominance, which is reflected in the carbon preference index ($CPI_{27\text{-}33}$), of 5.57±0.73.

The Average $ACL_{27\text{-}33}$ value is 30.16±0.40. In all samples long chain n-alkanes (C_{25}-C_{33}) dominate, with $n\text{-}C_{31}$ being always the most abundant homologue (Table 4-1).

96

The n-alkane distribution varies and shows three patterns: i) 4-6 ka BP: n-C_{31} > n-C_{29} > n-C_{27} > n-C_{33} > n-$C_{25;}$ ii) 8-10.2: n-C_{31} > n-C_{29} > n-C_{27} > n-C_{25} > n-C_{33}, and iii) around 16 ka BP: n-C_{31} > n-C_{33} > n-C_{29} > n-C_{27} > n-C_{25} (Figure 4-4). Apart from a local maximum (>30) from 0-0.5 ka BP ACL_{27-33} values are low and depict little variation in samples younger than 14 ka BP. Before 14 ka BP values are elevated with highest values in the oldest samples. Norm33 values are 0.46±0.11 on average. The trend Norm33 record mainly reflects trends of the ACL_{27-33} (Figure 4-7).

The ternary diagram in Figure 4-6 displays the relation between n-C_{29}, n-C_{31} and n-C_{33} alkanes. For samples from Omongwa Pan, the diagram depicts a low relative variation of n-C_{31} over the record. The plot clusters with low relative n-C_{29} content between 17-16 ka BP. Samples from the time interval 16 to 11 ka BP show a continuous increase of n-C_{29} accompanied by a decrease of n-C_{33}. After that, the relative composition of n-C_{29}, n-C_{31} and n-C_{33} is rather stable from 11-2 ka BP with highest n-C_{29} concentrations of the record. There is a decrease of n-C_{29} over time in samples after 2 ka BP.

4.4.2 Stable carbon isotopes

$\delta^{13}C$ values of long chain n-alkanes (C_{25} to C_{35}) vary from −25.0 ‰ to −20.7‰. All long chain n-alkanes show a drop of values at 16.0-16.4 ka BP and slightly decrease around 4 ka BP. Depleted values around 8 ka BP were detected for $\delta^{13}C_{29}$ and $\delta^{13}C_{31}$. Over the record $\delta^{13}C_{31}$ depicts the lowest values, except at 0.4 ka BP and in samples older than 15 ka BP when $\delta^{13}C_{29}$ is more depleted (Figure 4-5). Values of $LEWIS_{29-33}$ are 1.26±0.31 on average. The record reveals relatively high values (above 1.4) in the youngest sample (0.2 ka BP), at 3.6 ka BP, and in samples older than 16 ka BP (Table 1). Lowest values are detected in samples from 0.8 ka BP to 2.7 ka BP. Average values of $^{31}f_{woody}$ are 3.01±0.01 %, with the highest value at 3.6 ka BP and low values in samples older than 14 ka BP (Table 4-1). The Norm$^{13}C_{33}$ ratio shows little variation (Table 4-1). The highest divergence between $\delta^{13}C_{29}$ and $\delta^{13}C_{33}$ (below 0.4900) was calculated for 0.2 ka BP and samples older than 15 ka BP. Samples in an interval from 0.8 ka BP to 4.8 ka BP indicated a relatively high convergence (0.4977-0.5019).

Table 4-1. Leaf wax proxies in high-resolution sediment samples from Omongwa Pan

av. Depth (cm)	Age (ka)	Σ-*n*-Alkanes (C$_{17-35}$) μg/g$_{TOC}$	ACL (27-33)	Norm33	CPI (27-33)	δ^{13}C$_{31}$ (‰)	LEWIS (29-33)	$^{31}f_{woody}$	Normδ^{13}C$_{33}$
0.5	0.1	2901	30.08	0.43	5.63				
1.5	0.2	4291	30.10	0.42	5.54	-24.24	1.70	0.04	0.4836
3.5	0.4	3622	30.04	0.41	5.54	-24.11	0.90	0.03	0.4905
5.5	0.5	4333	29.91	0.37	5.40				
7.5	0.8	4390	29.86	0.36	5.31	-24.22	0.83	0.04	0.5012
9.5	1.7	4034	29.80	0.35	5.29	-24.08	0.96	0.03	0.4989
11.5	2.7	3525	29.76	0.34	5.25	-23.92	0.83	0.03	0.4978
12.5	3.0	3571	29.74	0.34	5.19				
13.5	3.2	3606	29.79	0.35	5.01				
14.5	3.4	3170	29.77	0.34	5.36				
15.5	3.6	2739	29.80	0.34	5.51	-24.96	1.49	0.06	0.5001
17.5	4.0	3322	29.86	0.35	5.47				
19.5	4.4	3948	29.76	0.34	5.35	-24.10	0.89	0.03	0.5019
21.5	4.8	3396	29.79	0.35	5.38	-23.99	1.06	0.03	0.4977
23.5	5.8	3519	29.75	0.34	5.36				
25.5	7.0	3837	29.86	0.38	5.33	-24.55	1.35	0.05	0.4952
27.5	8.1	4708	29.87	0.38	5.09	-24.41	1.34	0.04	0.4910
29.5	9.2	5290	29.83	0.37	4.93				
31.5	10.2	4261	29.81	0.37	4.89				
33.5	11.1	4848	29.86	0.38	4.79	-24.21	1.21	0.04	0.4948
35.5	12.0	3879	29.81	0.37	4.67				
37.5	12.8	5447	29.90	0.40	4.73	-24.21	1.17	0.04	0.4936
39.5	13.6	4583	29.97	0.42	4.72				
41.5	14.4	4253	30.07	0.45	4.61				
42.5	14.6	4195	30.12	0.47	4.60				

Table 4-1 continued.

av. Depth (cm)	Age (ka)	Σ-n-Alkanes (C$_{17-35}$) µg/g$_{TOC}$	ACL (27-33)	Norm33	CPI (27-33)	$\delta^{13}C_{31}$ (‰)	LEWIS (29-33)	$^{31}f_{woody}$	Norm$\delta^{13}C_{33}$
43.5	14.8	4505	30.17	0.49	4.73	-23.74	1.36	0.02	0.4902
45.5	15.1	3188	30.35	0.53	5.05				
46.5	15.3	2964	30.46	0.55	5.43				
47.5	15.5	2842	30.57	0.58	5.89	-23.25	1.09	0.01	0.4881
49.5	15.8	1941	30.65	0.59	5.94	-23.05	1.05	0.01	0.4884
50.5	16.0	2293	30.71	0.61	6.17	-23.75	1.09	0.02	0.4884
51.5	16.1	1928	30.73	0.62	6.56	-23.72	1.37	0.02	0.4856
52.5	16.3	1328	30.75	0.62	6.63	-23.67	1.78	0.02	0.4809
53.5	16.3	1520	30.73	0.61	7.18				
54.5	16.4	1266	30.74	0.62	6.31				
55.5	16.5	1258	30.76	0.63	6.07	-23.41	1.68	0.02	0.4822
56.5	16.6	1915	30.68	0.60	7.29	-23.59	1.84	0.02	0.4802
57.5	16.6	1931	30.78	0.61	6.77	-23.50	1.53	0.02	0.4832
58.5	16.8	1953	30.79	0.62	6.75				
59.5	16.9	1778	30.8	0.61	6.92				

4.5 Discussion

4.5.1 Comparison of Omongwa Pan high-resolution and low-resolution record

In this section we compare the results of this study with 1 cm sample intervals to older data from the same location from Omongwa Pan (Belz et al., 2020). In this old dataset sample were taken in intervals of 5 cm or larger. Each sample integrated the whole interval.

The average total organic carbon (TOC) normed concentrations of *n*-alkanes in the high-resolution record from Omongwa Pan are about 75% higher than average results from the low-resolution record. In

Figure **4-3**A a constant offset is visible while both records reflect similar trends. This is possibly caused by different applied methods for extraction. For extraction of the low-resolution record a solvent mixture of dichloromethane and methanol (99/1) at 75°C and 50 bar was used (Belz et al., 2020). Furthermore, the concentration of the internal standard (IS) for hydrocarbons 5α-Androstane was added in 11-fold concentration compared to the high-resolution record probably biasing compound/IS ratios.

For comparison of long chain *n*-alkane distribution and for calculation of all applied proxies, ratios of the abundances of individual compounds were used which bypass this source of methodical errors.
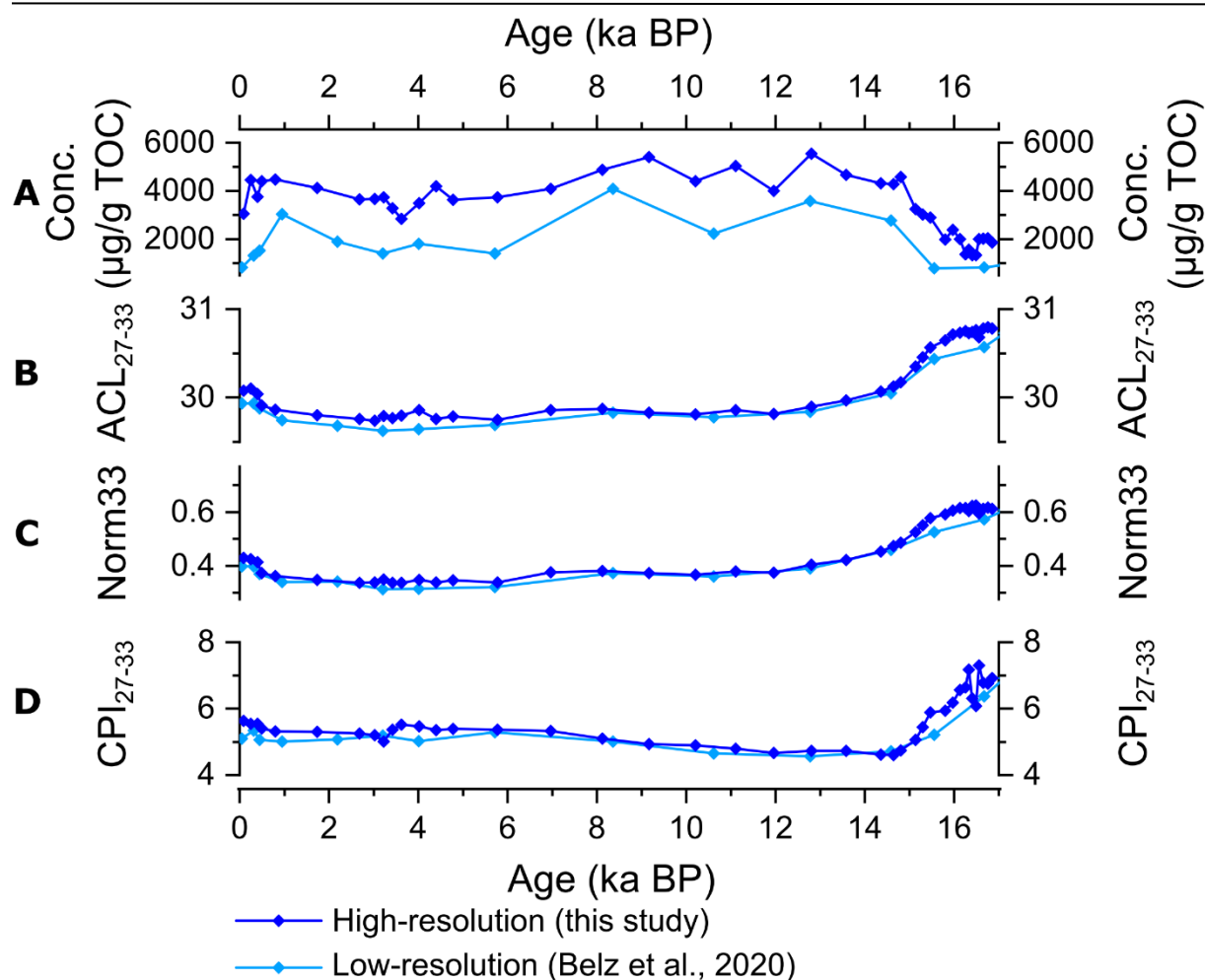
Figure 4-3 Comparison of Omongwa Pan leaf wax parameters between the high-resolution record (dark blue; this study) and an existing record with a lower resolution (light blue; Belz et al., 2020). A. Concentration. B. $ACL_{27\,33}$, C. Norm33, D. CPI_{27-33}.

In average, ACL_{27-33} and Norm33 values of the high-resolution record are elevated by 0.26 and 0.07, respectively. They follow trends of the low-resolution record but depict more variation and details (

Figure **4-3**). From 17 to 16 ka BP values are higher. The drop of ACL values starts later at 16.0 ka BP and is steeper. From 8 ka BP to 7 ka BP both records diverge. The high-resolution record depicts a local maximum around 4 ka BP to 3 ka BP. CPI_{27-33} values are also higher in the high-resolution record and show the same trend as ACL and Norm33 from 16.9 to 15 ka BP and from 4 ka BP to 3 ka BP.
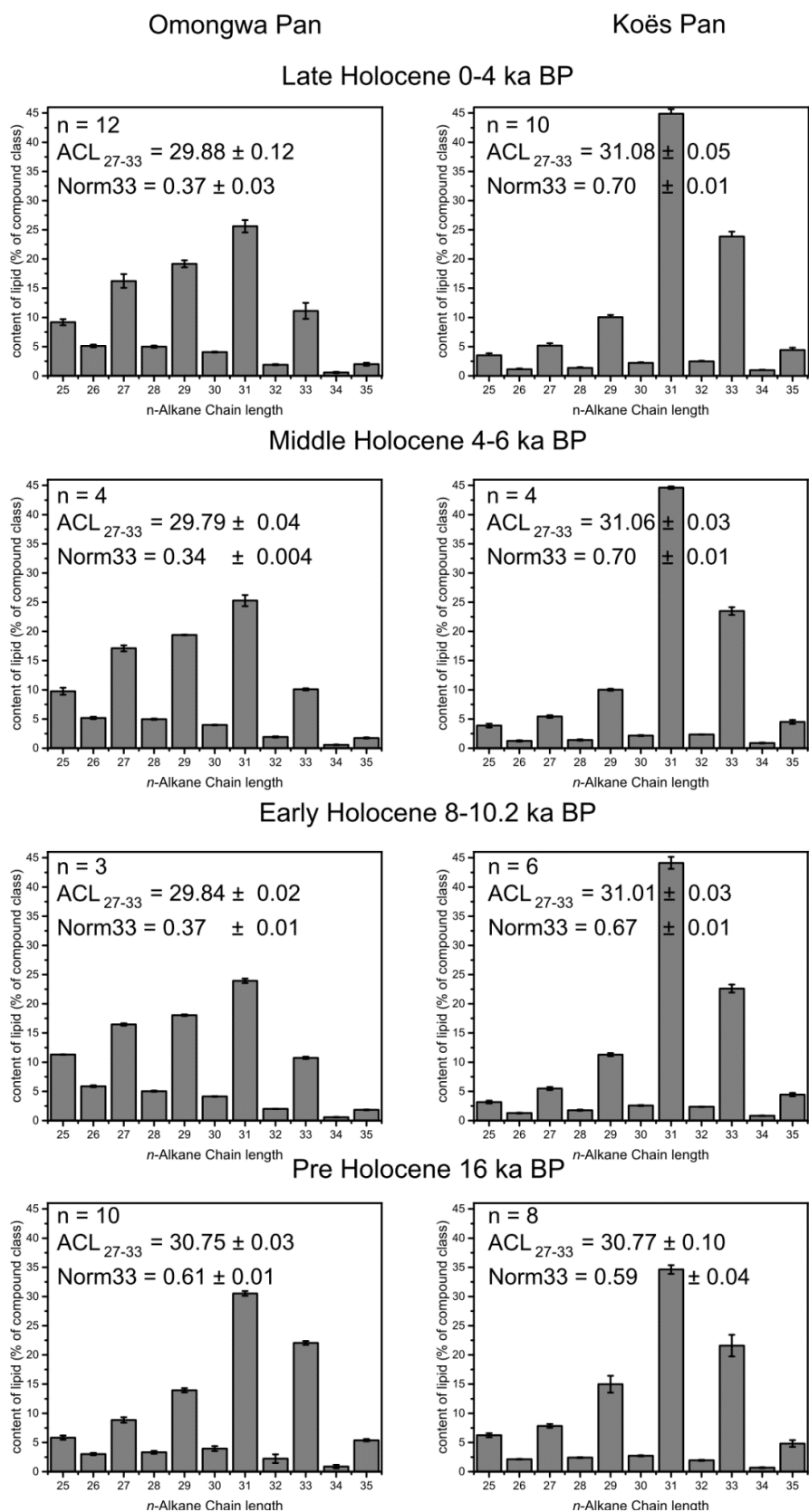
Figure 4-4 Relative chain length distributions of *n*-alkanes and mean average chain lengths (ACL27-33) of samples from different timespans of Omongwa Pan (left) and Koës Pan (right; data source: Belz et al., submitted).
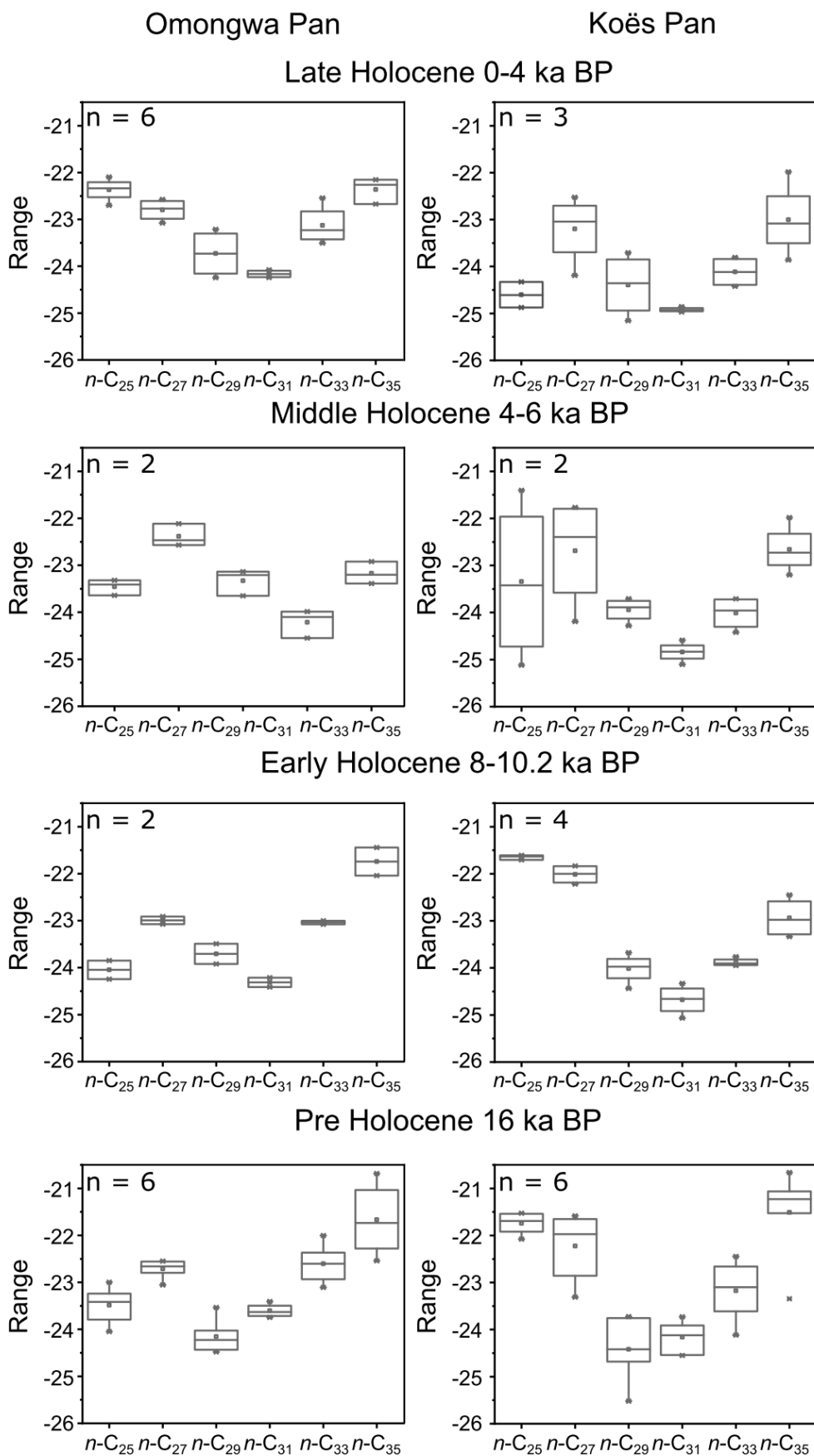
Figure 4-5 Box whisker plot of $\delta^{13}C$ of long chain n-alkanes of samples from different timespans for Omongwa Pan (left) and Koës Pan (right; data source: Belz et al., submitted).

The low-resolution record from Omongwa Pan comprised a longer time span from 27-0 ka BP. For a better comparison, all averages from the low-resolution record were recalculated from samples younger than 17 ka BP. Especially before 15 ka BP, during a period of fast change, the importance of high-resolution data is visible. Beside the differences in concentrations, the general similarity of trends in proxy values shows their reliability even considering the usage of differing methods.

In comparison to the low-resolution record from Omongwa Pan, $\delta^{13}C$ values of the high-resolution record are all increased and variation is much smaller. Differences may differ due to measurements using different GC-IRMS appliances and methods (cf. Belz et al., 2020). As the Koës Pan record was established using the same methodology as the high-resolution record of Omongwa Pan it is better suited for comparison.
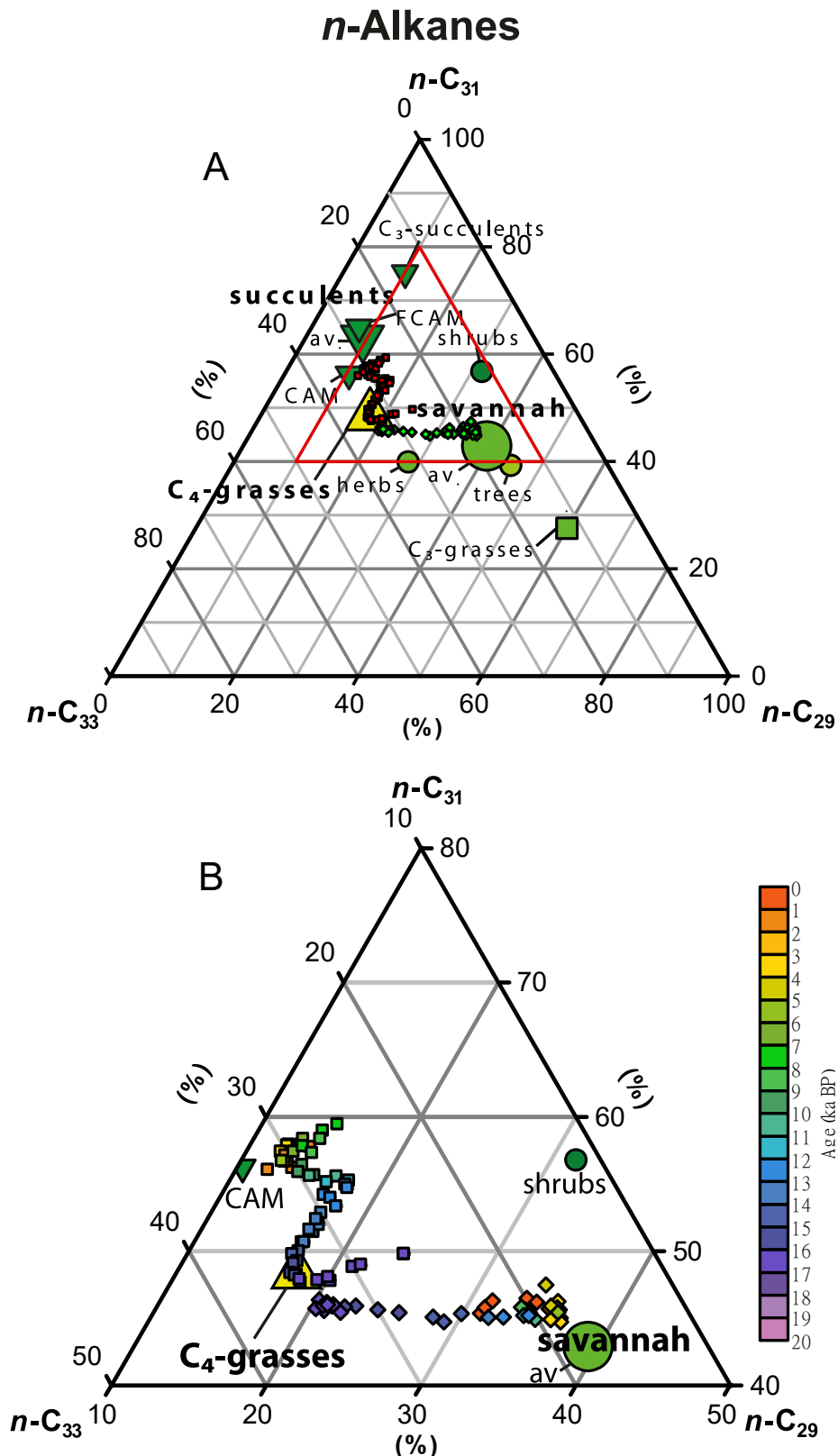
Figure 4-6. Relative distribution of long chain n-alkanes. A. Ternary diagram of n-C_{29}, n-C_{31} and n-C_{33} alkanes from Omongwa Pan (diamonds) and Koës Pan (squares). Average values are displayed for C_4 grasses (up-triangle), C_3 grasses (green square; Rommerskirchen et al., 2006b), succulents (down-triangle; Carr et al., 2014), C_3 savanna plants (circles; Vogts et al., 2009). B. Detailed section of ternary diagram of n-C_{29}, n-C_{31} and n-C_{33} alkanes from Koës Pan, sample colour indicates sediment age.
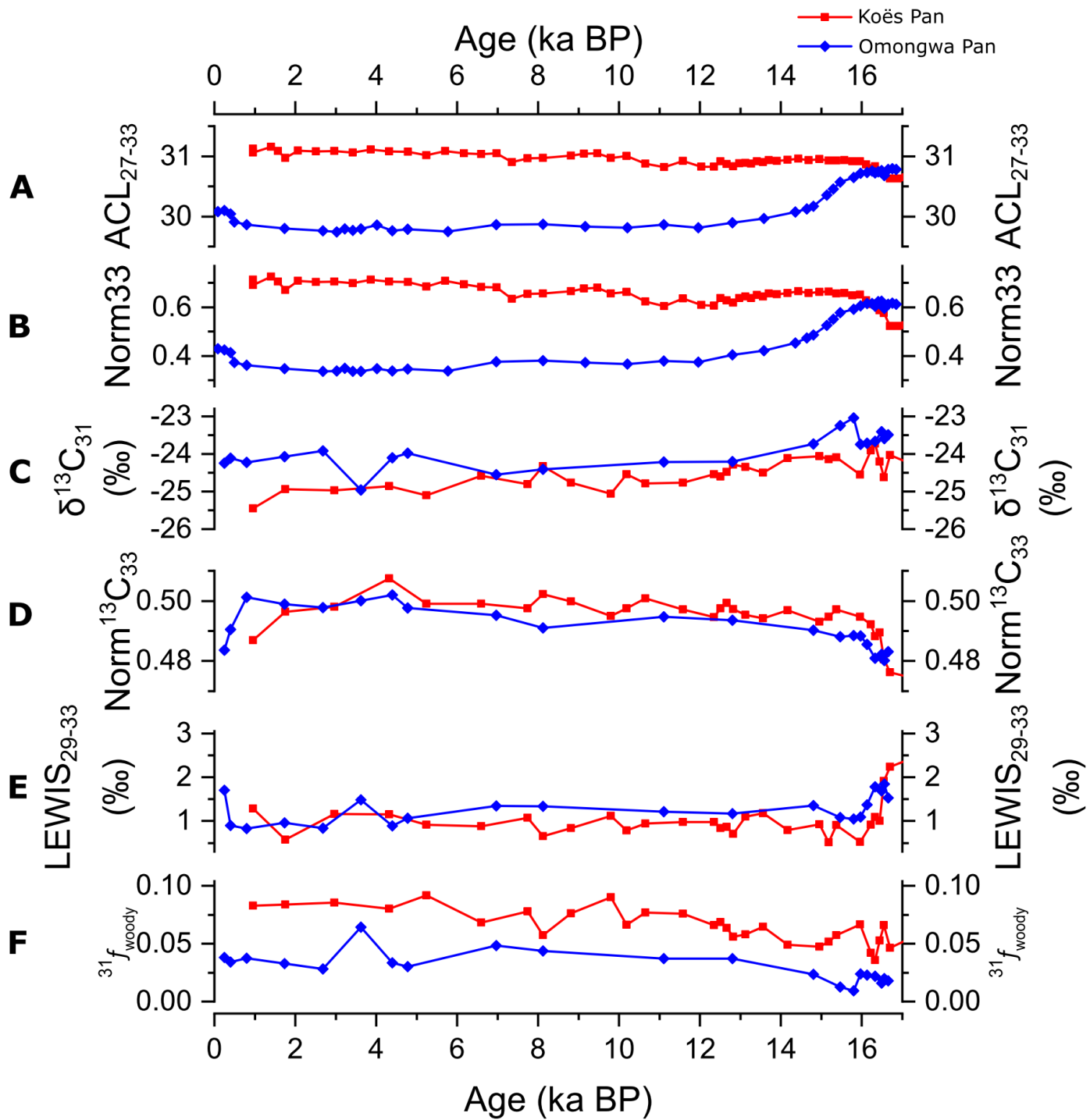
Figure 4-7 Comparison of leaf wax parameters between Omongwa Pan (blue diamonds) and Koës Pan (red squares; data source: Belz et al., submitted). A. $ACL_{27\ 33}$, B. Norm33, C. $\delta^{13}C_{31}$, D. $Norm\delta^{13}C_{33}$, E. $LEWIS_{29-33}$, F. $^{31}f_{woody}$.

4.5.2 Comparison of *n*-alkanes

Around 16 ka BP the long chain *n*-alkane distribution of Omongwa Pan and Koës Pan is almost identical. This is reflected in very similar ACL and Norm 33 values and visible in the ternary diagram (Figure 4-6), suggesting a dominance of C_4 grasses and comparable environmental conditions at both locations. *n*-Alkane proxies point towards an even higher contribution of C_4 grasses to leaf waxes compared to later time intervals. At both locations however, this was not a stable, prolonged state. At Omongwa Pan an abrupt shift of conditions with a higher water availability started with the beginning of Heinrich Stadial 1 (around 18 ka BP) which allowed a denser grass coverage (Belz et al., 2020). At Koës the distribution pattern was stable since 19.9 ka BP with an almost equal concentration of n-C_{29} and n-C_{33} alkanes as revealed in an average Norm33 value for the interval 19.9-17.0 ka BP of 0.51±0.01 (Belz et al., submitted). After 17 ka BP the *n*-alkane distribution, ACL_{27-33} and Norm33 changes dramatically (Figure 4-7). This development was likely caused by a shift from dominating winter precipitation to summer rainfall and accompanying changed environmental conditions during a shifted growing season (Belz et al., submitted).

Alkane distribution in sediments at Koës Pan and Omongwa Pan between 17 and 16 ka BP compare to that of fynbos soils (Herrmann et al., 2016; Belz et al., 2020; Belz et al., submitted). Several studies proposed an extension of fynbos during the northward expanded winter rainfall (Shi et al., 1998, 2000; Chase and Meadows, 2007). However, Lim et al. (2016) showed, that the expansion of fynbos did not reach the southern border of Namibia. Nonetheless, the alkane distribution could possibly point to colder conditions comparable to the fynbos biome.

After 16 ka BP, conditions at both locations start to diverge continuously towards different states. Until 11 ka BP the ternary diagram shows a continuous high-resolved change at both pans over time. The displayed steady variation is highly unlikely for such diagrams (Belz et al., submitted). At both locations inorganic proxies and sedimentation rate point to a shift towards dryer conditions prior to the Holocene (Schüller et al., 2018; Belz et al., 2020; Belz et al., submitted). During the Holocene the continuous change stopped and the relative long chain *n*-alkane

distribution clusters in both records pointing to stable condition at both pans (Figure 4-6).

The similar development towards dryer conditions before, the changes in leaf wax distributions led to completely different end members (fig.3). This indicates, that during the Holocene both pans were located in different biomes. It is likely that the Nama Karoo biome was expanded northward during the Holocene. The relative distribution of n-C_{29}, n-C_{31} and n-C_{33} in the Holocene is close to average C_3 savanna vegetation at Omongwa Pan.

4.5.3 Comparison of Carbon isotopes

In general, alkane $\delta^{13}C$ values of Omongwa Pan are slightly higher compared to Koës Pan. An exception are $\delta^{13}C_{27}$ values which are lower in Omongwa Pan before 6 ka BP (Figure 4-1). A similarity in both records is the relation between $\delta^{13}C_{29}$ and $\delta^{13}C_{33}$. Between 17 and 16 ka BP $\delta^{13}C_{33}$ values are distinctively higher than $\delta^{13}C_{29}$ values in both records. This changes over the record from both pans towards similar $\delta^{13}C_{29}$ and $\delta^{13}C_{33}$ values in the Holocene, which is reflected in $Norm^{13}C_{33}$ values around 0.5. The similarity between $\delta^{13}C$ values of both homologues is reached in Omongwa Pan after 5 ka BP, but starts in the Koës Pan record as early as 10 ka BP. This development can be explained with the source of the homologues. In the environmental setting of the western Kalahari, n-C_{29} and n-C_{33} are both synthesized by C_3 and C_4 plants. The relative amount of n-C_{33} created by C_3 plants is higher under dryer and or warmer conditions (Bush and McInerney, 2015). Therefore, when $\delta^{13}C_{31}$ does not change significantly (indicating that the C_3/C_4 plant ratio did not shift), a change from higher to lower $\delta^{13}C_{33}$ values points to conditions with more limited water availability or higher evapotranspiration, forcing C_3 plants to a higher production of n-C_{33}. On the other hand, n-C_{29} is produced by higher quantities by C_3 plants (Vogts et al., 2009). If the C_3/C_4 ratio is not shifted significantly, a rise of $\delta^{13}C_{29}$ potentially marks a change in the carbon fractionation of C_3 plants, which has been reported as a result of stomata closure to prevent water loss from evapotranspiration (Garcin et al., 2014). As the

production of n-C_{29} is higher in C_3 plants compared to C_4 plants, these changes would be more visible than in $\delta^{13}C_{31}$ and $\delta^{13}C_{33}$, where this effect is overprinted by the amount produced from C_4 plants. At both pans the rise in $Norm^{13}C_{33}$ points to more evaporative conditions during the Holocene. This correlates to a temperature rise in southwestern Africa at the end of LGIT and during the early Holocene (Stute and Talma, 1998; Lim et al., 2016).

The development of $\delta^{13}C_{29}$ and $\delta^{13}C_{33}$ at both locations is also visible in calculated $LEWIS_{29-31}$ values. The change from a higher towards a lower isotope spread from 17 to 16 ka BP potentially also be inferred from a decrease in species richness. During the Holocene the low $LEWIS_{29-31}$ variation in both pans indicates severe drop in species richness (Figure 4-7E). Woody cover as indicated by f_{woody} increases over the record This may be explained with the trend towards a less-dense grassy cover (Figure 4-7F). Throughout the record, the reconstructed woody cover between the two locations point to a denser woody cover at Koës Pan, which is invers in modern condition. However, the application of the f_{woody} proxy on Kalahari pans may be insignificant due to low vegetation density of the area.

4.5.4 Environmental implications

From 17 to 16 ka BP Omongwa Pan and Koës Pan feature wetter conditions compared to later phases. This is reflected as well in n-alkane parameters as in the higher sedimentation rate which leads to the high-resolution of this phase (Schüller et al., 2018). The nature of this wet phase is different. At Koës Pan this is continuation of an ongoing state with occurrence of winter rainfall that existed since the LGM (Belz et al., submitted). At Omongwa Pan this is the end of a short phase with increased summer rainfall visible in many sites in north Namibia and Botswana (e.g. Brook et al., 1999; Gasse et al., 2008; Cordova et al., 2017; Belz et al., 2020). It seems unlikely, however not impossible, that this intensification of summer rainfall reached Koës Pan as well, but it seems rather unlikely. The transition to Holocene conditions at Koës Pan is already completed when the short, wet phase at Omongwa Pan begins to fade out between 15 and 14 ka BP (Figure

4-7). Since Koës Pan is located to the south, it might also be possible, that a potential overlapping only existed at the peak of the southward shift of the ITCZ. If this is the case, it would have occurred directly in the transition from dominant winter to dominant summer rainfall. The expected effects probably resulted in more dynamic changes at Koës Pan. On the other hand, the stable conditions at Koës before 17 ka BP rather exclude the possibility of pulses of intensified winter rainfall extending further to the north. Therefore, winter rainfall did probably not reach Omongwa Pan during the LGM.

There are some locations north of Omongwa Pan featuring wet conditions between 10-8 ka BP (Burrough et al., 2007; Burrough et al., 2009; Burrough and Thomas, 2013; Cordova et al., 2017). However, these changes are not visible at Koes Pan and only to a very limited extent at Omongwa Pan. During this period the *n*-alkane distribution in Koes sediments is closest to that of Nama Karoo soils possibly indicating a northward extention of the Nama Karoo biome. The wet conditions did not reach Omongwa Pan as the *n*-alkane distribution changed in the different direction.

Schüller et al. (2018) showed, that towards recent times sedimentation rate rises at both pans. Relative distribution of *n*-alkanes and Norm33 possible indicate less dryer conditions. This is more visible at Omongwa Pan compared to Koes Pan (Figure 4-6). It points to an intensification of summer rain which decreases westward, so that a limited rise in rainfall amount might reach Omongwa Pan but not Koës Pan.

4.6 Conclusions

This study is a comparison of two high-resolution Holocene leaf wax records of Kalahari pans. The results indicate the high spatial dynamic of continental southern Africa climate. The different conditions reconstructed from two archives so close from each other, highlights the potential of pans as source for regionally limited paleo data. This is important to understand intracontinental shifts.

Furthermore, results show that leaf wax parameters are able to distinguish the different ecoregions at both pans. The record suggests past changes of biomes like the northward shift of the Nama Karoo to Koës Pan and the exclusion of a northward expansion of the Fynbos biome. The record at both pans depicts how sensitive relative abundances of n-C_{29}, n-C_{31} and n-C_{33} data from high-resolution pan sediments can be.

The isotopic carbon composition of individual long chain n-alkane homologues can be a valuable parameter for environmental conditions beside the ratio between C_3 and C_4 plants. We introduce the Norm$^{13}C_{33}$ as a potential proxy for evaporative conditions. Future studies should compare Norm$^{13}C_{33}$ in different soils for a better classification of this proxy.

The comparison of high-resolution compared to integrated low-resolution samples illustrates that high-resolution geochemical sampling yielded a more detailed, continuous record of dynamically changing environmental conditions.

Acknowledgments

5. Concluding remarks and future perspectives

5.1 Conclusions

The main aim of this thesis was to investigate the potential of Kalahari pans as an environmental archive and to assess their utility for paleoclimate reconstruction through the application of organic geochemical methods.

This thesis contains the first climate-related biomarker and isotope record from Kalahari pans (Chapter 2). The results show that pans are promising archives that can help to fill gaps in the paleoclimate and paleoenvironmental records, in the semi-arid to arid continental interior of southern Africa. Reliable and reproducible n-alkane data could be retrieved from pan sediment, even at very low TOC contents (<0.1%). The reproducibility of proxies was proved by the comparison of high and low-resolution data from nearby excavation pits in the Omongwa Pan (Chapter 4). In addition to the n-alkane record, in most samples it was possible to also obtain compound-specific carbon and hydrogen isotope data. In some samples the low concentration of n-alkanes impeded isotope analyses. All presented n-alkane and isotope data always were within ranges comparable to published soil and vegetation data (Rommerskirchen et al., 2006b; Vogts et al., 2009; Badewien et al., 2015b; Herrmann et al., 2016). While the Omongwa Pan record displays possible signs of degradation, CPI values show no signs for diagenetic overprints.

Perhaps the most remarkable results are the relative n-alkane distributions of n-C_{29}, n-C_{31} and n-C_{33}. Plotted on ternary diagrams, the data display continuous highly-resolved and almost linear trends over small scales in parts of both pan records. This confirms a steady sedimentation and shows the sensitivity of leaf wax n-alkane chain lengths. The widely-used ACL proxy obscures these trends, and does not show the same continuous signal revealed by the n-alkanes.

Compound-specific carbon isotopes from n-alkane homologues depict different trends in certain phases. This applies mainly to $\delta^{13}C_{29}$, $\delta^{13}C_{31}$ and $\delta^{13}C_{33}$. While $\delta^{13}C_{31}$ is probably the best indicator for changes in the ratio of C_3/C_4 plants, $\delta^{13}C_{29}$

and $\delta^{13}C_{33}$ are likely to be influenced by environmental factors like temperature and potential evapotranspiration.

An unexpected feature of the records from both pans is the discrepancy between the bulk and compound-specific carbon isotopes. Even large shifts in leaf wax $\delta^{13}C$ are not visible in the bulk record and vice versa. This indicates that the carbon cycle in pans is not fully understood. Another challenge was the interpretation of δD values. Although some information like ice volume changes, temperatures, or larger changes in the C_3/C_4 plant ratio can be roughly determined, a lot of important factors to estimate apparent fractionation including potential evapotranspiration, magnitude of continental effect, and seasonal temperature changes are vague and change over time, making a reconstruction for δD_p complex and sketchy. Furthermore, the δD_{31} is affected in a way that it cannot be relied upon as an indicator of relative precipitation changes alone, but it must always be reconsidered as an integration of all of the above factors.

In two analysed pans, Omongwa Pan in the western Kalahari and Koës Pan located 250 km further south, it was possible to reconstruct environmental conditions at least as far back as the end of the LGM. In Omongwa Pan, evidence was found for a moderate intensification of summer rain during HS1, which is in agreement with a previously postulated southward shift of the ITCZ during Northern Hemisphere cold spells (Lancaster, 1979; van Zinderen Bakker, 1983; Dahl et al., 2005; Schefuß et al., 2011). The results also correlate with existing archives in northeast Namibia and Botswana. The area around Omongwa Pan is probably close to the southern edge of the intensification of summer rainfall, as there are no signs for abrupt wetness reflected in the Koës Pan record around HS1. At Koës Pan we can see signs for changing around 17 ka BP from a winter rainfall-dominated to a summer rainfall-dominated environment, which confirms inorganic data from nearby Branddam Pan (Schüller et al., 2018). There are no similar signs from Omongwa Pan. Consequently, the northern border of the winter rainfall zone was probably located between both pans during the LGM. In both cases the biggest change happened within a millennium, highlighting the ability of pan records to detect and resolve abrupt environmental change.

Analyses of both pans also show that under dry conditions, such as during the Holocene, proxies vary little and environmental conditions are more difficult to reconstruct. This is exacerbated because dry conditions minimize sediment input by surface runoff and enhance the probability of pan dust emission.

Differences between pans indicate high intracontinental variability and that pans primarily record conditions of their catchment, and thus, are local archives suited to measure the expansion and boundaries of intracontinental environmental shifts.

The results and conclusions presented in this thesis illustrate the potential that Kalahari pans have as environmental archives. In the dry interior of southern Africa, where lakes are unavailable, pans can be used to fill gaps in the record of paleo-climate evolution. The abrupt shifts demonstrate that conditions changed at the end of the last glacial, confirming that variations on global scale can have severe effects on the regional climate dynamic of central southern Africa.

5.2 Outlook

This thesis can be a start in establishing pans as archives for leaf wax proxies in southern Africa. Prospects for reconstruction of environmental conditions can be complemented combined with inorganic proxies, (Schüller et al., 2018). Although this thesis focuses on two specific pans, the approach is not pan specific and can be transferred to other pans. Based on the results and findings from this thesis, more pans in the Kalahari could be used as paleoclimate archives. Promising would be pans in areas, where paleoenvironmental studies scarce. Besides eastern Namibia this is the case in parts of the Northern Cape in South Africa, especially north of Uppington and in the Kgalagadi Transfrontier Park, and in large parts of central and south western Botswana. A transect of pans in these areas could improve the knowledge on shifts of winter and summer rainfall and their extents during the last glacial and the following deglaciation. Due to the individuality of pans it is important to know the characteristics of a pan and its catchment. Despite the net sediment accumulation that was detected in analysed Kalahari pans it cannot be excluded that other pans have a low net sedimentation. Other pans might feature discontinuous sedimentation and hiatuses.

Every archive has potential pitfalls and for several aspects of pans there are still knowledge gaps. Certain aspects of sedimentation processes within pans are unknown. The distribution of sediment and organic carbon is not homogenous. TOC contents in a transect of Omongwa Pan with surface samples taken below the salt crust variated from below 0.2 % at the windward rim to 0.9 % in the pan centre (Belz, unpublished). By analysing profiles of transects of a pan, internal dynamics could be discovered possibly indicating the most promising profile site in a pan.

TIC was used as a different proxy in both pans. As a proxy for surface runoff at Omongwa Pan and to reconstruct aeolian input at Koës Pan. Still, TIC and the isotopic composition of inorganic carbon in the sediment could be influenced by formation and solution of evaporites and interaction with ground water. For a

better understanding and application of TIC as an environmental proxy these influences should be further investigated.

For a better comparison of central southern African leaf wax studies, the data base of soils (Herrmann et al., 2016), which is restricted to South Africa needs to be extended to Namibia and Botswana as well. The savanna biome is the largest in southern Africa with a high spatial variation in conditions and vegetation. One focus of this thesis laid on the identification of changes in seasonal precipitation and impacts on vegetation. In order to better retrace changes in growing season, epicuticular waxes of plants from SRZ, WRZ and YRZ could be analysed in different seasons. Especially the isotopic hydrogen composition of n-alkanes could contribute to a better reconstruction of regional paleo-hydrology. Another focus should lie on the relative distribution of n-C$_{29}$, n-C$_{31}$ and n-C$_{33}$. The continuous change in this distribution in both pan records gave insights on ongoing changes in conditions and/or. It is however, necessary to further determine drivers of variation in n-alkane homologue synthesis for a more detailed analysis of environmental evolution.

6. References

Badewien, T., Vogts, A., Dupont, L., Rullkötter, J., 2015a. Influence of Late Pleistocene and Holocene climate on vegetation distributions in southwest Africa elucidated from sedimentary n-alkanes – Differences between 12°S and 20°S. Quaternary Science Reviews 125, 160-171.

Badewien, T., Vogts, A., Rullkötter, J., 2015b. *n*-Alkane distribution and carbon stable isotope composition in leaf waxes of C_3 and C_4 plants from Angola. Organic Geochemistry 89–90, 71-79.

Bassham, J.A., Benson, A.A., Kay, L.D., Harris, A.Z., Wilson, A.T., Calvin, M., 1954. The Path of Carbon in Photosynthesis. XXI. The Cyclic Regeneration of Carbon Dioxide Acceptor1. Journal of the American Chemical Society 76, 1760-1770.

Belz, L., Schüller, I., Köster, J., Vieth-Hillebrand, A., Wehrmann, A., Wilkes, H., submitted. Changes in southern Kalahari rain seasonality during Last Glacial-Interglacial Transition and its impact on vegetation: A leaf wax study from salt pan sediments Journal of Quaternary Science.

Belz, L., Schüller, I., Wehrmann, A., Köster, J., Wilkes, H., 2020. The leaf wax biomarker record of a Namibian salt pan reveals enhanced summer rainfall during the Last Glacial-Interglacial Transition. Palaeogeography, Palaeoclimatology, Palaeoecology 543.

Berry, R.S., Kulmatiski, A., 2017. A savanna response to precipitation intensity. PLOS ONE 12, e0175402.

Bester, F.V., van Eck, J.A.J., Kolling, H., van Rooyen, B., 2003. Grazing capacity in the Sandveld Camel Thorn Savanna of Namibia. Spotlight on Agriculture 72.

Bickert, T., 2006. Influence of Geochemical Processes on Stable Isotope Distribution in Marine Sediments, in: Schulz, H.D., Zabel, M. (Eds.), Marine Geochemistry. Springer Berlin Heidelberg, Berlin, Heidelberg, pp. 339-369.

Björck, S., Walker, M.J.C., Cwynar, L.C., Johnsen, S., Knudsen, K.-L., Lowe, J.J., Wohlfarth, B., 1998. An event stratigraphy for the Last Termination in the North Atlantic region based on the Greenland ice-core record: a proposal by the INTIMATE group. Journal of Quaternary Science 13, 283-292.

Blaauw, M., Christen, J.A., 2011. Flexible paleoclimate age-depth models using an autoregressive gamma process. Bayesian Analysis 6, 457-474.

Bonner, W., Bonner, J., 1948. The Role of Carbon Dioxide in Acid Formation by Succulent Plants. American Journal of Botany 35, 113-117.

Boocock, C., van Straten, O.J., 1962. Notes on the geology and hydrogeology of the central Kalahari region, Bechuanaland Protectorate. South African Journal of Geology 65, 125-176.

Bowen, G.J., 2021. Gridded maps of the isotopic composition of meteoric waters. . http://www.waterisotopes.org. 10.01.2021.

Bowen, G.J., Wassenaar, L.I., Hobson, K.A., 2005. Global application of stable hydrogen and oxygen isotopes to wildlife forensics. Oecologia 143, 337-348.

Bredenkamp, G.J., Spada, F., Kazmierczak, E., 2002. On the origin of northern and southern hemisphere grasslands. Plant Ecology 163, 209-229.

Broccoli, A.J., Dahl, K.A., Stouffer, R.J., 2006. Response of the ITCZ to Northern Hemisphere cooling. Geophysical Research Letters 33.

Broecker, W.S., 1994. Massive iceberg discharges as triggers for global climate change. Nature 372, 421-424.

Broecker, W.S., Denton, G.H., Edwards, R.L., Cheng, H., Alley, R.B., Putnam, A.E., 2010. Putting the Younger Dryas cold event into context. Quaternary Science Reviews 29, 1078-1081.

References

Broecker, W.S., Kennett, J.P., Flower, B.P., Teller, J.T., Trumbore, S., Bonani, G., Wolfli, W., 1989. Routing of meltwater from the Laurentide Ice Sheet during the Younger Dryas cold episode. Nature 341, 318-321.

Brook, G., Scott, L., Railsback, L.B., Goddard, E., 2010. A 35ka pollen and isotope record of environmental change along the southern margin of the Kalahari from a stalagmite and animal dung deposits in Wonderwerk Cave, South Africa.

Brook, G.A., Cherkinsky, A., Railsback, L.B., Marais, E., Hipondoka, M.H.T., 2013. Radiocarbon dating of organic residue and carbonate in stromatolites from Etosha Pan, Namibia: the radiocarbon reservoir effect, correction of published carbonate ages, and evidence of a >8 m deep lake during the Late Pleistocene. Radiocarbon, 1156-1163.

Brook, G.A., Cowart, J.B., A., B.S., 1998. Comparison of Quaternary environmental change in eastern and southern Africa using cave speleothem, tufa and rock shelter sediment data, in: Alsharan, A., Glennie, K.W., Wintle, G.L., Kendall, C.G. (Eds.), Quaternary Deserts and Climate Change. Balkema, Rotterdam, pp. 239–250.

Brook, G.A., Cowart, J.B., Marais, E., 1996. Wet and dry periods in the southern African summer rainfall zone during the last 330 kyr from speleothem, tufa and sand dune age data. Palaeoecology of Africa, 147-158.

Brook, G.A., Marais, E., Cowart, J.B., 1999. Evidence of wetter and drier conditions in Namibia from tufas and submerged speleothems. Cimbebasia, 29-39.

Brook, G.A., Railsback, L.B., Scott, L., Voarintsoa, N.R.G., Liang, F., 2015. Late Holocene Stalagmite and Tufa Climate Records for Wonderwerk Cave: Relationships Between Archaeology and Climate in Southern Africa. African Archaeological Review 32, 669-700.

Burdanowitz, N., Dupont, L., Zabel, M., Schefuß, E., 2018. Holocene hydrologic and vegetation developments in the Orange River catchment (South Africa) and their controls. The Holocene 28, 1288-1300.

Burrough, S.L., Thomas, D.S.G., 2013. Central southern Africa at the time of the African Humid Period: a new analysis of Holocene palaeoenvironmental and palaeoclimate data. Quaternary Science Reviews 80, 29-46.

Burrough, S.L., Thomas, D.S.G., Bailey, R.M., 2009. Mega-Lake in the Kalahari: A Late Pleistocene record of the Palaeolake Makgadikgadi system. Quaternary Science Reviews 28, 1392-1411.

Burrough, S.L., Thomas, D.S.G., Shaw, P.A., Bailey, R.M., 2007. Multiphase Quaternary highstands at Lake Ngami, Kalahari, northern Botswana. Palaeogeography, Palaeoclimatology, Palaeoecology 253, 280-299.

Bush, A.B.G., Philander, S.G.H., 1999. The climate of the Last Glacial Maximum: Results from a coupled atmosphere-ocean general circulation model. Journal of Geophysical Research: Atmospheres 104, 24509-24525.

Bush, R.T., McInerney, F.A., 2013. Leaf wax *n*-alkane distributions in and across modern plants: Implications for paleoecology and chemotaxonomy. Geochimica et Cosmochimica Acta 117, 161-179.

Bush, R.T., McInerney, F.A., 2015. Influence of temperature and C_4 abundance on *n*-alkane chain length distributions across the central USA. Organic Geochemistry 79, 65-73.

Carr, A.S., Boom, A., Chase, B.M., Meadows, M.E., Grimes, H.L., 2015. Holocene sea level and environmental change on the west coast of South Africa: evidence from plant biomarkers, stable isotopes and pollen. Journal of Paleolimnology 53, 415-432.

Carr, A.S., Boom, A., Grimes, H.L., Chase, B.M., Meadows, M.E., Harris, A., 2014. Leaf wax n-alkane distributions in arid zone South African flora: Environmental controls, chemotaxonomy and palaeoecological implications. Organic Geochemistry 67, 72-84.

Chase, B., 2009. Evaluating the use of dune sediments as a proxy for palaeo-aridity: A southern African case study. Earth-Science Reviews 93, 31-45.

Chase, B.M., Chevalier, M., Boom, A., Carr, A.S., 2017. The dynamic relationship between temperate and tropical circulation systems across South Africa since the last glacial maximum. Quaternary Science Reviews 174, 54-62.

References

Chase, B.M., Lim, S., Chevalier, M., Boom, A., Carr, A.S., Meadows, M.E., Reimer, P.J., 2015. Influence of tropical easterlies in southern Africa's winter rainfall zone during the Holocene. Quaternary Science Reviews 107, 138-148.

Chase, B.M., Meadows, M.E., 2007. Late Quaternary dynamics of southern Africa's winter rainfall zone. Earth-Science Reviews 84, 103-138.

Chase, B.M., Niedermeyer, E.M., Boom, A., Carr, A.S., Chevalier, M., He, F., Meadows, M.E., Ogle, N., Reimer, P.J., 2019. Orbital controls on Namib Desert hydroclimate over the past 50,000 years. Geology 47, 867-871.

Chase, B.M., Scott, L., Meadows, M.E., Gil-Romera, G., Boom, A., Carr, A.S., Reimer, P.J., Truc, L., Valsecchi, V., Quick, L.J., 2012. Rock hyrax middens: A palaeoenvironmental archive for southern African drylands. Quaternary Science Reviews 56, 107-125.

Chevalier, M., Chase, B.M., 2015. Southeast African records reveal a coherent shift from high- to low-latitude forcing mechanisms along the east African margin across last glacial–interglacial transition. Quaternary Science Reviews 125, 117-130.

Chevalier, M., Chase, B.M., 2016. Determining the drivers of long-term aridity variability: a southern African case study. Journal of Quaternary Science 31, 143-151.

Clift, P.D., Wan, S., Blusztajn, J., 2014. Reconstructing chemical weathering, physical erosion and monsoon intensity since 25Ma in the northern South China Sea: A review of competing proxies. Earth-Science Reviews 130, 86-102.

climate-data.org, 2020. Koës Climate (Namibia). https://en.climate-data.org/africa/namibia/karas-region/koes-169817/. 29.12.2020.

Cockcroft, M.J., Wilkinson, M.J., Tyson, P.D., 1987. The application of a present-day climatic model to the late quaternary in southern Africa. Climatic Change 10, 161-181.

Collins, J.A., Schefuß, E., Govin, A., Mulitza, S., Tiedemann, R., 2014. Insolation and glacial–interglacial control on southwestern African hydroclimate over the past 140 000 years. Earth and Planetary Science Letters 398, 1-10.

Collins, J.A., Schefuß, E., Mulitza, S., Prange, M., Werner, M., Tharammal, T., Paul, A., Wefer, G., 2013. Estimating the hydrogen isotopic composition of past precipitation using leaf-waxes from western Africa. Quaternary Science Reviews 65, 88-101.

Cooper, J.E., Bray, E.E., 1963. A postulated role of fatty acids in petroleum formation. Geochimica et Cosmochimica Acta 27, 1113-1127.

Coplen, T.B., Herczeg, A.L., Barnes, C., 2000. Isotope Engineering—Using Stable Isotopes of the Water Molecule to Solve Practical Problems, in: Cook, P.G., Herczeg, A.L. (Eds.), Environmental Tracers in Subsurface Hydrology. Springer US, Boston, MA, pp. 79-110.

Cordova, C.E., Scott, L., Chase, B.M., Chevalier, M., 2017. Late Pleistocene-Holocene vegetation and climate change in the Middle Kalahari, Lake Ngami, Botswana. Quaternary Science Reviews 171, 199-215.

Craig, H., 1961. Isotopic Variations in Meteoric Waters. Science 133, 1702-1703.

Crowley, T.J., 1992. North Atlantic Deep Water cools the southern hemisphere. Paleoceanography 7, 489-497.

Dahl, K.A., Broccoli, A.J., Stouffer, R.J., 2005. Assessing the role of North Atlantic freshwater forcing in millennial scale climate variability: a tropical Atlantic perspective. Climate Dynamics 24, 325-346.

Dansgaard, W., 1964. Stable isotopes in precipitation. Tellus 16, 436-468.

Dodd, A.N., Borland, A.M., Haslam, R.P., Griffiths, H., Maxwell, K., 2002. Crassulacean acid metabolism: plastic, fantastic. Journal of Experimental Botany 53, 569-580.

Eckardt, F.D., Kuring, N., 2005. SeaWiFS identifies dust sources in the Namib Desert. International Journal of Remote Sensing 26, 4159-4167.

Ecker, M., Brink, J., Horwitz, L.K., Scott, L., Lee-Thorp, J.A., 2018. A 12,000 year record of changes in herbivore niche separation and palaeoclimate (Wonderwerk Cave, South Africa). Quaternary Science Reviews 180, 132-144.

Eglinton, G., Hamilton, R.J., 1967. Leaf Epicuticular Waxes. Science 156, 1322-1335.

Eglinton, T.I., Eglinton, G., 2008. Molecular proxies for paleoclimatology. Earth and Planetary Science Letters 275, 1-16.

Ellis, R.P., Vogel, J.C., Fuls, A., 1980. Photosynthetic pathways and the geographical distribution of grasses in south west Africa Namibia. South African Journal of Science 76, 307-314.

Feakins, S.J., Sessions, A.L., 2010. Controls on the D/H ratios of plant leaf waxes in an arid ecosystem. Geochimica et Cosmochimica Acta 74, 2128-2141.

February, E.C., Higgins, S.I., Bond, W.J., Swemmer, L., 2013. Influence of competition and rainfall manipulation on the growth responses of savanna trees and grasses. Ecology 94, 1155-1164.

Garcin, Y., Schefuß, E., Schwab, V.F., Garreta, V., Gleixner, G., Vincens, A., Todou, G., Séné, O., Onana, J.-M., Achoundong, G., Sachse, D., 2014. Reconstructing C_3 and C_4 vegetation cover using n-alkane carbon isotope ratios in recent lake sediments from Cameroon, Western Central Africa. Geochimica et Cosmochimica Acta 142, 482-500.

Garcin, Y., Schwab, V.F., Gleixner, G., Kahmen, A., Todou, G., Séné, O., Onana, J.-M., Achoundong, G., Sachse, D., 2012. Hydrogen isotope ratios of lacustrine sedimentary n-alkanes as proxies of tropical African hydrology: Insights from a calibration transect across Cameroon. Geochimica et Cosmochimica Acta 79, 106-126.

Gasse, F., Chalié, F., Vincens, A., Williams, M.A.J., Williamson, D., 2008. Climatic patterns in equatorial and southern Africa from 30,000 to 10,000 years ago reconstructed from terrestrial and near-shore proxy data. Quaternary Science Reviews 27, 2316-2340.

Genderjahn, S., Alawi, M., Kallmeyer, J., Belz, L., Wagner, D., Mangelsdorf, K., 2017. Present and past microbial life in continental pan sediments and its response to climate variability in the southern Kalahari. Organic Geochemistry 108, 30-42.

Genderjahn, S., Alawi, M., Mangelsdorf, K., Horn, F., Wagner, D., 2018a. Desiccation- and Saline-Tolerant Bacteria and Archaea in Kalahari Pan Sediments. Frontiers in Microbiology 9.

Genderjahn, S., Alawi, M., Wagner, D., Schüller, I., Wanke, A., Mangelsdorf, K., 2018b. Microbial community responses to modern environmental and past climatic conditions in Omongwa Pan, western Kalahari: A paired 16S rRNA gene profiling and lipid biomarker approach. Journal of Geophysical Research: Biogeosciences 123, 1333-1351.

Gersonde, R., Crosta, X., Abelmann, A., Armand, L., 2005. Sea-surface temperature and sea ice distribution of the Southern Ocean at the EPILOG Last Glacial Maximum—a circum-Antarctic view based on siliceous microfossil records. Quaternary Science Reviews 24, 869-896.

Griffiths, J.F., 1972. Climates of Africa. Elsevier, Amsterdam.

Hays, J.D., Imbrie, J., Shackleton, N.J., 1976. Variations in the Earth's Orbit: Pacemaker of the Ice Ages. Science 194, 1121-1132.

Heinrich, H., 1988. Origin and consequences of cyclic ice rafting in the Northeast Atlantic Ocean during the past 130,000 years. Quaternary Research 29, 142-152.

Held, I.M., Soden, B.J., 2006. Robust Responses of the Hydrological Cycle to Global Warming. Journal of Climate 19, 5686-5699.

Herrmann, N., Boom, A., Carr, A.S., Chase, B.M., Granger, R., Hahn, A., Zabel, M., Schefuß, E., 2016. Sources, transport and deposition of terrestrial organic material: A case study from southwestern Africa. Quaternary Science Reviews 149, 215-229.

Herrmann, N., Boom, A., Carr, A.S., Chase, B.M., West, A.G., Zabel, M., Schefuß, E., 2017. Hydrogen isotope fractionation of leaf wax n-alkanes in southern African soils. Organic Geochemistry 109, 1-13.

Hinrichs, K.-U., Rinna, J., Rullkötter, J., 1998. Late Quaternary paleoenvironmental conditions indicated by marine and terrestrial molecular biomarkers in sediments from the Santa Barbara basin. , in: Wilson, R.C., Tharp, V.L. (Eds.), Proceedings of the fourteenth annual Pacific climate

References

(PACLIM) workshop, April 6-9, 1997. Interagency Ecological Program, Technical Report 57, California Department of Water Resources., Marysville (CA), pp. 125-133.

Hoefs, J., 2009. Stable Isotope Geochemistry, 6th ed. ed. Springer, Berlin.

Hoefs, J., 2018. Variations of Stable Isotope Ratios in Nature, Stable Isotope Geochemistry. Springer International Publishing, Cham, pp. 229-432.

Howard, S., McInerney, F.A., Caddy-Retalic, S., Hall, P.A., Andrae, J.W., 2018. Modelling leaf wax n - alkane inputs to soils along a latitudinal transect across Australia. Organic Geochemistry 121, 126-137.

Hürkamp, K., Völkel, J., Heine, K., Bens, O., Leopold, M., Winkelbauer, J., 2011. Late Quaternary environmental changes from aeolian and fluvial geoarchives in the southwestern Kalahari, South Africa: Implications for past African climate dynamics. South African Journal of Geology 114, 459-474.

Imbrie, J., Berger, A., Boyle, E.A., Clemens, S.C., Duffy, A., Howard, W.R., Kukla, G., Kutzbach, J., Martinson, D.G., McIntyre, A., Mix, A.C., Molfino, B., Morley, J.J., Peterson, L.C., Pisias, N.G., Prell, W.L., Raymo, M.E., Shackleton, N.J., Toggweiler, J.R., 1993. On the structure and origin of major glaciation cycles 2. The 100,000-year cycle. Paleoceanography 8, 699-735.

IPCC, 2021. Climate Change 2021: The Physical Science Basis. Contribution of Working Group I to the Sixth Assessment Report of the Intergovernmental Panel on Climate Change. Cambridge University Press. In Press.

Jambrina-Enríquez, M., Sachse, D., Valero-Garcés, B.L., 2016. A deglaciation and Holocene biomarker-based reconstruction of climate and environmental variability in NW Iberian Peninsula: the Sanabria Lake sequence. Journal of Paleolimnology 56, 49-66.

Jones, C.R., 1980. The Geology of the Kalahari. Botswana Notes and Records 12, 1-14.

Joubert, D.F., Rothauge, A., Smit, G.N., 2008. A conceptual model of vegetation dynamics in the semiarid Highland savanna of Namibia, with particular reference to bush thickening by *Acacia mellifera*. Journal of Arid Environments 72, 2201-2210.

Joubert, D.F., Smit, G.N., Hoffman, M.T., 2012. The role of fire in preventing transitions from a grass dominated state to a bush thickened state in arid savannas. Journal of Arid Environments 87, 1-7.

Joubert, D.F., Smit, G.N., Hoffman, M.T., 2013. The influence of rainfall, competition and predation on seed production, germination and establishment of an encroaching Acacia in an arid Namibian savanna. Journal of Arid Environments 91, 7-13.

Koch, K., Barthlott, W., 2009. Superhydrophobic and superhydrophilic plant surfaces: an inspiration for biomimetic materials. Philos Trans A Math Phys Eng Sci 367, 1487-1509.

Koch, K., Ensikat, H.-J., 2008. The hydrophobic coatings of plant surfaces: Epicuticular wax crystals and their morphologies, crystallinity and molecular self-assembly. Micron 39, 759-772.

Kolattukudy, P.E., 1976. Introduction to natural waxes., in: Kolattukudy, P.E. (Ed.), Chemistry and Biochemistry of Natural Waxes. Elsevier Scientific Publishing Company, Amsterdam, pp. 1-17.

Kristen, I., Fuhrmann, A., Thorpe, J., Röhl, U., Wilkes, H., Oberhänsli, H., 2007. Hydrological changes in southern Africa over the last 200 Ka as recorded in lake sediments from the Tswaing impact crater. South African Journal of Geology 110, 311-326.

Kristen, I., Wilkes, H., Vieth, A., Zink, K.-G., Plessen, B., Thorpe, J., Partridge, T.C., Oberhänsli, H., 2010. Biomarker and stable carbon isotope analyses of sedimentary organic matter from Lake Tswaing: evidence for deglacial wetness and early Holocene drought from South Africa. Journal of Paleolimnology 44, 143-160.

Kuhn, T.K., Krull, E.S., Bowater, A., Grice, K., Gleixner, G., 2010. The occurrence of short chain n-alkanes with an even over odd predominance in higher plants and soils. Organic Geochemistry 41, 88-95.

Kunst, L., Samuels, A.L., 2003. Biosynthesis and secretion of plant cuticular wax. Progress in Lipid Research 42, 51-80.

References

Labeyrie, L., Cole, J., Alverson, K., Stocker, T., 2003. The history of climate dynamics in the Late Quaternary, in: Alverson, K.D., Pedersen, T.F., Bradley, R.S. (Eds.), Paleoclimate, Global Change and the Future. Springer Berlin Heidelberg, Berlin, Heidelberg, pp. 33-61.

Lancaster, I.N., 1978. The pans of the southern Kalahari, Botswana. The Geographical Journal 144, 81-98.

Lancaster, I.N., 1979. Evidence for a widespread late Pleistocene humid period in the Kalahari. Nature 279, 145.

Lancaster, N., 1986. Pans in the southwestern Kalahari: a preliminary report. Palaeoecology of Africa 17, 9.

Lemma, B., Mekonnen, B., Glaser, B., Zech, W., Nemomissa, S., Bekele, T., Bittner, L., Zech, M., 2019. Chemotaxonomic patterns of vegetation and soils along altitudinal transects of the Bale Mountains, Ethiopia, and implications for paleovegetation reconstructions – Part II: lignin-derived phenols and leaf-wax-derived n-alkanes. E&G Quaternary Sci. J. 68, 189-200.

Leng, M.J., Marshall, J.D., 2004. Palaeoclimate interpretation of stable isotope data from lake sediment archives. Quaternary Science Reviews 23, 811-831.

Lewis, S.C., LeGrande, A.N., Kelley, M., Schmidt, G.A., 2010. Water vapour source impacts on oxygen isotope variability in tropical precipitation during Heinrich events. Clim. Past 6, 325-343.

Lim, S., Chase, B.M., Chevalier, M., Reimer, P.J., 2016. 50,000 years of vegetation and climate change in the southern Namib Desert, Pella, South Africa. Palaeogeography, Palaeoclimatology, Palaeoecology 451, 197-209.

Lisiecki, L.E., Raymo, M.E., 2005. A Pliocene-Pleistocene stack of 57 globally distributed benthic $\delta^{18}O$ records. Paleoceanography 20, PA1003.

Magill, C.R., Eglinton, G., Eglinton, T.I., 2019. Isotopic variance among plant lipid homologues correlates with biodiversity patterns of their source communities. PLOS ONE 14, e0212211.

Mees, F., 1999. Distribution patterns of gypsum and kalistrontite in a dry lake basin of the southwestern Kalahari (Omongwa pan, Namibia). Earth Surface Processes and Landforms 24, 731-744.

Meyers, P.A., 2003. Applications of organic geochemistry to paleolimnological reconstructions: a summary of examples from the Laurentian Great Lakes. Organic Geochemistry 34, 261-289.

Milanković, M., 1941. Kanon der Erdbestrahlungen und seine Anwendung auf das Eiszeitenproblem. Königliche Serbische Akademie, Belgrade.

Milewski, R., Chabrillat, S., Behling, R., 2017. Analyses of recent sediment surface dynamic of a Namibian Kalahari salt pan based on multitemporal landsat and hyperspectral Hyperion data. Remote Sensing 9, 170.

Milewski, R., Chabrillat, S., Bookhagen, B., 2020. Analyses of Namibian Seasonal Salt Pan Crust Dynamics and Climatic Drivers Using Landsat 8 Time-Series and Ground Data. Remote Sensing 12, 474.

Mix, A.C., Bard, E., Schneider, R., 2001. Environmental processes of the ice age: land, oceans, glaciers (EPILOG). Quaternary Science Reviews 20, 627-657.

Mucina, L., Rutherford, M.C., 2006. The vegetation of South Africa, Lesotho and Swaziland. South African National Biodiversity Institute, Pretoria.

Nicholson, S.E., 2000. The nature of rainfall variability over Africa on time scales of decades to millenia. Global and Planetary Change 26, 137-158.

Nicholson, S.E., 2009. A revised picture of the structure of the "monsoon" and land ITCZ over West Africa. Climate Dynamics 32, 1155-1171.

Niedermeyer, E.M., Prange, M., Mulitza, S., Mollenhauer, G., Schefuß, E., Schulz, M., 2009. Extratropical forcing of Sahel aridity during Heinrich stadials. Geophysical Research Letters 36.

Nield, J., Bryant, R., Wiggs, G., King, J., Thomas, D., Eckardt, F., Washington, R., 2015. The dynamism of salt crust patterns on playas. Geology 43, 31-34.

O'Leary, M.H., 1981. Carbon isotope fractionation in plants. Phytochemistry 20, 15.

Olson, D.M., Dinerstein, E., Wikramanayake, E.D., Burgess, N.D., Powell, G.V.N., Underwood, E.C., D'Amico, J.A., Itoua, I., Strand, H.E., Morrison, J.C., Loucks, C.J., Allnutt, T.F., Ricketts, T.H., Kura,

References

Y., Lamoreux, J.F., Wettengel, W.W., Hedao, P., Kassem, K.R., 2001. Terrestrial Ecoregions of the World: A New Map of Life on Earth. A new global map of terrestrial ecoregions provides an innovative tool for conserving biodiversity. BioScience 51, 933-938.

Osborne, C.P., Sack, L., 2012. Evolution of C4 plants: a new hypothesis for an interaction of CO2 and water relations mediated by plant hydraulics. Philos Trans R Soc Lond B Biol Sci 367, 583-600.

Peters, K.E., Walters, C.C., Moldowan, J.M., 2005. Biodegradation parameters, The Biomarker Guide, 2 ed. Cambridge University Press, Cambridge, pp. 645-708.

Rach, O., Brauer, A., Wilkes, H., Sachse, D., 2014. Delayed hydrological response to Greenland cooling at the onset of the Younger Dryas in western Europe. Nature Geoscience 7, 109-112.

Radke, M., Wilsch, H., Welte, D.H., 1980. Preparative hydrocarbon group type determination by automated medium pressure liquid chromatography. Analytical Chemistry 52, 6.

Railsback, L.B., Brook, G.A., Liang, F., Marais, E., Cheng, H., Edwards, R.L., 2016. A multi-proxy stalagmite record from northwestern Namibia of regional drying with increasing global-scale warmth over the last 47kyr: The interplay of a globally shifting ITCZ with regional currents, winds, and rainfall. Palaeogeography, Palaeoclimatology, Palaeoecology 461, 109-121.

Ramisch, A., Bens, O., Buylaert, J.-P., Eden, M., Heine, K., Hürkamp, K., Schwindt, D., Völkel, J., 2017. Fluvial landscape development in the southwestern Kalahari during the Holocene – Chronology and provenance of fluvial deposits in the Molopo Canyon. Geomorphology 281, 94-107.

Reynolds, R.L., Yount, J.C., Reheis, M., Goldstein, H., Chavez Jr., P., Fulton, R., Whitney, J., Fuller, C., Forester, R.M., 2007. Dust emission from wet and dry playas in the Mojave Desert, USA. Earth Surface Processes and Landforms 32, 1811-1827.

Risi, C., Bony, S., Vimeux, F., 2008. Influence of convective processes on the isotopic composition ($\delta18O$ and δD) of precipitation and water vapor in the tropics: 2. Physical interpretation of the amount effect. Journal of Geophysical Research: Atmospheres 113.

Roberts, N., Allcock, S.L., Arnaud, F., Dean, J.R., Eastwood, W.J., Jones, M.D., Leng, M.J., Metcalfe, S.E., Malet, E., Woodbridge, J., Yiğitbaşıoğlu, H., 2016. A tale of two lakes: a multi-proxy comparison of Lateglacial and Holocene environmental change in Cappadocia, Turkey. Journal of Quaternary Science 31, 348-362.

Rommerskirchen, F., Eglinton, G., Dupont, L., Güntner, U., Wenzel, C., Rullkötter, J., 2003. A north to south transect of Holocene southeast Atlantic continental margin sediments: Relationship between aerosol transport and compound-specific $\delta^{13}C$ land plant biomarker and pollen records. Geochemistry, Geophysics, Geosystems 4, 1101.

Rommerskirchen, F., Eglinton, G., Dupont, L., Rullkötter, J., 2006a. Glacial/interglacial changes in southern Africa: Compound-specific $\delta^{13}C$ land plant biomarker and pollen records from southeast Atlantic continental margin sediments. Geochemistry, Geophysics, Geosystems 7, Q08010.

Rommerskirchen, F., Plader, A., Eglinton, G., Chikaraishi, Y., Rullkötter, J., 2006b. Chemotaxonomic significance of distribution and stable carbon isotopic composition of long-chain alkanes and alkan-1-ols in C_4 grass waxes. Organic Geochemistry 37, 1303-1332.

Rosen, M.R., 1994. The importance of groundwater in playas: A review of playa classifications and the sedimentology and hydrology of playas, Paleoclimate and Basin Evolution of Playa Systems. Geological Society of America, p. 0.

Roy, P.D., Sinha, R., Smykatz-Kloss, W., Singhvi, A.K., Nagar, Y.C., 2008. Playas of the Thar Desert: Mineralogical and Geochemical Archives of Late Holocene Climate Asian Journal of Earth Sciences 1, 43-61.

Rullkötter, J., 2006. Organic Matter: The Driving Force for Early Diagenesis, in: Schulz, H.D., Zabel, M. (Eds.), Marine Geochemistry, 2nd edition ed. Springer Berlin Heidelberg, Berlin, Heidelberg, pp. 129-172.

Rutherford, M.C., Mucina, L., W., P.L., 2006. Biomes and Bioregions of Southern Africa, in: Mucina, L., Rutherford, M.C. (Eds.), The vegetation of South Africa, Lesotho and Swaziland. South African National Biodiversity Institute, Pretoria, pp. 30-51.

References

Rutherford, M.C., O'Farrel, P., Goldberg, K., Midgley, G.F., Powrie, L.W., Ringrose, S., Matheson, W., Timberlake, J., 2005. SAFARI 2000 NBI Vegetation Map of the Savannas of Southern Africa. ORNL Distributed Active Archive Center.

Sachse, D., Billault, I., Bowen, G.J., Chikaraishi, Y., Dawson, T.E., Feakins, S.J., Freeman, K.H., Magill, C.R., McInerney, F.A., van der Meer, M.T.J., Polissar, P., Robins, R.J., Sachs, J.P., Schmidt, H.-L., Sessions, A.L., White, J.W.C., West, J.B., Kahmen, A., 2012. Molecular paleohydrology: interpreting the hydrogen-isotopic composition of lipid biomarkers from photosynthesizing organisms. Annual Review of Earth and Planetary Sciences 40, 221-249.

SAHRA, 2021. Sustainability of Semi-Arid Hydrology and Riparian Areas. http://web.sahra.arizona.edu/programs/isotopes/oxygen.html.

Sarnthein, M., Stattegger, K., Dreger, D., Erlenkeuser, H., Grootes, P., Haupt, B.J., Jung, S., Kiefer, T., Kuhnt, W., Pflaumann, U., Schäfer-Neth, C., Schulz, H., Schulz, M., Seidov, D., Simstich, J., Kreveld, S.v., Vogelsang, E., Völker, A., Weinelt, M., 2001. Fundamental Modes and Abrupt Changes in North Atlantic Circulation and Climate over the last 60 ky — Concepts, Reconstruction and Numerical Modeling, in: Schäfer, P., Ritzrau, W., Schlüter, M., Thiede, J. (Eds.), The Northern North Atlantic: A Changing Environment. Springer Berlin Heidelberg, Berlin, Heidelberg, pp. 365-410.

Schefuß, E., Kuhlmann, H., Mollenhauer, G., Prange, M., Patzold, J., 2011. Forcing of wet phases in southeast Africa over the past 17,000 years. Nature 480, 509-512.

Schefuß, E., Ratmeyer, V., Stuut, J.-B.W., Jansen, J.H.F., Sinninghe Damsté, J.S., 2003. Carbon isotope analyses of n-alkanes in dust from the lower atmosphere over the central eastern Atlantic. Geochimica et Cosmochimica Acta 67, 1757-1767.

Schefuß, E., Schouten, S., Schneider, R.R., 2005. Climatic controls on central African hydrology during the past 20,000 years. Nature 437, 1003-1006.

Schmidt, F., Oberhänsli, H., Wilkes, H., 2014. Biocoenosis response to hydrological variability in Southern Africa during the last 84 ka BP: A study of lipid biomarkers and compound-specific stable carbon and hydrogen isotopes from the hypersaline Lake Tswaing. Global and Planetary Change 112, 92-104.

Schüller, I., Belz, L., Wilkes, H., Wehrmann, A., 2018. Late Quaternary shift in southern African rainfall zones: sedimentary and geochemical data from Kalahari pans. Zeitschrift für Geomorphologie 61, 339-362.

Schüller, I., Belz, L., Wilkes, H., Wehrmann, A., 2022. Kalahari Pans: Quaternary evolution and processes of ephemeral lakes., in: Eckhardt, F. (Ed.), Landscapes and Landforms of Botswana. Springer, Dordrecht, in press.

Schüller, I., Wehrmann, A., 2018. [14]C age determinations, grain size analyses and X-ray fluorescence analyses of Southwestern Kalahari pan sediments, Project GeoArchives, Spaces, Supplement to: Schüller, Irka; Belz, Lukas; Wilkes, Heinz; Wehrmann, Achim (2018): Late Quaternary shift in southern African rainfall zones: sedimentary and geochemical data from Kalahari pans. Zeitschrift für Geomorphologie, 61(4), 339-362, https://doi.org/10.1127/zfg/2018/0556. PANGAEA.

Schwark, L., Zink, K., Lechterbeck, J., 2002. Reconstruction of postglacial to early Holocene vegetation history in terrestrial Central Europe via cuticular lipid biomarkers and pollen records from lake sediments. Geology 30, 463-466.

Scott, L., 1982. A late quaternary pollen record from the Transvaal bushveld, South Africa. Quaternary Research 17, 339-370.

Scott, L., 2016. Fluctuations of vegetation and climate over the last 75 000 years in the Savanna Biome, South Africa: Tswaing Crater and Wonderkrater pollen sequences reviewed. Quaternary Science Reviews 145, 117-133.

Scott, L., Gil Romera, G., Marais, E., Brook, G.A., 2018. Pollen in fossil hyrax dung from Marine Isotope Stages 2 and 3 reveals past environments in Namibia. Quaternary International 464, 260-272.

Scott, L., Marais, E., Brook, G.A., 2004. Fossil hyrax dung and evidence of Late Pleistocene and Holocene vegetation types in the Namib Desert. Journal of Quaternary Science 19, 829-832.

References

Scott, L., Nyakale, M., 2002. Pollen indications of Holocene palaeoenvironments at Florisbad spring in the central Free State, South Africa. The Holocene 12, 497-503.

Scott, L., Thackeray, J.F., 2015. Palynology of Holocene Deposits in Excavation 1 at Wonderwerk Cave, Northern Cape (South Africa). African Archaeological Review 32, 839-855.

Shanahan, T.M., McKay, N.P., Hughen, K.A., Overpeck, J.T., Otto-Bliesner, B., Heil, C.W., King, J., Scholz, C.A., Peck, J., 2015. The time-transgressive termination of the African Humid Period. Nature Geoscience 8, 140-144.

Sharkey, T.D., 2019. Discovery of the canonical Calvin–Benson cycle. Photosynthesis Research 140, 235-252.

Shaw, P.A., Bryant, R.G., 2011. Pans, Playas and Salt Lakes, Arid Zone Geomorphology, pp. 373-401.

Shaw, P.A., Thomas, D.S.G., 1996. The Quaternary Palaeoenvironmental history of the Kalahari, Southern Africa. Journal of Arid Environments 32, 9-22.

Shepherd, T., 2003. Wax pathways, in: Murphy, D.J., Murray, B.C. (Eds.), Encyclopedia of applied plant sciences. Elsevier, Oxford, UK, pp. 1204-1225.

Shepherd, T., Wynne Griffiths, D., 2006. The effects of stress on plant cuticular waxes. New Phytol 171, 469-499.

Shi, N., Dupont, L.M., Beug, H.-J., Schneider, R., 1998. Vegetation and climate changes during the last 21 000 years in S.W. Africa based on a marine pollen record. Vegetation History and Archaeobotany 7, 127-140.

Shi, N., Dupont, L.M., Beug, H.-J., Schneider, R., 2000. Correlation between Vegetation in Southwestern Africa and Oceanic Upwelling in the Past 21,000 Years. Quaternary Research 54, 72-80.

Singarayer, J.S., Burrough, S.L., 2015. Interhemispheric dynamics of the African rainbelt during the late Quaternary. Quaternary Science Reviews 124, 48-67.

Slack, C.R., Hatch, M.D., 1967. Comparative studies on the activity of carboxylases and other enzymes in relation to the new pathway of photosynthetic carbon dioxide fixation in tropical grasses. Biochem J 103, 660-665.

Spötl, C., Vennemann, T.W., 2003. Continuous-flow isotope ratio mass spectrometric analysis of carbonate minerals. Rapid Communications in Mass Spectrometry 17, 1004-1006.

Stager, J.C., Ryves, D.B., Chase, B.M., Pausata, F.S.R., 2011. Catastrophic drought in the Afro-Asian monsoon region during Heinrich Event 1. Science 331, 1299-1302.

Stamp, S.L.D., Morgan, W.T.W., 1972. Africa: A Study in Tropical Development, third ed. ed. Wiley, New York.

Stone, A.E.C., 2014. Last Glacial Maximum conditions in southern Africa:Are we any closer to understanding the climate of this time period? Progress in Physical Geography: Earth and Environment 38, 519-542.

Stute, M., Talma, A.S., 1998. Glacial temperatures and moisture transport regimes reconstructed from noble gases and $\delta^{18}O$, Stampriet aquifer, Namibia. IAEA, International Atomic Energy Agency (IAEA).

Tabares, X., Zimmermann, H., Dietze, E., Ratzmann, G., Belz, L., Vieth-Hillebrand, A., Dupont, L., Wilkes, H., Mapani, B., Herzschuh, U., 2020. Vegetation state changes in the course of shrub encroachment in an African savanna since about 1850 CE and their potential drivers. Ecology and Evolution 10, 962-979.

Telfer, M.W., Thomas, D.S.G., 2006. Complex Holocene lunette dune development, South Africa: Implications for paleoclimate and models of pan development in arid regions. Geology 34, 853-856.

Thomas, D.S.G., Brook, G., Shaw, P., Bateman, M., Haberyan, K., Appleton, C., Nash, D., McLaren, S., Davies, F., 2003. Late Pleistocene wetting and drying in the NW Kalahari: an integrated study from the Tsodilo Hills, Botswana. Quaternary International 104, 53-67.

Thomas, D.S.G., Shaw, P.A., 1990. The deposition and development of the Kalahari Group sediments, Central Southern Africa. Journal of African Earth Sciences (and the Middle East) 10, 187-197.

Thomas, D.S.G., Shaw, P.A., 2002. Late Quaternary environmental change in central southern Africa: new data, synthesis, issues and prospects. Quaternary Science Reviews 21, 783-797.

References

Truc, L., Chevalier, M., Favier, C., Cheddadi, R., Meadows, M.E., Scott, L., Carr, A.S., Smith, G.F., Chase, B.M., 2013. Quantification of climate change for the last 20,000years from Wonderkrater, South Africa: Implications for the long-term dynamics of the Intertropical Convergence Zone. Palaeogeography, Palaeoclimatology, Palaeoecology 386, 575-587.

Tyson, P.D., Garstang, M., Swap, R., Kållberg, P., Edwards, M., 1996. An ait transport climatology for subtropical southern Africa. International Journal of Climatology 16, 265-291.

van Zinderen Bakker, E.M., 1983. The Late Quaternary history of climate and vegetation in East and southern Africa. Bothalia 14, 7.

Vickery, K.J., Eckardt, F.D., Bryant, R.G., 2013. A sub-basin scale dust plume source frequency inventory for southern Africa, 2005–2008. Geophysical Research Letters 40, 5274-5279.

Vogel, J.C., Fuls, A., Ellis, R.P., 1978. The geographical distribution of kranz grasses in South Africa. South African Journal of Science 74, 209-215.

Vogts, A., Badewien, T., Rullkötter, J., Schefuß, E., 2016. Near-constant apparent hydrogen isotope fractionation between leaf wax *n*-alkanes and precipitation in tropical regions: Evidence from a marine sediment transect off SW Africa. Organic Geochemistry 96, 18-27.

Vogts, A., Moossen, H., Rommerskirchen, F., Rullkötter, J., 2009. Distribution patterns and stable carbon isotopic composition of alkanes and alkan-1-ols from plant waxes of African rain forest and savanna C_3 species. Organic Geochemistry 40, 1037-1054.

Wacey, D., Wright, D.T., Boyce, A.J., 2007. A stable isotope study of microbial dolomite formation in the Coorong Region, South Australia. Chemical Geology 244, 155-174.

Weldeab, S., Stuut, J.B.W., Schneider, R.R., Siebel, W., 2013. Holocene climate variability in the winter rainfall zone of South Africa. Clim. Past 9, 2347-2364.

Wessel, P., Smith, W.H.F., Scharroo, R., Luis, J., Wobbe, F., 2013. Generic Mapping Tools: Improved version released. EOS, Transactions American Geophysical Union 94, 409-410.

Wiesenberg, G.L.B., Schwarzbauer, J., Schmidt, M.W.I., Schwark, L., 2004. Source and turnover of organic matter in agricultural soils derived from *n*-alkane/*n*-carboxylic acid compositions and C-isotope signatures. Organic Geochemistry 35, 1371-1393.

Wündsch, M., Haberzettl, T., Meadows, M.E., Kirsten, K.L., Kasper, T., Baade, J., Daut, G., Stoner, J.S., Mäusbacher, R., 2016. The impact of changing reservoir effects on the 14C chronology of a Holocene sediment record from South Africa. Quaternary Geochronology 36, 148-160.

Xie, P., Arkin, P.A., 1997. Global Precipitation: A 17-Year monthly analysis based on gauge observations, satellite estimates, and numerical model outputs. Bulletin of the American Meteorological Society 78, 2539-2558.

Zhang, Z., Zhao, M., Eglinton, G., Lu, H., Huang, C., 2006. Leaf wax lipids as paleovegetational and paleoenvironmental proxies for the Chinese Loess Plateau over the last 170kyr. Quaternary Science Reviews 25, 575-594.

Danksagung

Ich danke Prof. Dr. Heinz Wilkes für die Möglichkeit mit diesem Thema in seiner Arbeitsgruppe zu promovieren. Vielen Dank für fachliche Unterstützung und das entgegengebrachte Vertrauen. Außerdem möchte ich mich bei Prof. Dr. Hans-Jürgen Brumsack bedanken für die Bereitschaft das Zweitgutachten zu übernehmen.

Weiterhin möchte ich mich bei allen Projektmitgliedern von GeoArchives für die gute Zusammenarbeit und die aufregende Zeit im südlichen Afrika bedanken. Ein besonderer Dank geht an Steffi Genderjahn und Irka Schüller, die gemeinsam mit mir alle Höhen und Tiefen des Projekts durchstanden und mich mit großem fachlichem und moralischem Beistand bei den Probenkampagnen und auch sonst unterstützt haben.

Ich möchte mich bei den Mitgliedern den Arbeitsgruppen der Organische Geochemie am Deutschen GeoForschungsZentrum (GFZ) in Potsdam und am Institut für Chemie und Biologie des Meeres (ICBM) für die fachliche Unterstützung und die freundliche Arbeitsatmosphäre bedanken. Herzlich bedanken möchte ich mich bei Jürgen Köster für geologische Unterstützung bei der Feldarbeit und viele hilfreiche Fachdiskussionen und Anregungen. Für Unterstützung im Labor bei Fragen aller Art danke ich Kerstin Adolph, Kristin Günther, Regina Grundmann, Cornelia Karger, Anke Kaminsky, Petra Meier, Anke Müllenmeister-Sawall. Für die große Unterstützung bei den Isotopenmessungen bedanke ich mich bei Bernd Kopke.

Weiterhin möchte ich mich bei zahlreichen Auszubildenden und studentischen Hilfskräften bedanken, die mich im Labor tatkräftig und zuverlässig unterstützt haben: Nicolas Bill, Timo Brengelmann, Fenja Martins, Lea Mohrmann, Malte Stoltnow, Irina Weimer und May-Franzis Zastrau.

Vielen Dank auch an das Büroumfeld Anja, Ann-Katrin, Daniel, Melanie, Nana, Nena, René, Tanja und Tobias, fürs auflockern des Alltags auch in stressigen

Zeiten, ganz besonders auch an Julia und Simone für geduldige Antworten auf alle meine Fragen.

Auch möchte ich mich bei allen Mitgliedern der Arbeitsgruppe Schifffahrtsmedizin am Zentralinstitut für Arbeitsmedizin und Maritime Medizin (ZfAM), insbesondere PD Dr. Marcus Oldenburg für das Gewähren der nötigen Flexibilität die das Fertigstellen dieser Arbeit benötigte.

Zum Schluss möchte ich mich bei meiner Familie und meinen Freunden und ganz besonders Hannah für das Aushalten, Motivieren, Unterstützen und Ablenken in dieser doch recht langen Zeit. Danke! Ohne Euch wäre diese Arbeit niemals fertig geworden.

Curriculum Vitae

Name	Lukas Belz
Date of birth	15.11.1983
Place of birth	Wiesbaden

Education

2015 – 2021	PhD student, Research Group for Organic Geochemistry, Institute for Chemistry and Biology of the Marine Environment (ICBM), Carl von Ossietzky University Oldenburg, Germany
2010 – 2013	M. Sc. Marine Geoscience, University of Bremen, Germany
2007 – 2010	B. Sc. Geosciene, University of Bremen, Germany
2003 – 2007	Dipl. Ing. (FH) Nautical Science, University of Applied Science Oldnburg/Ostfriesland/Wilhelmshaven, Elsfleth, Germany

Eidesstattliche Erklärung

Hiermit versichere ich, dass ich die vorliegende Arbeit unter Berücksichtigung der Leitlinien guter wissenschaftlicher Praxis an der Carl von Ossietzky Universität Oldenburg selbstständig angefertigt und keine anderen als die angegebenen Quellen und Hilfsmittel verwendet habe. Zusätzlich erkläre ich, dass diese Dissertation weder in ihrer Gesamtheit noch in Teilen einer anderen wissenschaftlichen Hochschule zur Begutachtung in einem Promotionsvorhaben vorliegt oder vorgelegen hat und dass im Zusammenhang mit dem Promotionsvorhaben keine kommerziellen Vermittlungs- oder Beratungsdienste in Anspruch genommen worden sind.

Oldenburg, den 29.10.2021

‾‾‾‾‾‾‾‾‾‾‾‾‾‾‾‾‾‾‾‾‾‾‾‾‾‾‾‾

Lukas Belz